

This work was written as part of one of the author's official duties as an Employee of the United States Government and is therefore a work of the United States Government. In accordance with 17 U.S.C. 105, no copyright protection is available for such works under U.S. Law. Access to this work was provided by the University of Maryland, Baltimore County (UMBC) ScholarWorks@UMBC digital repository on the Maryland Shared Open Access (MD-SOAR) platform.

Please provide feedback

Please support the ScholarWorks@UMBC repository by emailing [scholarworks-group@umbc.edu](mailto:scholarworks-group@umbc.edu) and telling us what having access to this work means to you and why it's important to you. Thank you.



# Sensitivity projections for dark matter searches with the *Fermi* large area telescope



E. Charles<sup>a,b,\*</sup>, M. Sánchez-Conde<sup>c,d</sup>, B. Anderson<sup>c,d</sup>, R. Caputo<sup>e,f</sup>, A. Cuoco<sup>g,h</sup>,  
M. Di Mauro<sup>a,b</sup>, A. Drlica-Wagner<sup>i</sup>, G.A. Gomez-Vargas<sup>j,k</sup>, M. Meyer<sup>c,d</sup>,  
L. Tibaldo<sup>l</sup>, M. Wood<sup>a,b</sup>, G. Zaharijas<sup>m,n</sup>, S. Zimmer<sup>o,c,d</sup>, M. Ajello<sup>p</sup>, A. Albert<sup>a,b</sup>,  
L. Baldini<sup>q,y,a,b</sup>, K. Bechtol<sup>r,s</sup>, E.D. Bloom<sup>a,b</sup>, F. Ceraudo<sup>a,b</sup>, J. Cohen-Tanugi<sup>t</sup>,  
S.W. Digel<sup>a,b</sup>, J. Gaskins<sup>u</sup>, M. Gustafsson<sup>v</sup>, N. Mirabal<sup>w,x</sup>, M. Razzano<sup>y</sup>

<sup>a</sup> W. W. Hansen Experimental Physics Laboratory, Kavli Institute for Particle Astrophysics and Cosmology, Department of Physics, Stanford University, Stanford, CA 94305, USA

<sup>b</sup> SLAC National Accelerator Laboratory, Stanford University, Stanford, CA 94305, USA

<sup>c</sup> Department of Physics, Stockholm University, AlbaNova, SE-106 91 Stockholm, Sweden

<sup>d</sup> The Oskar Klein Centre for Cosmoparticle Physics, AlbaNova, SE-106 91 Stockholm, Sweden

<sup>e</sup> Santa Cruz Institute for Particle Physics, Department of Physics, University of California at Santa Cruz, Santa Cruz, CA 95064, USA

<sup>f</sup> Department of Astronomy and Astrophysics, University of California at Santa Cruz, Santa Cruz, CA 95064, USA

<sup>g</sup> RWTH Aachen University, Institute for Theoretical Particle Physics and Cosmology, (TTK), D-52056 Aachen, Germany

<sup>h</sup> Istituto Nazionale di Fisica Nucleare, Sezione di Torino, I-10125 Torino, Italy

<sup>i</sup> Center for Particle Astrophysics, Fermi National Accelerator Laboratory, Batavia, IL 60510, USA

<sup>j</sup> Instituto de Astrofísica, Facultad de Física, Pontificia Universidad Católica de Chile, Casilla 306, Santiago 22, Chile

<sup>k</sup> Istituto Nazionale di Fisica Nucleare, Sezione di Roma "Tor Vergata", I-00133 Roma, Italy

<sup>l</sup> Max-Planck-Institut für Kernphysik, D-69029 Heidelberg, Germany

<sup>m</sup> Istituto Nazionale di Fisica Nucleare, Sezione di Trieste, and Università di Trieste, I-34127 Trieste, Italy

<sup>n</sup> Laboratory for Astroparticle Physics, University of Nova Gorica, Vipavska 13, SI-5000 Nova Gorica, Slovenia

<sup>o</sup> University of Geneva, Département de physique nucléaire et corpusculaire (DPNC), 24 quai Ernest-Ansermet, CH-1211 Genève 4, Switzerland

<sup>p</sup> Department of Physics and Astronomy, Clemson University, Kinard Lab of Physics, Clemson, SC 29634-0978, USA

<sup>q</sup> Università di Pisa, I-56127 Pisa, Italy

<sup>r</sup> Department of Physics, University of Wisconsin, Madison, WI 53706, USA

<sup>s</sup> Wisconsin IceCube Particle Astrophysics Center, University of Wisconsin, Madison, WI 53706, USA

<sup>t</sup> Laboratoire Univers et Particules de Montpellier, Université Montpellier, CNRS/IN2P3, F-34095 Montpellier, France

<sup>u</sup> GRAPPA, University of Amsterdam, Science Park 904, 1098XH Amsterdam, Netherlands

<sup>v</sup> Georg-August University Göttingen, Institute for theoretical Physics - Faculty of Physics, Friedrich-Hund-Platz 1, D-37077 Göttingen, Germany

<sup>w</sup> NASA Goddard Space Flight Center, Greenbelt, MD 20771, USA

<sup>x</sup> NASA Postdoctoral Program Fellow, USA

<sup>y</sup> Istituto Nazionale di Fisica Nucleare, Sezione di Pisa, I-56127 Pisa, Italy

## ARTICLE INFO

### Article history:

Accepted 13 May 2016

Available online 20 May 2016

## ABSTRACT

The nature of dark matter is a longstanding enigma of physics; it may consist of particles beyond the Standard Model that are still elusive to experiments. Among indirect search

\* Corresponding author at: SLAC National Accelerator Laboratory, Stanford University, Stanford, CA 94305, USA.  
E-mail address: [echarles@slac.stanford.edu](mailto:echarles@slac.stanford.edu) (E. Charles).

editor: M.P. Kamionkowski

**Keywords:**

Gamma-ray observations

Dark matter

Fermi-LAT

techniques, which look for stable products from the annihilation or decay of dark matter particles, or from axions coupling to high-energy photons, observations of the  $\gamma$ -ray sky have come to prominence over the last few years, because of the excellent sensitivity of the Large Area Telescope (LAT) on the *Fermi Gamma-ray Space Telescope* mission. The LAT energy range from 20 MeV to above 300 GeV is particularly well suited for searching for products of the interactions of dark matter particles. In this report we describe methods used to search for evidence of dark matter with the LAT, and review the status of searches performed with up to six years of LAT data. We also discuss the factors that determine the sensitivities of these searches, including the magnitudes of the signals and the relevant backgrounds, considering both statistical and systematic uncertainties. We project the expected sensitivities of each search method for 10 and 15 years of LAT data taking. In particular, we find that the sensitivity of searches targeting dwarf galaxies, which provide the best limits currently, will improve faster than the square root of observing time. Current LAT limits for dwarf galaxies using six years of data reach the thermal relic level for masses up to 120 GeV for the  $b\bar{b}$  annihilation channel for reasonable dark matter density profiles. With projected discoveries of additional dwarfs, these limits could extend to about 250 GeV. With as much as 15 years of LAT data these searches would be sensitive to dark matter annihilations at the thermal relic cross section for masses to greater than 400 GeV (200 GeV) in the  $b\bar{b}(\tau^+\tau^-)$  annihilation channels.

© 2016 Elsevier B.V. All rights reserved.

## Contents

1.	Introduction.....	3
2.	Dark matter and dark matter particle candidates.....	3
2.1.	Weakly interacting massive particles.....	4
2.1.1.	Characterizing a WIMP signal in the gamma-ray sky .....	4
2.1.2.	Spectrum of gamma rays from WIMP interactions .....	5
2.2.	Axions and axion-like particles.....	5
3.	Astrophysical backgrounds for dark matter searches .....	6
3.1.	Cataloged sources .....	6
3.2.	Diffuse emission from the Milky Way .....	8
3.3.	Unresolved Galactic source populations .....	8
3.4.	Isotropic background and extragalactic source populations .....	9
3.5.	Residual charged-particle backgrounds .....	10
4.	Search strategies, status, and projections for dark matter detection with the LAT .....	11
4.1.	Dark matter WIMP search targets .....	11
4.2.	Current WIMP search sensitivity .....	11
4.3.	Limiting factors in search sensitivity.....	11
4.4.	The Milky Way Galactic halo.....	13
4.4.1.	Galactic halo: Status of current searches .....	13
4.4.2.	Galactic halo: Sensitivity projections .....	14
4.5.	Known satellites of the Milky Way .....	15
4.5.1.	Known satellites: Current status .....	16
4.5.2.	Known satellites: Sensitivity projections.....	16
4.6.	Undiscovered satellites of the Milky Way .....	18
4.6.1.	Undiscovered satellites: Current status .....	18
4.6.2.	Undiscovered satellites: Sensitivity projections.....	19
4.7.	Galaxy clusters .....	20
4.7.1.	Galaxy clusters: Current status .....	20
4.7.2.	Galaxy clusters: Sensitivity projections .....	21
4.8.	Cosmological WIMP searches .....	21
4.8.1.	Searches for contributions to the IGRB spectrum: Current status .....	21
4.8.2.	Searches for contributions to the IGRB spectrum: Sensitivity projections .....	22
4.8.3.	IGRB anisotropies and cross-correlation measurements: Current status .....	22
4.8.4.	IGRB anisotropies and cross-correlation measurements: Sensitivity projections .....	23
4.9.	Spectral lines .....	24
4.9.1.	Spectral lines: Current status .....	24
4.9.2.	Spectral lines: Sensitivity projections .....	24
4.10.	Axions and axion-like particles.....	26
4.10.1.	Axions and ALPs: Current status .....	26
4.10.2.	Axions and ALPs: Sensitivity projections .....	27
5.	Discussion .....	27

5.1.	Summary of projected limits .....	27
5.2.	Relation to other indirect-detection efforts .....	28
5.3.	Role of indirect-detection searches for dark matter .....	30
6.	Summary .....	31
	Acknowledgments .....	32
Appendix A.	Dark matter density profiles .....	32
Appendix B.	Calculating gamma-ray spectra from WIMP annihilation .....	33
Appendix C.	The <i>Fermi</i> LAT and LAT data .....	33
Appendix D.	Monte Carlo simulations .....	34
Appendix E.	Modeling the Galactic diffuse emission .....	34
Appendix F.	Likelihood formalism and effective background .....	35
Appendix G.	Projecting the uncertainty of contributions to the extragalactic gamma-ray background .....	36
Appendix H.	Projecting the sensitivity of the angular power spectrum analysis .....	37
Appendix I.	List of acronyms and abbreviations .....	38
	References .....	38

## 1. Introduction

Since its launch in June 2008, the *Fermi* Gamma-ray Space Telescope (*Fermi*) has surveyed the high-energy sky from 20 MeV to above 300 GeV with its main instrument, the Large Area Telescope (LAT) [1]. The LAT has opened new experimental windows into physics beyond the Standard Model. In this report we consider one such window, the indirect search for dark matter via observations of high-energy  $\gamma$  rays. Annihilation or decay of massive dark matter (DM) particles could produce  $\gamma$  rays, and the coupling of light axions or axion-like particles (ALPs) to photons in a magnetic field would alter the  $\gamma$ -ray spectra of distant sources. For these reasons,  $\gamma$ -ray observations could provide compelling indirect evidence for particle DM. Analyses of LAT data have provided hints of a potential signal of DM annihilation from the Galactic center (e.g., [2–4]) (and see Section 4.4.1) and in observations of other regions have set the strongest constraints on DM annihilation cross sections [5].

Several comprehensive and detailed reviews of the particle physics and particle astrophysics related to DM searches with the LAT and other instruments have been published recently—see, e.g., [6–8], expanding on earlier summaries, e.g., [9]. In this paper we will focus in particular on the details that are relevant for understanding the sensitivity of indirect DM searches with the LAT data and quantifying the expected sensitivity gains with additional data taking.

This paper is organized as follows. In Section 2 we summarize the phenomenology of DM searches in  $\gamma$ -ray data. In Section 3 we describe the astrophysical backgrounds for these searches, and discuss both the statistical and systematic uncertainties arising from those backgrounds. In Section 4 we present the primary astrophysical targets for DM searches with the LAT, providing the status of current searches and estimates of the sensitivity for DM searches projecting to 10 and 15 years of data taking. In Section 5 we examine the projected search sensitivities and compare them with indirect DM searches based on observations at other energies and of cosmic rays and neutrinos. We also compare them with current and projected constraints on DM derived from underground detector searches (“direct-detection” DM searches) and from searches for new physics at the Large Hadron Collider (LHC, “production” searches). We then summarize our findings and present the expected sensitivity reach for DM searches with the continuing *Fermi* mission Section 6. Finally, we provide technical details in several appendices.

## 2. Dark matter and dark matter particle candidates

Overwhelming evidence indicates that the observed structure of the Universe cannot be explained by the Standard Model of particle physics alone. In particular, measurements of Galactic rotation curves (e.g., [10]) and galaxy cluster dynamics (e.g., [11]), precision measurements of the cosmic microwave background (e.g., [12,13]), observations of the primordial abundances of heavy isotopes produced by Big Bang nucleosynthesis (e.g., [14]), and other lines of evidence all point to a substantial fraction of the Universe’s energy density being in a form of matter without significant interaction with the Standard Model particles. Numerical simulations of large-scale structure also support this conclusion; such simulations require non-relativistic DM in order to be consistent with observations (e.g., [15], and references therein).

From the observational evidence, we infer that DM interacts gravitationally, is non-relativistic (i.e., “cold”) during the formation of large-scale structure (e.g., [12,13]), and does not have large scattering cross sections with either itself (e.g., [16]) or Standard Model particles (e.g., [17]). No particle in the Standard Model meets the requirements. We have no other solid experimental or theoretical understanding of the fundamental nature of DM.

In the standard cosmology, because DM is cold, its distribution is structured over a wide range of mass scales. Small, dense DM clumps form first and later merge to form larger structures. Each of these structures, such as the DM *halo* in which the Milky Way resides, retains a population of less massive *subhalos*. In this report we consider searches that target DM halos and subhalos at distance scales from kpc (e.g., Section 4.4) to Gpc (Section 4.8).

Many particles have been posited as DM candidates. Here we focus in particular on weakly interactive massive particles (WIMPs) and axions or ALPs, as these are well-motivated candidates that may leave detectable signatures in the LAT data.

## 2.1. Weakly interacting massive particles

A heavy ( $m_\chi \gtrsim 1$  GeV) particle with a finite annihilation cross section into Standard Model particles would be theoretically well motivated as DM. The canonical example of such DM is a non-relativistic thermal relic that froze out of equilibrium with the particle bath in the early Universe. While significant annihilation would cease during freeze-out, if the DM pair annihilation is due to an  $s$ -wave process and therefore velocity independent, low rates of annihilation would continue to the present day. Such a DM particle could yield the measured DM energy density today,  $\Omega h^2 = 0.1199 \pm 0.0027$  [12,13], provided the annihilation cross section averaged over the velocity distribution is near  $\langle\sigma v\rangle \sim 3 \times 10^{-26} \text{ cm}^3 \text{ s}^{-1}$  [18].<sup>1</sup> This can be realized in models with supersymmetry (e.g., [20,21]), though other models can also work (e.g., [22]).

However, relatively simple modifications of the canonical thermal relic theory can result in present-day annihilation cross sections that differ by orders of magnitude from the standard assumption of  $\langle\sigma v\rangle \sim 3 \times 10^{-26} \text{ cm}^3 \text{ s}^{-1}$  [23]. Furthermore, in some theoretical frameworks, the DM particles may decay with lifetimes that are large compared to the age of the Universe, at rates that may be observable (see [24] for a recent review). Therefore in our searches we do not presuppose anything about the intensity of the expected DM signals.

The end products of such DM annihilation can be searched for as signals correlated with astrophysical objects known to have large DM content. Because  $\gamma$  rays are not deflected by magnetic fields, regions where DM is densest are directions with the greatest intensity of  $\gamma$  rays from DM annihilations. However, these signals must be measured relative to backgrounds from products of Standard Model astrophysical processes (Section 3).

Final states including  $\gamma$  rays are a generic expectation of DM annihilation and can result from many different annihilation channels. Two-body final states (with one or both a photon) produce  $\gamma$  rays that have a characteristic line spectrum (see Section 4.9). DM may also convert into pairs (or a larger multiplicity) of quarks, leptons, gluons, or  $SU(2)_L$  gauge bosons, all of which will decay or hadronize, resulting in a continuum spectrum of  $\gamma$  rays and other stable particles (see Section 2.1.2). The LAT is also able to measure spectra of electrons [25–27], positrons [28], and other cosmic rays, but we will not discuss sensitivity projections for those measurements in this report.

### 2.1.1. Characterizing a WIMP signal in the gamma-ray sky

The  $\gamma$ -ray flux from DM annihilation (or decay) depends on the product of factors related to the particle physics and the spatial distribution of the DM.

We do not know the mass and annihilation (or decay) channels of DM particles. However, if DM annihilates into a pair of Standard Model particles other than neutrinos, be they gauge bosons, quarks, or charged leptons, then (with the exception of the stable particles such as  $e^\pm$ ), those particles must decay or hadronize. This leads to a cascade of Standard Model particles, decaying down to electrons, protons, their anti-partners, and a large multiplicity of photons with  $\gamma$ -ray energies. Photons are also emitted as final-state radiation from charged particles, including  $e^+e^-$  pairs. Finally, secondary  $\gamma$  rays can be emitted as the final state particles propagate from the interaction point by such processes as inverse-Compton scattering (from  $e^\pm$  interactions with radiation fields) or pion production (from hadronic interactions with interstellar gas and dust).

The differential flux of prompt  $\gamma$  rays from DM annihilation within a solid angle  $\Delta\Omega$  is typically expressed as:

$$\frac{d\phi(\Delta\Omega)}{dE_\gamma} = \left( \frac{x\langle\sigma v\rangle}{8\pi} \frac{dN_\gamma}{dE_\gamma} \frac{1}{m_\chi^2} \right) \left( \int_{\Delta\Omega} d\Omega \frac{dJ_{\text{ann}}}{d\Omega} \right) \quad (1)$$

where  $x = 1$  if DM is its own antiparticle and  $x = 1/2$  if it is not (in this paper we will assume that  $x = 1$ ),  $\langle\sigma v\rangle$  is the velocity-averaged annihilation cross section,  $m_\chi$  is the WIMP mass, and  $dN_\gamma/dE_\gamma$  is the differential spectrum of  $\gamma$  rays from annihilation of a pair of DM particles (see Section 2.1.2). Eq. (1) does not include the secondary  $\gamma$  rays, which can modify both the spectrum and spatial distribution of the emission.

The “ $J$  factor” depends on the details of the spatial distribution of the DM:

$$\frac{dJ_{\text{ann}}}{d\Omega} = \int_{\text{l.o.s.}} d\ell \rho(\vec{\ell})^2. \quad (2)$$

The integration is performed along the line of sight, and  $\rho(\vec{\ell})$  is the density of the DM particles [29]. For DM decay (as opposed to annihilation) the factor of  $\left( \frac{x\langle\sigma v\rangle}{8\pi} \frac{1}{m_\chi^2} \right)$  becomes  $\left( \frac{1}{4\pi} \frac{1}{\tau m_\chi} \right)$ , where  $\tau$  is the lifetime of the DM particle, and  $\frac{dJ_{\text{dec}}}{d\Omega} = \int_{\text{l.o.s.}} d\ell \rho(\vec{\ell})$ . As we are concerned primarily with exploring the case for additional data-taking with the LAT in this paper we will focus on DM annihilation for concreteness. However, as we will discuss in Section 4 our estimates of the scaling of the detection sensitivity would be very similar for the case of DM decay.

The  $J$  factor is an astrophysical quantity that is target dependent. Finding an astronomical object that maximizes this quantity is a key step in designing a sensitive search for indirect signals of DM. (It is also important to consider the

<sup>1</sup> Unless the  $s$ -wave amplitude is  $\lesssim 10$  times smaller than the  $p$ -wave amplitude, the current annihilation rate should be within an order of magnitude of the required rate for thermal relic DM [19].

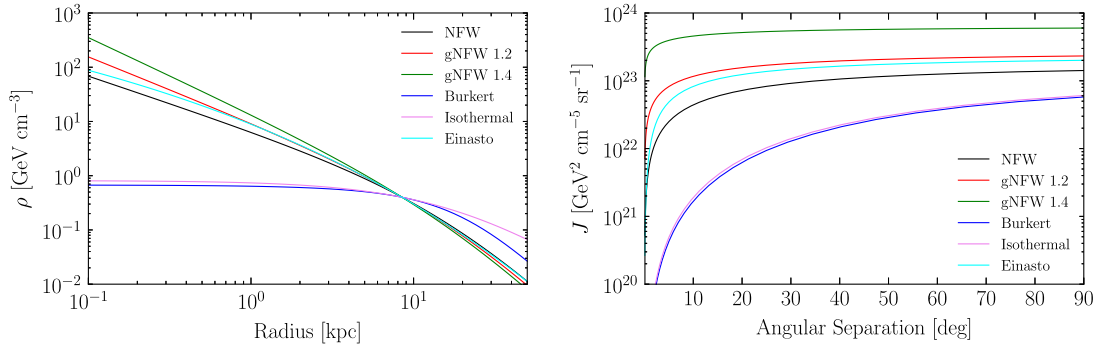


**Fig. 1.** The density as a function of Galactocentric radius (left) and the integrated  $J$  factor as a function of angular separation from the Galactic center for several widely considered radial profiles of the DM halo of the Milky Way.

astrophysical backgrounds associated with potential targets, see Section 3.) Typically the total  $J$  factor integrated over the solid angle of a region of interest (ROI,  $\Delta\Omega$ ) is quoted for a given target:

$$J(\Delta\Omega) \equiv \int_{\Delta\Omega} d\Omega \int_{\text{l.o.s.}} d\ell \rho_\chi^2(\vec{\ell}). \quad (3)$$

Note that  $J$  depends implicitly on the distance to the DM target. The density profiles of DM halos must be determined from a combination of observation and simulation, and depend on the search target.

As an example, the densities and resulting integrated  $J$  factors for various potential DM density profiles for the Milky Way are shown in Fig. 1. For this comparison we adopted a scale radius of  $r_s = 20$  kpc, and selected  $\rho_0$  such that the local DM density (at 8.5 kpc from the Galactic center) is  $0.4 \text{ GeV cm}^{-3}$  (see, e.g., [30–32]). The parameters were chosen to be consistent with dynamical constraints (e.g., [33–35]). Details for the various radial profile models are given in Appendix A.

With the exception of annihilation to leptons in relatively dense environments, such as near the Galactic center [36–39], secondary processes are sub-dominant for  $\gamma$ -ray emission and we will not consider them in this paper. (See, however, Section 5.2 for discussion of constraints on lepton-dominated channels from cosmic-ray and radio observations.)

### 2.1.2. Spectrum of gamma rays from WIMP interactions

Fig. 2 shows the prompt-emission spectra,  $dN_\gamma/dE_\gamma$ , per pair annihilation, for a variety of channels and DM masses [40]. We typically present results for the  $b\bar{b}$  channel in this report. Similar results apply to other channels, but in some cases we highlight how the results depend on the channel considered, in particular for the  $\tau^+\tau^-$  channel, for which  $dN_\gamma/dE_\gamma$  peaks at higher energies.

## 2.2. Axions and axion-like particles

Alternative classes of DM candidates include axions and ALPs. Axions were originally considered to be pseudo-Nambu–Goldstone bosons (pNGBs) that arise when an additional symmetry of the standard-model Lagrangian is spontaneously broken [41,42]. This additional shift symmetry was introduced to solve the strong CP problem in quantum chromodynamics [43]. The axion mass  $m_a$  is inversely proportional to the breaking scale  $f_a$  of the additional symmetry,  $m_a \sim 0.6 \text{ meV}(10^{10} \text{ GeV}/f_a)$  [44]. For ALPs, which are commonly predicted in string theories (e.g. [45,46]), these two parameters are independent. If produced non-thermally in the early Universe via the so-called misalignment mechanism, the coherent oscillations of the pNGB field can act as cold DM [47–51].

Axions and ALPs can be detected through their coupling to photons described by the Lagrangian (e.g. [52]),

$$\mathcal{L}_{a\gamma} = -\frac{1}{4}g_{a\gamma}F_{\mu\nu}\tilde{F}^{\mu\nu}a, \quad (4)$$

where  $F_{\mu\nu}$  ( $\tilde{F}_{\mu\nu}$ ) is the (dual) electromagnetic field tensor,  $a$  the pNGB field strength, and  $g_{a\gamma}$  the coupling constant to photons. The coupling is related to the symmetry breaking scale via

$$g_{a\gamma} = \frac{\alpha}{2\pi} \frac{\mathcal{N}}{f_a}, \quad (5)$$

with the fine-structure constant  $\alpha$  and a model-dependent factor  $\mathcal{N}$ , usually assumed to be of the order one. As a consequence of two-photon coupling, ALPs and axions can be detected either through their decay to photons (as a  $\gamma$ -ray flux associated with objects with extreme magnetic fields, such as neutron stars) or an oscillation to photons in external magnetic fields (as irregularities in the spectra of  $\gamma$ -ray sources).

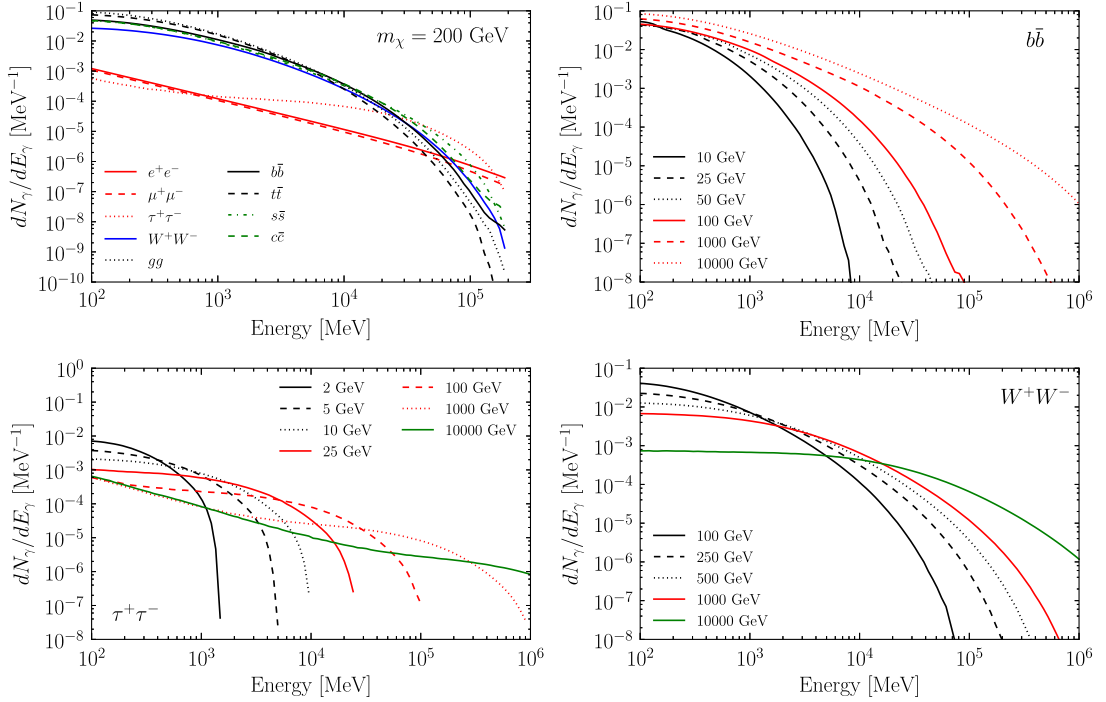


**Fig. 2.** Spectra,  $dN_\gamma/dE_\gamma$ , of prompt  $\gamma$  rays per DM pair annihilation for different annihilation channels and DM masses. (Upper left) Annihilation spectra of 200 GeV DM into various annihilation channels. Annihilation spectra into  $b\bar{b}$  (upper right),  $\tau^+\tau^-$  (lower left), and  $W^+W^-$  (lower right) for a range of DM masses. See Ref. [40] and Appendix B for details of the calculation of these spectra. These spectra do not include secondary emission of  $\gamma$  rays, which will enhance the emission at lower energies in the leptonic channels and can be important in dense environments.

The pNGB lifetime for photon decay in vacuum is given by [48]

$$\tau_{a\gamma} = \frac{64\pi}{m_a^3 g_{a\gamma}^2} = 1.3 \times 10^{27} \text{ s} \left( \frac{g_{a\gamma}}{10^{-11} \text{ GeV}^{-1}} \right)^{-2} \left( \frac{m_a}{\text{eV}} \right)^{-3}. \quad (6)$$

For axions and ALPs to be cold DM, we require that they are sufficiently stable, i.e.,  $\tau_{a\gamma}$  must be larger than the age of the Universe  $\sim 13.7$  Gyr. A further requirement is that the pNGB field should have started to oscillate no later than when the expanding early Universe reached matter–radiation equality. Also, we require that mass does not receive any further radiative corrections, so that the energy density  $\Omega_a$  is diluted with the expanding Universe. For an axion or ALP making up a fraction  $\Omega_a/\Omega$  of the total DM, these requirements lead to an upper limit on the photon coupling in terms of the mass [51],

$$\frac{g_{a\gamma}}{10^{-11} \text{ GeV}^{-1}} \lesssim 2.20 \times 10^3 \theta_1 \mathcal{N} \sqrt{\frac{m_a}{\text{eV}}} \sqrt{\frac{\Omega}{\Omega_a}}, \quad (7)$$

where  $\theta_1$  is the initial misalignment angle of the pNGB field.

### 3. Astrophysical backgrounds for dark matter searches

All DM searches using the LAT must contend with backgrounds from a variety of astrophysical sources as well as instrumental backgrounds. (Details about the LAT instrument and data are provided in Appendix C.) The effect of the different backgrounds depends on the location and size of the DM search target as well as on the methodology of the particular search technique. In this section we summarize five major astrophysical backgrounds for DM searches. Simulated all-sky maps for 15 years of data for each background type are shown in Fig. 3. (See Appendix D for simulation details.)

#### 3.1. Cataloged sources

The third *Fermi* LAT source catalog (3FGL, [53]) was constructed based on the analysis of the first four years of LAT data, and contains more than 3000 individual sources. Of those, more than 2000 are associated with multi-wavelength counterparts of known  $\gamma$ -ray emitting source classes. Although follow-up studies on the earlier 1FGL [54] and 2FGL [55] catalogs found plausible associations for  $\sim 80\%$  of the sources in those catalogs [56], the 1010 unassociated sources in the 3FGL catalog could conceivably include signals from DM subhalos (see Section 4.6).



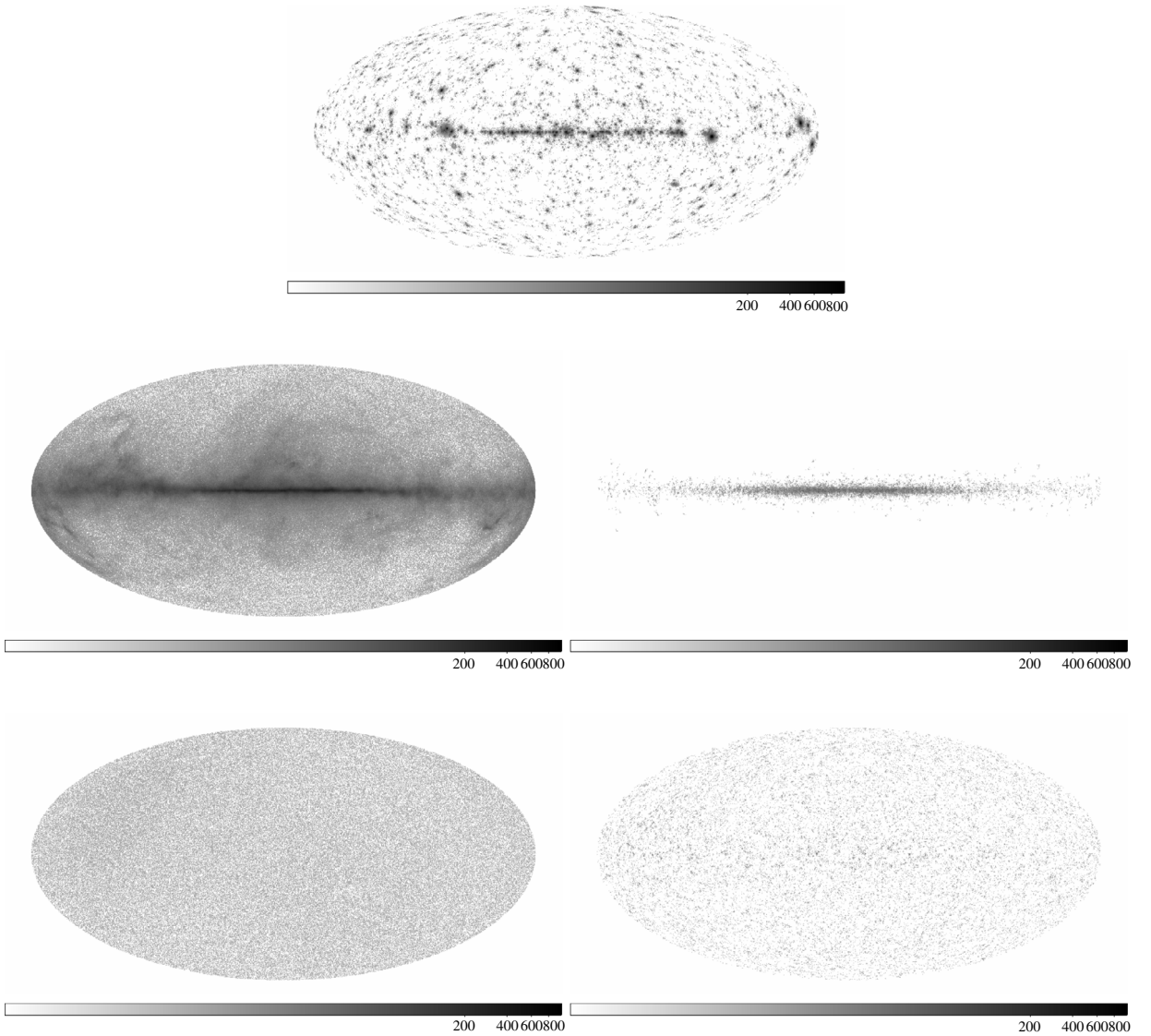


**Fig. 3.** Counts maps of all  $\gamma$  rays with reconstructed energy above 1 GeV for 15 years of simulated data for the P8R2\_SOURCE event class. The maps are shown in a Hammer–Aitoff projection in Galactic coordinates with  $1^\circ \times 1^\circ$  pixels. The individual maps show cataloged sources (Section 3.1, top), the diffuse Galactic emissions (Section 3.2, middle left), unresolved Galactic sources (Section 3.3, middle right) isotropic background emission (Section 3.4 and Section 3.5, bottom left), and unresolved extragalactic sources (Section 3.4, bottom right). The maps have the same gray scale to facilitate comparisons.

For analyses of DM targets that have spatial extents of less than a few degrees, we typically include all of the cataloged sources in the ROI in the baseline model (i.e., DM-free null hypothesis) and allow the spectral parameters (including overall flux normalizations) of the nearest sources to vary when fitting for the DM targets. This avoids incorrectly setting limits that exclude DM signals that were mis-attributed as already-known sources. If a DM target were placed at the position of a cataloged source, the two would be at least partially degenerate in the likelihood fitting and any limits on the DM cross section would consequently worsen since some or all of the flux from the target location was potentially attributable to DM. Allowing the spectral parameters of sources to vary also helps to account for any variability in the source, particularly if an analysis uses a different integration time from the catalog analysis.

For searches for DM signals from large regions of the sky, e.g., in a spectral line search (Section 4.9, see also, e.g., Refs. [57–59]), or for  $\gamma$  rays from WIMPs at cosmological distances (Section 4.8, see also, e.g., Refs. [60,61]) we typically choose to mask regions around the brightest cataloged sources. This is done to reduce the background and increase the signal-to-noise of the analysis, and to simplify the analysis by avoiding the need to re-optimize the spectral parameters of thousands of sources.

Therefore, when estimating the sensitivity for a DM search, depending on the analysis considered, we either include the cataloged sources in the background model or account for the reduced search area (and reduced signal) from masking parts of the sky.



The 4FGL catalog now under development will be based on seven years of LAT data and is projected to include more than 4000  $\gamma$  ray sources. For sources at a given flux level, the deepening exposure of the LAT observations also results in more precise localization of sources, consequently increasing the power to classify sources based on associations with counterparts at other wavelengths. This helps to increase the numbers of classified sources for population studies. The remaining unassociated sources also become ‘cleaner’ targets in searches for undiscovered dark satellites of the Milky Way (Section 4.6).

The collected emission from sources that are too faint to be detected individually will contribute to both the Galactic (Section 3.3) and isotropic background (Section 3.4). After detailed accounting for the detection efficiencies, the intrinsic flux distributions  $dN/dS$  of sources of a given class are essential for population studies that dissect these backgrounds.

### 3.2. Diffuse emission from the Milky Way

Diffuse emission, i.e., emission not associated with discrete sources, accounts for the majority of the  $\gamma$  rays detected by the LAT. Diffuse  $\gamma$ -ray emission can be categorized as Galactic, associated with the Milky Way, or extragalactic, which has a nearly isotropic distribution over the sky. An unresolved source component may constitute less than 10% of the Galactic diffuse emission [53]. Therefore, the majority is due to interactions of high-energy cosmic rays with interstellar gas and radiation fields in the Milky Way. The production processes are inelastic collisions of cosmic-ray nuclei with nuclei in the interstellar medium, which produce  $\gamma$ -rays mainly through production and decay of neutral mesons like  $\pi^0$ , bremsstrahlung of cosmic-ray electrons and positrons off gas nuclei, and inverse-Compton scattering of cosmic-ray electrons and positrons off interstellar photons from radio to optical/UV. Predicting the intensities of interstellar  $\gamma$ -ray emission requires knowing the densities of cosmic rays, interstellar gas, and radiation fields everywhere in the Milky Way. In practice, we use realistic, but simplified, models of these quantities. Details of the modeling procedure are provided in Appendix E.

Detailed studies comparing models of the diffuse Galactic emission [62] to LAT data have found that the models are fairly accurate, with typical residuals of 10% or better over much of the sky. This is compatible with, and in some cases somewhat better than, estimates of the uncertainties of the modeling procedures (that are closer to 20% to 30% for the local emissions alone, see Ref. [63]). However, as mentioned above, large-scale residuals associated with specific structures and source populations do exist, and in some parts of the sky and for some energy ranges the observed Galactic diffuse emission can exceed the modeling predictions by 100% or more.

Similarly, the intensity of the Galactic diffuse emission, and hence its contribution to the background in particular analyses, varies significantly across the sky (see Fig. 3, middle left). Therefore, treatment of the uncertainties arising from the model of the Galactic diffuse emission depends on the search target. In searches targeting discrete sources at high Galactic latitudes (such as known Milky Way satellites, see Section 4.5), the Galactic diffuse emission was found to be faint enough that the systematic uncertainties of the model can be neglected (e.g., [5]). For searches targeting larger regions of the sky away from the Galactic plane it is often sufficient to use a small set of representative Galactic diffuse emission models to quantify the uncertainties arising from the Galactic fore- and backgrounds [64]. Finally, searches targeting the Galactic center and inner Galactic halo must contend with very large backgrounds with large uncertainties, and typically either mask the Galactic plane (e.g., Ref. [65]), perform detailed studies of the uncertainties (e.g., Ref. [66]), undertake detailed fitting of the Galactic diffuse emission and point sources (e.g., Ref. [67]) or do some of all of these.

In the context of developing a new model of the Galactic diffuse emission to support Pass 8 analyses of seven-year and longer data sets, we are investigating ways to increase the accuracy and reduce the systematic uncertainty of the model. These include incorporating higher-resolution surveys of the interstellar gas in the Galactic plane that became available recently (e.g., [68,69]), improving the derivation of gas distributions along lines of sight toward the inner Galaxy using recently published analyses of the distribution of interstellar dust in the Galactic plane based on reddening of stars, refining the evaluation of the dark neutral medium using *Planck* microwave data, and of course iterating the fitting with deep searches for point sources in the Pass 8 data. Each of these is expected to increase the accuracy of the modeling in the challenging directions near the Galactic plane.

### 3.3. Unresolved Galactic source populations

Although unresolved Galactic sources make a relatively small contribution to the total  $\gamma$ -ray luminosity of the Milky Way, their distribution is unlikely to follow the dust and gas that dominate the diffuse Galactic  $\gamma$ -ray distributions. The template fitting procedure used to generate the model of diffuse Galactic emission does have some freedom to absorb contributions from unresolved sources, but exactly how much is difficult to predict as it depends on the correlation between the morphology of the distribution of unresolved sources and the templates used to model the diffuse Galactic  $\gamma$ -ray emission. Furthermore, as can be seen in Fig. 4, the flux threshold for the detection of a point source depends strongly on the diffuse Galactic background. The LAT sensitivity is also slightly better near the celestial poles, as those regions have the largest exposure.

The population of unresolved Galactic sources was studied in detail in § 6 of the 3FGL catalog paper [53]. A mock catalog (with ten times the number of expected Galactic  $\gamma$ -ray sources) was produced for that work. We have simulated populations of both detected and undetected Galactic sources by applying thresholding using the map shown in Fig. 4. Fig. 5 shows the

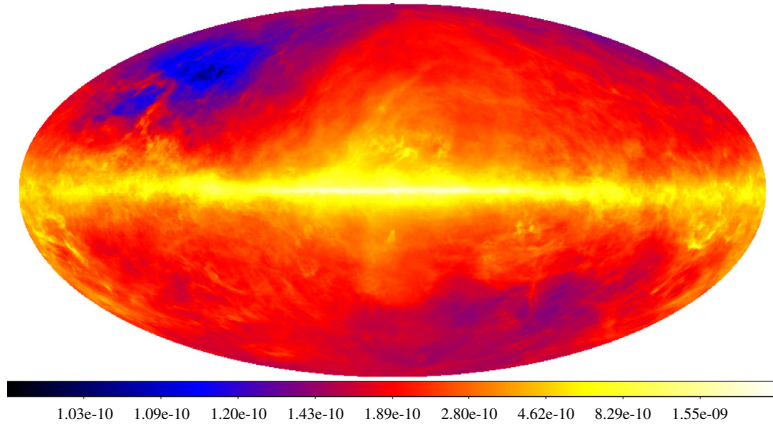


**Fig. 4.** Map of the source detection threshold flux above 1 GeV (in  $\text{cm}^{-2} \text{s}^{-1}$ ) for a point source with a power-law spectrum and a spectral index  $\Gamma = 2.2$ . The map is in Hammer–Aitoff projection in Galactic coordinates and is derived for the first four years of LAT observations.

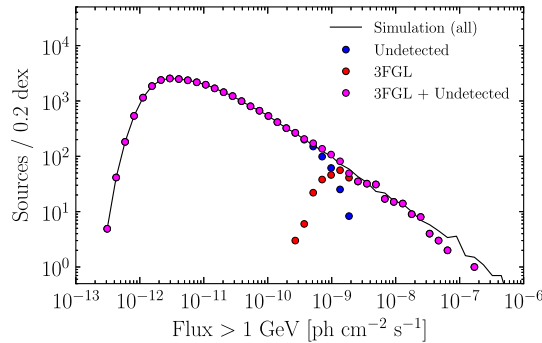


**Fig. 5.** Integral photon flux above 1 GeV for Galactic sources. The black line shows the total simulated distribution, the blue points show the simulated sources below the detection threshold for the 3FGL catalog and the red points show the distribution of 3FGL sources. Finally, the magenta points show the sum of the simulated distribution below the detection threshold and the 3FGL catalog sources. (For interpretation of the references to colour in this figure legend, the reader is referred to the web version of this article.)

simulated source counts as a function of integral photon flux above 1 GeV for both detected and undetected Galactic sources, illustrating that the total simulated distribution of sources is well modeled by the sum of the simulated undetected sources and the 3FGL catalog of detected sources. (We applied the thresholding in energy flux, rather than photon flux, to reduce the dependence on the spectral index of the source.)

The unresolved Galactic sources are not an important background for most LAT searches. Search targets typically are at high Galactic latitudes (such as the dwarf galaxies, Section 4.5), and often low Galactic latitude regions are masked. The exception is searches targeting the Galactic center, where unresolved Galactic sources are potentially a very challenging background (see Section 4.4). Pulsars pose a particular challenge, as their  $\gamma$ -ray spectra are similar to the expected DM signal for some parts of the parameter space we are searching, e.g.,  $\sim 50$  GeV (20 GeV) DM annihilating to  $b$ -quarks ( $\tau$ -leptons) [70–75].

### 3.4. Isotropic background and extragalactic source populations

The isotropic gamma-ray background (IGRB) comprises all extragalactic emissions too faint or too diffuse to be resolved in a given survey, as well as any residual Galactic foregrounds that are approximately isotropic (see, e.g., [76] for a recent review). In contrast, the extragalactic  $\gamma$ -ray background (EGB) includes the IGRB as well as the emission from resolved extragalactic point sources.

Population studies of the source classes contributing to the EGB have shown that known  $\gamma$ -ray emitting source classes can account for most of it [77]. This can be seen in Fig. 6 (see also Section 4.8).

The distinction between a truly isotropic background and one composed primarily of unresolved sources is potentially very important for projecting search sensitivities. This is because the nature of the statistical fluctuations is quite different in the two cases. In the former case the background is characterized by Poisson fluctuations in the  $\gamma$ -ray counts, while in the latter it is characterized by Poisson fluctuations in the number of sub-threshold sources overlapping the search target. Since the sub-threshold sources are generally not modeled, the distribution in the null-hypothesis case will have more high test-statistic ( $TS$ , defined as twice the difference in log-likelihood between the null hypothesis and the best-fit model) values than

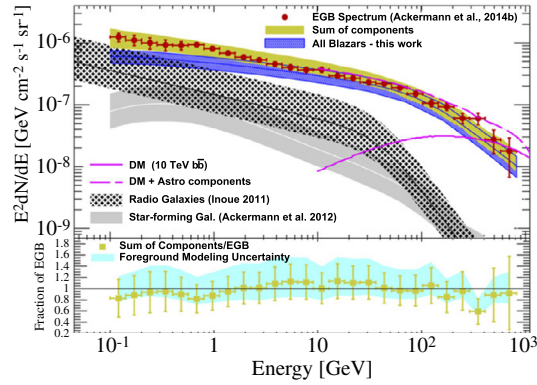


**Fig. 6.** EGB (i.e. IGRB plus resolved extragalactic sources) as measured by the LAT in [64] (red points with error bars). The yellow band indicates the sum of contributions for unresolved sources of different types (blazars, star-forming galaxies and radio galaxies). The lower inset shows the ratio of this summed contribution to the EGB measurement, as well as the uncertainty due to the foreground emission models. (For interpretation of the references to colour in this figure legend, the reader is referred to the web version of this article.)

Source: This figure appeared as Fig. 3 of Ref. [77]; additional details are available there; reproduced by permission of the AAS.

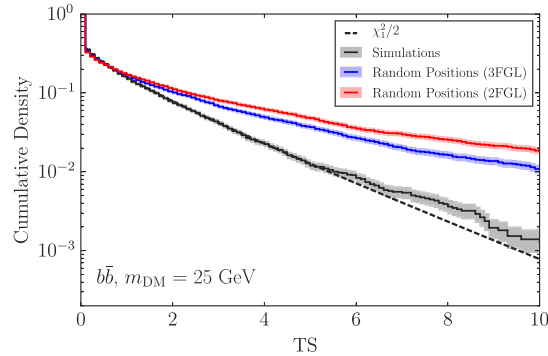


**Fig. 7.** Distribution of TS values obtained when testing for the existence of a point-like source with a spectrum characteristic of DM annihilation. The dotted line shows the expected asymptotic distribution for the null hypothesis (a  $\chi^2$ -distribution with 1 degree of freedom). The gray band shows the distribution obtained from simulations without unresolved sources, while the red and blue bands show the distributions obtained from random locations in the sky, when the background model used in the analysis included the 2FGL (red) and 3FGL (blue) catalog sources. (For interpretation of the references to colour in this figure legend, the reader is referred to the web version of this article.)

Source: This figure appeared as Fig. 5 of Ref. [5], additional details are available there, reproduced by permission of the APS and the authors.

would be expected for truly isotropic backgrounds. An example of this can be seen in studies of the TS distribution of random fields in flight data as compared to *all-sky photon simulations* shown in Fig. 7. Interestingly, although the fraction of high-TS trials does increase because of the unresolved source background, the median expected upper limits are not affected. This is because the large majority of randomly selected positions do not overlap with any  $\gamma$  rays from unresolved sources.

### 3.5. Residual charged-particle backgrounds

A final component of the background is the residual charged particles that contaminate the LAT  $\gamma$ -ray sample. In this context we define *particle backgrounds* as all events that are classified as  $\gamma$  rays in a given LAT event class but originate from cosmic rays or the interactions of cosmic rays in the Earth's atmosphere. Therefore, the particle backgrounds include both charged and neutral particles—including secondary  $\gamma$  rays.

Models of the particle background fluxes incident on the LAT are described in detail in Ref. [78]. Discussion of the calibration of the particle background contamination in the high-purity event classes, i.e., the event selections used for single source, source population and diffuse emission analyses (SOURCE class and cleaner) can be found in Ref. [79]. Details of the residual charged particle contamination for Pass 8 event classes can be found in Ref. [80].

For the studies described in this paper it is sufficient to note that the residual charged particle backgrounds are treated as part of the isotropic  $\gamma$ -ray template, and that the isotropic templates used for data analysis were derived from fits to the flight data.

Estimates of the residual charged particle contamination for the various Pass 8 event classes are shown in Fig. 8. The contamination of the P8R2\_ULTRACLEAN event classes is at or below the IGRB level for all energy  $> 100$  MeV.

The simplest approach for dealing with residual charged particle backgrounds is to choose an event class with low enough levels of residual charged particles that they may safely be neglected. This is possible for most of the analyses

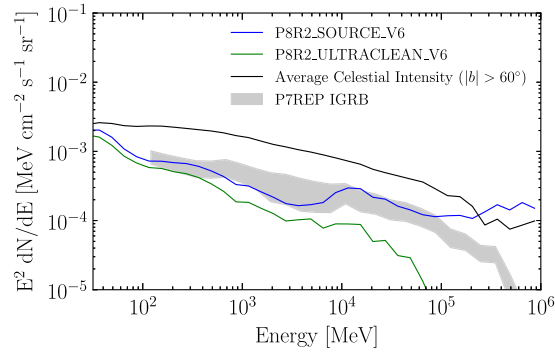


**Fig. 8.** Comparison of the residual charged-particle background contamination for the P8R2\_SOURCE and P8R2\_ULTRACLEAN event classes with the average brightness of the  $\gamma$ -ray sky at intermediate and high latitudes and the estimated IGRB.

**Table 1**

Summary table of DM search targets discussed in this paper.

Target	Distance (kpc)	$J$ factor ( $\text{GeV}^2 \text{cm}^{-5}$ )	Angular extent ( $^\circ$ )
Galactic center/halo (Section 4.4)	8.5	$3 \times 10^{22} - 5 \times 10^{23}$	$>10$
Known Milky Way satellites (Section 4.5)	25–300	$3 \times 10^{17} - 3 \times 10^{19}$	$<0.5$
Dark satellites (Section 4.6)	Up to 300	Up to $3 \times 10^{19}$	$<0.5$
Galaxy Clusters (Section 4.7)	$>5 \times 10^4$	Up to $1 \times 10^{18}$	Up to $\sim 3$
Cosmological DM (Section 4.8)	$>10^6$	–	Isotropic

described in this paper, the exceptions being those targeting large fractions (or all) of the sky, as even for the cleanest event class, the integrated contributions from residual charged particle backgrounds can become important. Specifically, searches for spectral lines (Section 4.9) and large-scale, cosmological DM signatures (Section 4.8) must consider this background component.

#### 4. Search strategies, status, and projections for dark matter detection with the LAT

In this section we describe astrophysical objects that are the primary targets for searching for signals from DM annihilation. We first present an overview of the various WIMP search targets and results; then for each target we summarize the status of current searches, and project how the sensitivity will improve with continued LAT data taking. Finally we discuss searches for axion or ALP DM and how the sensitivity of those searches will improve with additional LAT data.

##### 4.1. Dark matter WIMP search targets

Table 1 summarizes the targets for WIMP searches. The differences between the targets are pronounced enough to warrant significant modifications in the search techniques, as discussed earlier in this section. For example, searches targeting known dark-matter dominated Milky Way satellites (Section 4.5.1) are very similar to blind searches for point-like emission performed when creating catalogs of  $\gamma$ -ray point sources such as the 3FGL; on the other hand, extracting a isotropic signal from DM halos of galaxies at cosmological distances (Section 4.8) requires very detailed modeling of both the Galactic foreground emission and the contributions of unresolved sources.

##### 4.2. Current WIMP search sensitivity

We show a subset of published results for various DM targets for the  $b\bar{b}$  channel in Fig. 9. For each target, we selected recent results that used moderate assumptions, i.e., neither the most conservative nor the most optimistic cases. Because of differences in the data sets, DM profiles, and background modeling, these results should be taken as representative and absolute comparisons should be interpreted with caution. Details about the scenarios considered (e.g., the DM distribution) for each of the targets are provided in Table 2.

##### 4.3. Limiting factors in search sensitivity

To understand the benefits of additional data taking for DM searches we consider three cases. Because of the rapidly falling power-law backgrounds, individual search targets might fall under different cases at low and high energies.

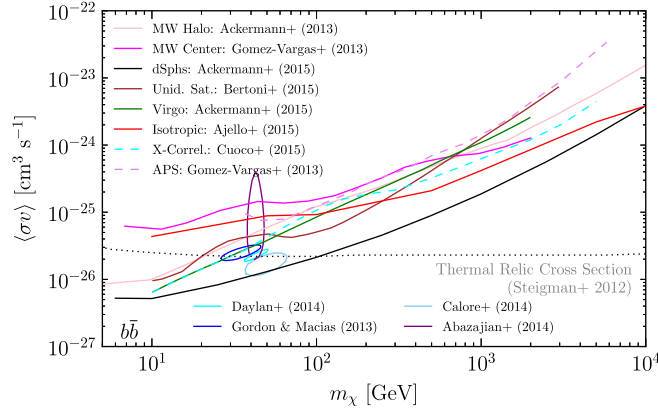


**Fig. 9.** Comparison of representative published limits (curves) and best-fit regions (ellipses) for the  $b\bar{b}$  channel found using LAT data for several DM targets. References and details about the scenario selected as the representative limit or best-fit values for each DM target are provided in Table 2.

**Table 2**

The works referenced here for the various DM targets are the representative results shown in Fig. 9. The scenarios given in quotation marks appear as they were named in the original reference to distinguish them from other scenarios presented in the same papers. For details about the exact parametrization of the various DM signals as well as the modeling of astrophysical backgrounds the reader is referred to the original references.

Target	Ref.	Scenario	Other Refs.
Galactic halo (Section 4.4)	[65]	NFW profile “constrained free source fits” $3\sigma$ ULs	–
Galactic center (limits, Section 4.4)	[39]	NFW profile, $3\sigma$ ULs	–
Galactic center (best-fits, Section 4.4)	[3,4,81–84]	gNFW profile with $\gamma \sim 1.2$	[2,85]
dSphs (Section 4.5)	[5]	NFW profile	[86–94]
Unid. Satellites (Section 4.6)	[95]	95% CL ULs	[88,96–99]
Galaxy clusters (Section 4.7)	[100]	Virgo, “DM-I” conservative boost model	[101–108]
Isotropic (Section 4.8)	[77]	$2\sigma$ ULs	[109–111]
Cross-correlation (Section 4.8)	[112]	“annLOW, ALLGeV”, 95% CL ULs	[61,113–122]
Ang. Power Spectrum (Section 4.8)	[123]	“Galactic + Extragal HIGH DM”	[123–137]

1. *Searches that are or will be systematics limited:* for these we cannot expect to improve the sensitivity dramatically. We do expect that the sensitivity will improve as our knowledge of the  $\gamma$ -ray sky and the astrophysical backgrounds improve, but these improvements are likely to be incremental.
2. *Searches that are background limited:* here we can expect the sensitivity to improve as  $\sqrt{t}$ . As the mission continues, the relative gain in sensitivity from these searches is moderate. Doubling the current data set would result in a good, but not overwhelming,  $\sim 40\%$  improvement in sensitivity for these searches.
3. *Searches that are signal limited:* here we can expect the sensitivity to improve proportionately with time. These are the searches that constitute the strongest case for continued data taking.

For many of the targets that we will discuss, the searches are for a small signal against a large background. For those cases the largest and most problematic systematic uncertainties come for mis-modeling the background in a way that would induce a fake signal or mask a real signal. Typically such uncertainties will scale roughly linearly with the background. We have developed and applied a technique for DM searches with significant systematic uncertainties, namely calculating the “effective background”  $b_{\text{eff}}$  (i.e., the background weighted by how strongly it overlaps with the signal) for the search [58,138,139]. We estimate systematic uncertainties by positing that they can be expressed as a fraction of  $b_{\text{eff}}$ , i.e.,  $f = n_{\text{sig}}/b_{\text{eff}}$  and measuring the observed signal in control regions, where no DM signal should be present. This effective background methodology is discussed in more detail in Appendix F and in Refs. [140–143].

The statistical uncertainties on the number of counts assigned to a signal arising from fluctuation in the background are expected to be roughly  $\delta n_{\text{sig}} = b_{\text{eff}}^{1/2}$ . To include the effect of systematic uncertainties we estimate the total uncertainty of the signal as a fraction of the effective background added in quadrature with the statistical uncertainty:  $\delta n_{\text{sig}} = f_{\text{syst}} b_{\text{eff}} \oplus b_{\text{eff}}^{1/2}$ . The value of  $f_{\text{syst}}$  depends on the analysis (and ranges from 0.015 [139] to 0.05 [138]) and for each analysis we estimate it with the judicious use of control samples in the flight data.

Given the observed range of  $f_{\text{syst}}$ , we can roughly state that we expect searches to be systematics limited when  $b_{\text{eff}} \gtrsim 2000$  ph, background limited when  $2000 \text{ ph} \gtrsim b_{\text{eff}} \gtrsim 50$  ph and signal limited when  $b_{\text{eff}} \lesssim 50$  ph. The ranges are shown in comparison with values of  $b_{\text{eff}}$  as a function of  $m_\chi$  for the  $b\bar{b}$  channel in Fig. 10.

The main difference when considering DM decay, as opposed to annihilation, is that  $\gamma$ -ray emission is less concentrated spatially since it scales as the DM density  $\rho$  instead of  $\rho^2$ . This will change the relative powers of different search targets, reducing the impact of very high densities in the cores of DM halos. In terms of the scaling behavior with additional data, targets that are larger than the LAT angular resolution (such as the Galactic Halo or local clusters of galaxies) will have larger

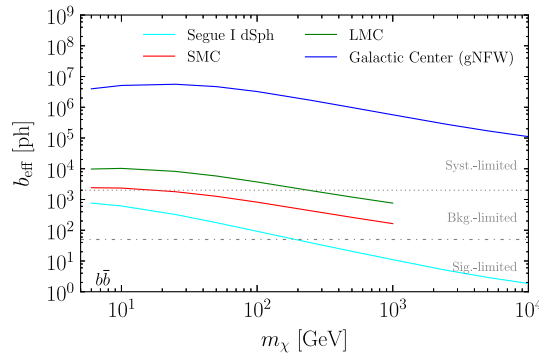


**Fig. 10.** Effective background for six years of P8R2\_SOURCE data, as a function of  $m_\chi$  for the  $b\bar{b}$  channel, for four DM search targets with different angular scales and astrophysical backgrounds: the Galactic center (Section 4.4) the Large and Small Magellanic clouds (Section 4.5) and the Segue I dwarf galaxy. Also shown are the approximate cross-over levels between different search sensitivity limiting factors.

$b_{\text{eff}}$ . Conversely, targets smaller than the LAT angular resolution, such as the dSphs or unidentified satellites will have the same  $b_{\text{eff}}$ , and hence the same scaling behavior.

#### 4.4. The Milky Way Galactic halo

The halo of our own Milky Way is by far the brightest potential source of LAT-detectable  $\gamma$  rays from DM particle interactions. However, as we discussed in Section 3, DM searches targeting the Milky Way halo must contend with large backgrounds from standard astrophysical processes in the Milky Way.

Although  $N$ -body simulations lead to the expectation that DM halos of galaxies exhibit some degree of triaxiality and sub-structure (see [143] and references therein), the Milky Way's DM distribution is generally assumed to be approximately spherically symmetric, with the density a function of only the distance from the Galactic center,  $r$ . As discussed above, in this paper we consider a generalized NFW profile for the radial density profile of the DM (Eq. (A.1)). When considering the Milky Way, we adopt a scale radius of  $r_{\text{rms}} = 20$  kpc, and select  $\rho_0$  such that the local DM density (at 8.5 kpc from the Galactic center) is  $0.4 \text{ GeV cm}^{-3}$ , consistent with dynamical constraints (e.g., [33–35]). Note, however, that the actual DM density profile in the inner galaxy (e.g., [32,144,145]), and the local density (e.g., [31,146–149]) are the subjects of vigorous debate.

DM-only simulations generally favor inner slopes near the canonical NFW value ( $\gamma = 1$ ) [150,151], although baryonic effects are expected to have a non-negligible impact on the DM distribution within the inner  $\sim 10$  kpc of the Milky Way [152–155]. The magnitude of such effects, however, is currently uncertain. With this in mind, we consider different DM radial profiles when estimating the sensitivity of searches for DM signals from the Galactic halo. The radial profiles of both the density and the integrated  $J$  factors for several density profiles were shown in Fig. 1 in Section 2.1.1.

##### 4.4.1. Galactic halo: Status of current searches

Several groups have reported an excess of  $\gamma$  rays in the 1–10 GeV energy range from the region of the Galactic center with respect to expectations based on cataloged point sources and detailed models predicting the Galactic diffuse  $\gamma$ -ray emission (see, e.g., [2–4]).

Although the existence and spatial extension of the excess have been found to be robust against uncertainties of modeling the Galactic diffuse  $\gamma$ -ray emission, the measured spectrum of the excess has been shown to depend strongly on the Galactic diffuse emission model [67,67,81,84,85]. Fig. 11 shows four different fitted spectra that are extracted with for different representative Galactic diffuse emission models.

The bright, structured and relatively uncertain astrophysical fore/backgrounds toward the Galactic center complicate the interpretation of the excess. Some authors have argued that the excess is consistent with DM, and that other interpretations are disfavored (e.g., [3,72,75]). Others have pointed out that the spectrum of the excess is very similar to spectra observed from pulsars and argued that the excess is more likely attributable to a large population of either young pulsars [73] or older millisecond pulsars [71,74,156–159] near the Galactic center. In particular, several analyses of the spatial fluctuations of the  $\gamma$ -ray emission within the Galactic center excess found that they are more consistent with arising from a population of unresolved sources (such as pulsars) than from a smooth distribution (as might be expected for DM) [74,158,159]. To summarize, in the LAT energy band, the  $\gamma$ -ray spectrum expected from a population of pulsars is very similar to the  $\gamma$ -ray spectrum expected from 50 GeV DM annihilating to  $b\bar{b}$ , and additional data, either relating to the spatial distribution of the signal, observations in other energy bands, or  $\gamma$ -ray observations of other targets are required to clarify the interpretation of the excess.

The morphology of the excess has also been studied in detail and found to be consistent with spherical symmetry, in particular an NFW profile with an inner slope of  $\gamma = 1.2$  [3,4,81]. Refs. [160,161] compared this to  $N$ -body simulations of Milky Way-like structures and found it to be broadly consistent with expectations, though somewhat more peaked than the simulations in the innermost  $\sim 2^\circ$ , see Fig. 12.



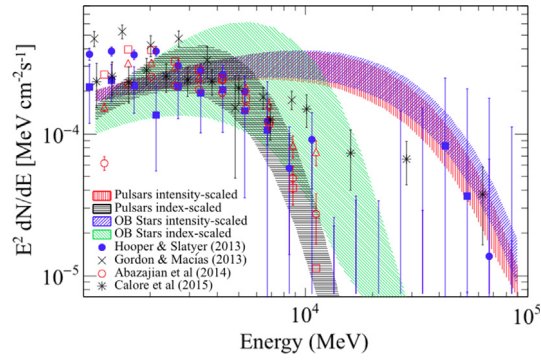


**Fig. 11.** Spectrum of the Galactic center excess in the inner  $15^\circ \times 15^\circ$  region obtained with four different models of the Galactic diffuse emission compared with spectra obtained from other published analyses based on still-different models of the Galactic diffuse emission.

Source: This figure is from Ref. [67] (reproduced by permission of the AAS); see that reference for additional details about the Galactic emission diffuse models and fitting.

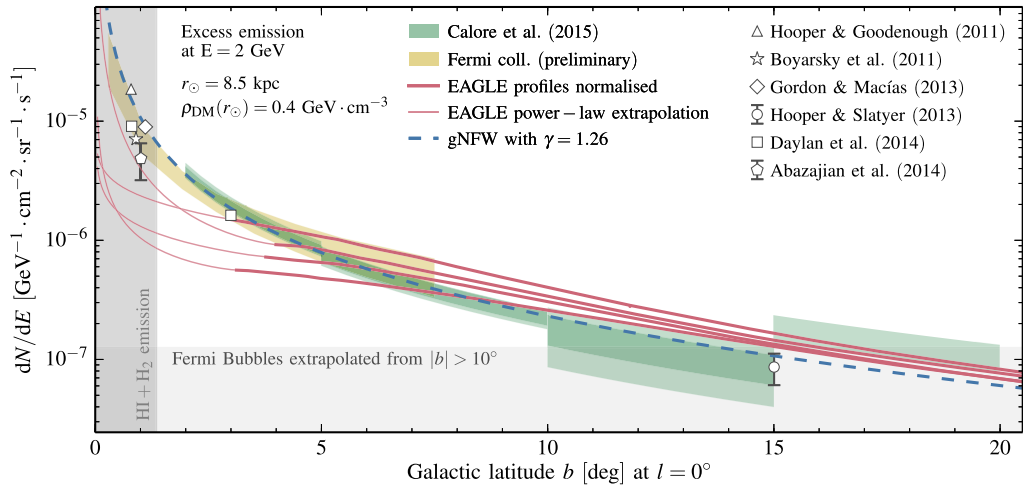


**Fig. 12.** Measurements of the radial profile of the Galactic center excess (markers and bands) compared with predictions of hydrodynamical and  $N$ -body simulations of Milky Way-like structures (red lines).

Source: This figure is from Ref. [160] (reproduced by permission of the AAS); see that reference for additional details.

Finally, the best-fit cross-section and mass range for a DM interpretation of the Galactic center excess is in mild tension with the current limits from a joint analysis of several Milky Way satellite dwarf galaxies (see Section 4.5).

#### 4.4.2. Galactic halo: Sensitivity projections

Although the DM signal from the Galactic center would be much larger than for any other target, the astrophysical backgrounds are also very large and imperfectly known toward the Galactic center. Furthermore, it is important to distinguish between measuring an excess with respect to models of  $\gamma$ -ray emission from predicted cosmic-ray populations interacting with estimated dust, gas and radiation field, and being able to interpret that excess as a clear signal of DM. Accordingly, we can expect systematic uncertainties in modeling the Galactic fore/background to significantly limit the sensitivity of searches for DM signals from the Galactic center. Furthermore, as described above, a population of unresolved pulsars in the inner Galaxy would be a difficult-to-reduce background for the best-fit DM models.

Therefore, in projecting the search sensitivity we account for such systematic limitations. The  $b_{\text{eff}}$  (in counts) for several radial profiles are shown in Fig. 13.<sup>2</sup>

Fig. 14 shows the expected upper-limit bands for the statistical errors-only case as well as for indicative values of  $f_{\text{sys}}$  (0.01 and 0.1).

Fits for DM-like excesses in a scan of positions along the Galactic plane but away from the Galactic center (i.e., where one does not expect signals from DM) find several other locations along the plane with putative signals similar in size to the Galactic center excess (see, e.g., Fig. 11 of [66]). From a scan along the Galactic plane in  $10^\circ$  steps with 6 years of P8R2\_CLEAN

<sup>2</sup> Fig. 13 was made using the “binned model map simulations” for the diffuse Galactic and isotropic background components, together with the “all-sky photon simulations” of the cataloged point sources as described in Appendix D.

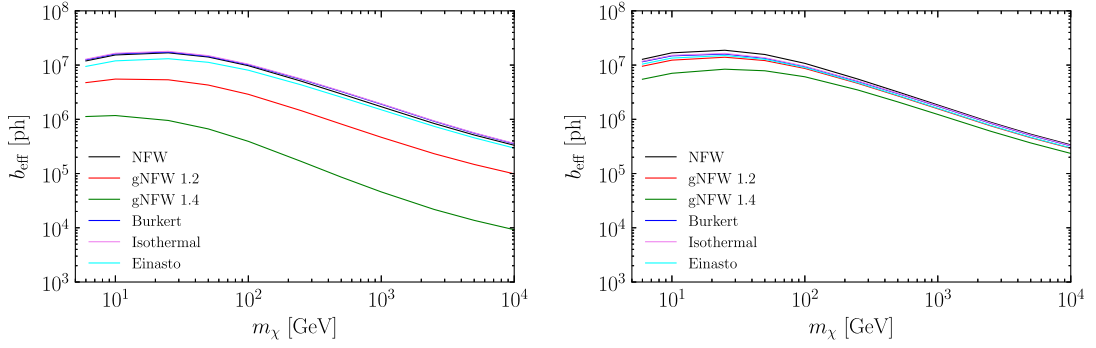


**Fig. 13.** Estimated  $b_{\text{eff}}$  for several DM radial profiles, for a  $60^\circ \times 60^\circ$  area centered on the Galactic center for 15 years of P8R2\_SOURCE data. The plot shows the total integrated  $b_{\text{eff}}$  for annihilations to  $b\bar{b}$  as a function of the WIMP mass,  $m_\chi$ . The left-hand plot includes all Galactic latitudes  $|b| < 30^\circ$ , the right-hand plot excludes the Galactic plane ( $|b| < 2^\circ$ ).

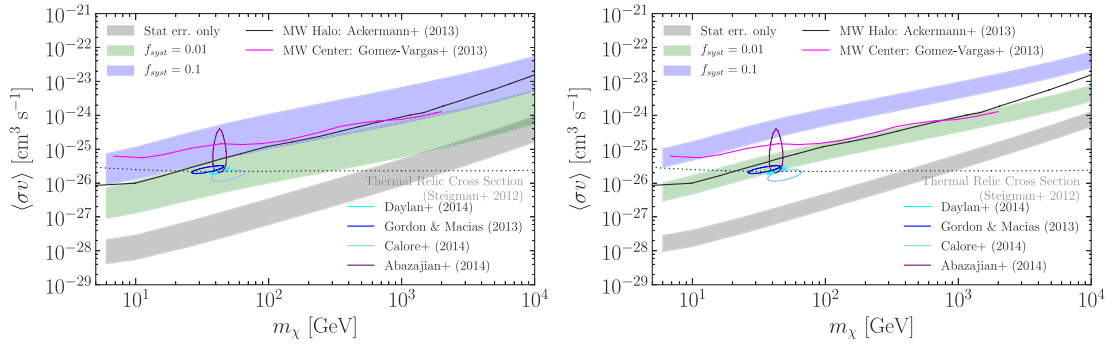


**Fig. 14.** Projected limits for 15 years of P8R2\_SOURCE data, for annihilations to  $b\bar{b}$  as a function of the WIMP mass,  $m_\chi$ , when various levels of systematic uncertainty are included. The extrema of the color bands give the projected limits for the NFW and gNFW with  $\gamma = 1.2$  radial profiles for a given level of systematic uncertainty. The left plot includes all Galactic latitudes  $|b| < 30^\circ$ , the right plot excludes the Galactic plane ( $|b| < 2^\circ$ ). The ellipses and cross indicate the best-fit region obtained if the Galactic center excess is interpreted as a DM signal. (For interpretation of the references to colour in this figure legend, the reader is referred to the web version of this article.)

data we estimate that the systematic uncertainties are of the order of  $f_{\text{syst}} = 0.02$ , though they depend somewhat on energy and can reach  $f_{\text{syst}} \sim 0.06$ . The fore/backgrounds are much brighter within a few degrees of the Galactic plane, and some authors (e.g., [466,81]) have chosen to mask the plane and confine the analysis to  $|b| > 2^\circ$ , reducing both the signal and the systematic uncertainties of the fore/background modeling.

It is difficult to estimate how our understanding and modeling of the fore/backgrounds will evolve, or our ability to rule out other contributors such as pulsars. However, as shown in Fig. 14, even if the modeling uncertainties can be reduced to  $f_{\text{syst}} = 0.01$  the interpretation of the nature of the Galactic center excess will be limited by systematic uncertainties of the background modeling. Thus, we believe that definitively confirming or ruling out a DM interpretation of the Galactic center excess will require inputs from searches of other DM targets or from other multi-wavelength data. In particular, if the Galactic center excess is due to unresolved emission from pulsars, then additional LAT data should resolve some of those sources robustly and provide targets for dedicated radio pulsation searches. If fact, arguments against pulsar interpretations have relied on the non-observation of many pulsars in the Galactic center region in the LAT data [72,75,162].

#### 4.5. Known satellites of the Milky Way

Many DM subhalos have been discovered from optical surveys and follow-up spectroscopy as dark-matter-dominated dwarf spheroidal galaxies (dSphs) residing within the DM halo of our own Galaxy. The known dSphs have dynamical masses ranging from  $\sim 10^5$  to  $10^8 M_\odot$  and stellar half-light radii between 0.02 and 0.7 kpc [163].

The known dSphs are identified as collections of old, metal-poor stars, kinematic analyses of which reveals a binding DM halo up to a thousand times more massive than the stars themselves. Multi-wavelength observations show that the objects contain little besides stars and DM [164–166]. Without the requisite gas or cosmic-ray content, dSphs have no conventional mechanism for producing  $\gamma$  rays. This means that any DM signal originating from dSphs must contend only with the diffuse  $\gamma$ -ray background. As dSphs are primarily found far from the Galactic plane, the background intensity is often low and spectrally featureless.

Fitting the NFW density profile to the stellar velocity dispersions observed in the nearest dSphs yields  $J$  factors on the order of  $10^{19} \text{ GeV}^2 \text{ cm}^{-5}$ . These values are fairly robust; they are insensitive to both the shape of the inner density profile and

the level of substructure within the dSph. However, for particular dSphs different authors have found a range of estimated  $J$  factors that are larger than the quoted uncertainties of the individual studies, suggesting that the measurements are potentially impacted by systematic biases (see, e.g., [167–170]).

Although each individual  $J$  factor is smaller than that of the Galactic center, kinematically determined  $J$  factors are known for 19 dSphs, so far. The predicted annihilation signal from the population of dSphs is commensurately higher, and analyzing dSphs as a group results in sensitivity competitive with other targets. Furthermore, systematic disagreements of uncertainties of the  $J$  factors are peculiar to individual dSphs, rather than systematic across the set of dSphs. Decreasing the  $J$  factor of a single dSph, or increasing the uncertainty of that  $J$  factor, will lessen the impact of that dSph on the joint analysis, but will not greatly affect the overall result. The effect of the uncertainties in  $J$  factors in a joint likelihood analysis was studied in detail in Ref. [5] (see in particular Fig. 7), and the overall limits changed by less than 40% for all of the scenarios considered.

#### 4.5.1. Known satellites: Current status

Since early in the *Fermi* mission, dSph analyses have provided cutting-edge constraints on  $\langle\sigma v\rangle$  [89–92,94,171]. Upper limits using the new Pass 8 data set are some of the most constraining to date, ruling out WIMPs with masses below 100 GeV that annihilate through quark or  $\tau$ -lepton channels at the thermal relic cross section [5]. These limits are in mild tension with the masses and cross-sections best-fit for DM interpretations of the Galactic center excess (Section 4.4), and provide an essential cross-check for those claims.

In addition to the accumulation of  $\gamma$ -ray data, dSph searches for DM are now benefiting from a rapid increase in the number of known dSphs. Until recently, ultra-faint dSphs (those with luminosities  $\lesssim 5 \times 10^4 L_\odot$ ) had only been discovered by the Sloan Digital Sky Survey (SDSS), which primarily covered the northern hemisphere [172]. Over the past two years, the Dark Energy Survey (DES) [173] has begun to explore the southern hemisphere, discovering 17 new dSph candidates [174–177]. Over roughly the same time period, the PanSTARRS survey [178] contributed an additional 3 dSph candidates [179,180]. Two more candidates were also discovered in other optical surveys. If all of these are confirmed as dSphs with spectroscopic data, these surveys will have more than doubled the size of the ultra-faint dSph population. Indeed, Ref. [181] consider 28 kinematically confirmed dSphs galaxies, 13 candidates that are likely to be dSphs (based on their optical properties), and 4 systems that may be either dSphs or globular clusters. The initial DES discoveries were promptly investigated for  $\gamma$ -ray emission [86,93,169], and yield results consistent with the previous studies of dSphs. A projection of combined dSph sensitivity, including the future accumulation of both data and targets is discussed in Section 4.5.2.

Finally, searches have also targeted other DM-rich Milky Way satellites and structures, including the Large Magellanic Cloud (LMC, [138]), the Small Magellanic Cloud (SMC, [182]) and the Smith high-velocity cloud [183]. However, these targets are spatially extended, and in the cases of the LMC and SMC have significant astrophysical  $\gamma$ -ray emission. Therefore these searches are limited by the systematic uncertainties of the background modeling.

#### 4.5.2. Known satellites: Sensitivity projections

In the light of the active DES and PanSTARRS large-area optical surveys and the upcoming LSST survey [184], any projection of future dSph DM search sensitivity must include an estimate of an expanded set of targets. After two years (out of five) of operation, DES has contributed several new likely dSph candidates [174–177], including a few that have already been confirmed as dSphs with spectroscopic followups [86,169].

Predictions about the number and  $J$  factor distribution of undiscovered dSphs are very uncertain. In particular, the faint end of the dwarf galaxy luminosity function, the structural properties (and DM distributions) of the smallest satellites, and the radial distribution of subhalos that would host dSphs are not well known.

The SDSS survey covered roughly 1/3 of the sky and discovered 15 ultra-faint dSphs; DES, PanSTARRS, and in particular LSST, will cover complementary regions of the sky to significantly great depth. Combining the distribution of optical luminosities of known dSphs with  $N$ -body DM simulations and the expanded depth and sky coverage of the new surveys, we can anticipate 25–40 total dSphs to be discovered by DES, and possibly hundreds by LSST [185,186], however many of these dSphs would be more distant and have correspondingly smaller  $J$  factors. Even so, LSST is still likely to contribute many dSphs with  $J$  factors above  $10^{19} \text{ GeV}^{-2} \text{ cm}^{-5}$ , and is also likely to contribute at least some dSphs with larger  $J$  factors than any discovered by DES [187].

In practice, the distribution of  $J$  factors for the DES dSphs has been similar to previously discovered dSphs, in spite of the greater depth of the DES survey. This could reflect that the dwarf galaxy luminosity function continues below the faintest objects discovered by SDSS, or it could simply be that the DES survey region has an excess of dSphs, because of the influence of the nearby Magellanic clouds.

We will take 60 total dSphs as a conservative estimate of the total number of dSphs that can be used as targets for LAT searches, i.e., having  $J$  factors that are large enough and well determined enough to contribute the sensitivity of a joint analysis.

As an all-sky monitor, the LAT has already, and will continue to, observe the new targets for the duration of its lifetime. All that is required to incorporate them into a joint analysis are locations and  $J$  factors and their uncertainties. To project the increased sensitivity that will result, we simulated 200 realizations of our entire search using the “ROI-specific photon

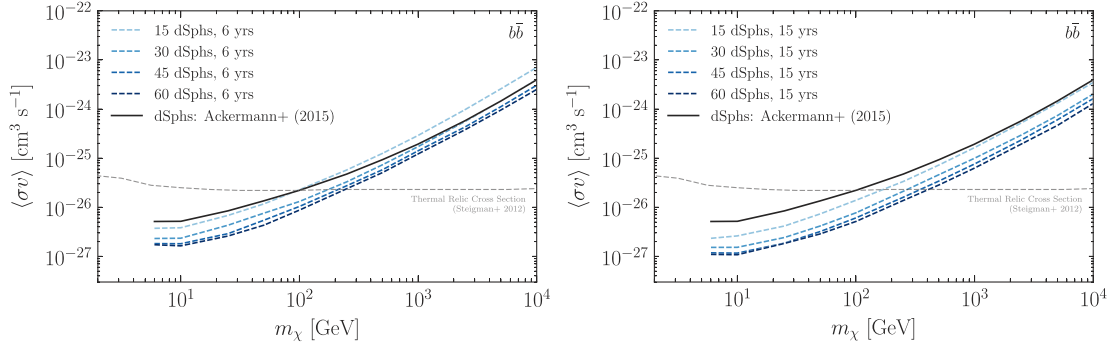


**Fig. 15.** Projected upper limits on the WIMP annihilation cross section from the joint analysis of dSphs as a function of the size of the dSph sample on the assumption of 6- (left) and 15-year (right) data sets with P8R2\_SOURCE data. The solid black curve shows the observed limit from the analysis of 15 known dSphs with 6 years of P8R2\_SOURCE data [5]. Projections correspond to the median expected limit for the given number of dSphs and observation period from 200 simulated realizations of the entire search (see text for details).

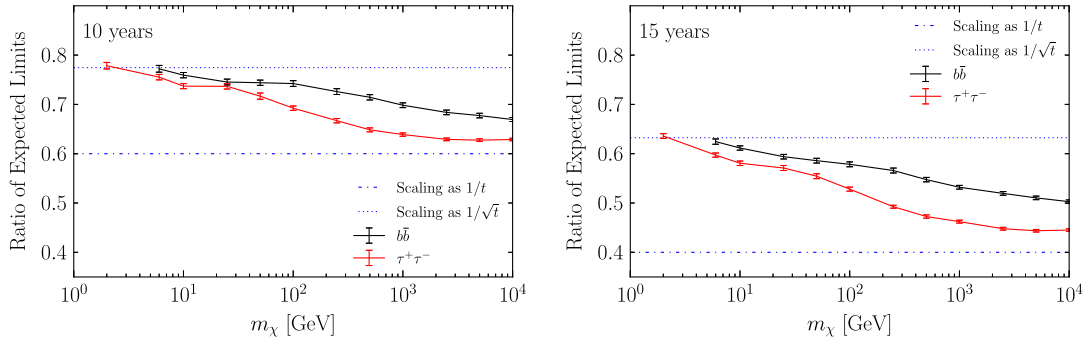


**Fig. 16.** Ratio of the median expected upper limits on the WIMP annihilation cross section for 10 years of LAT data relative to 6 years (left) and 15 years relative to 6 years (right) for the  $b\bar{b}$  and  $\tau^+\tau^-$  annihilation channels. The upper and lower horizontal lines are the expectations for the purely background limited (sensitivity scales as  $\sqrt{t}$ ) and purely signal limited (sensitivity scales linearly with  $t$ ) cases. We use the results for the projected sample of 60 dSphs (see Fig. 15) for these comparisons.

simulations” and “Binned model map simulations” described in Appendix D but duplicated our target set<sup>3</sup> up to three times to reach 60 in total. The effect of additional targets on the search sensitivity is illustrated in Fig. 15.

We also examined how the expected sensitivity scales with time for different masses and annihilation channels. Fig. 16 shows the mean of the ratio of expected limits for all of the simulated dSphs. Because of the softer spectrum in the  $b\bar{b}$  channel, the improvement in that channel is close to the expectation for a background-limited search (i.e., it scales as  $\sqrt{t}$ ) for low masses, improves with increasing mass, but does not reach the linear scaling we would expect for a purely signal limited search. On the other hand, in the harder  $\tau^+\tau^-$  channel, the scaling behavior transitions from the background limited to signal limited cases around 100 GeV.

The slope of the projected upper limit curve near 100 GeV is close to one ( $\sim 1.1$ – $1.2$ )  $\text{cm}^3 \text{s}^{-1}/\text{GeV}$ . The mass for which the thermal relic cross section will be excluded scales as the inverse of the slope times the improvement on the limits on  $\langle\sigma v\rangle$ . This results in considerable extension of the mass range with limits at or below the thermal relic cross section with additional data, up to  $>400$  GeV ( $>200$  GeV) in the  $b\bar{b}$  ( $\tau^+\tau^-$ ) channel with 60 dSphs and 15 years of data, see Fig. 17.

Finally, given that optical surveys will be discovering new targets for years to come, we consider the possibility that they discover a dSph that is near enough and massive enough that it would be clearly observable by the LAT for plausible DM annihilation cross-sections.

The  $J$  factors of known dSphs scale approximately with the square of distance, i.e., the dSphs would have similar  $J$  factors (within about 0.4 dex) if they were all at the same distance:  $J \sim 10^{18.3} \text{ GeV}^2 \text{ cm}^{-5} \times (d/100 \text{ kpc})$ . For a 100 GeV DM particle annihilating to  $b\bar{b}$  at the thermal relic cross section we currently could expect a  $5\sigma$  significance detection of any dSphs following that  $J$  factor scaling relation within  $\sim 8$  kpc and located away from the Galactic plane. That corresponds to a “discovery” volume of  $\sim 2100 \text{ kpc}^3$ . With 15 years of data that volume would at least double to  $\sim 4200 \text{ kpc}^3$ . For higher masses and in the harder  $\tau^+\tau^-$  channel the volume would increase by a factor of four.

<sup>3</sup> The targets were placed at random locations and with  $J$  factors (and  $J$  factor uncertainties) sampled from the posterior distribution.

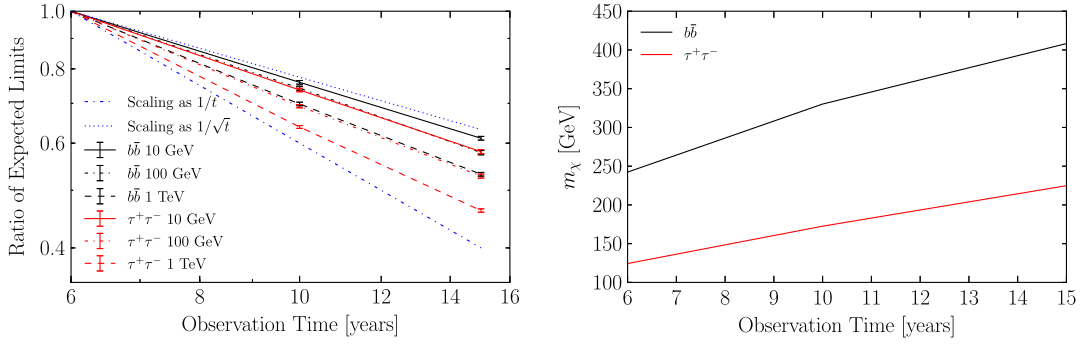


**Fig. 17.** Left: ratio of the median expected upper limits on the WIMP annihilation cross section from 6 years of LAT data as a function of time for 10 GeV, 100 GeV and 1 TeV for the  $b\bar{b}$  and  $\tau^+\tau^-$  channels. Right: upper extent of the mass range over which the thermal relic cross section can be excluded, as a function of observation time, for the  $b\bar{b}$  and  $\tau^+\tau^-$  channels. We use the results for the projected sample of 60 dSphs (see Fig. 15) for these comparisons.

#### 4.6. Undiscovered satellites of the Milky Way

Current simulations of Milky Way-sized halos [151,188] predict the existence of tens of thousands of Galactic DM subhalos. The most massive of these subhalos are expected to host the known dSphs, while the stellar/baryonic component of smaller subhalos may be negligible. In fact, some of these subhalos may completely lack any astrophysical counterparts [189]. Indeed, this leaves the exciting possibility that  $\gamma$  rays from DM annihilation in these as *dark satellites* may be the only way to detect them. Given the typical masses and distances of dark satellites, they may represent excellent targets for DM searches in  $\gamma$  rays, e.g., [88,96–99,190,191].

Since the LAT surveys the entire  $\gamma$ -ray sky with unprecedented sensitivity, it is an ideal instrument for the discovery of new source classes. In fact,  $\sim 1/3$  of the sources in the 3FGL catalog lack firm associations with known counterparts at other wavelengths [53]. Some fraction of the unassociated  $\gamma$ -ray source population may be composed of dark satellites. By comparing the predictions of  $N$ -body cosmological simulations with the observed number of unassociated sources, it is possible to place firm constraints on the DM annihilation cross section. Additionally, if a population of candidate dark satellites is found in  $\gamma$ -ray observations, the findings could be used to target deep optical searches for hyper-faint dwarf galaxies.

##### 4.6.1. Undiscovered satellites: Current status

Several diagnostics have been explored to distinguish a potential population of dark satellites from more conventional astrophysical sources in  $\gamma$ -rays:

1. *Multi-wavelength associations and identified sources:* Dark satellites are not expected to emit in other wavelengths, so cataloged sources with such associations are excluded. Likewise, the detection of pulsations, typically either in  $\gamma$ -ray or radio data, can rule out sources as potential dark satellite.
2. *Temporal variability:* Dark satellites are expected to be steady sources. This distinguishes them from background blazars, which can vary on minute-to-month time scales.
3. *Spatial distribution:* Dark satellites are expected to be nearly isotropically distributed on the sky. Thus, selecting sources at high Galactic latitudes can increase the contrast with respect to a population of Galactic sources, such as young pulsars.
4. *Spatial extension:* Nearby dark satellites may have spatial extensions that are measurable in  $\gamma$  rays. This is unlikely for astrophysical sources at high Galactic latitudes, which are primarily either blazars or millisecond pulsars [192]. When considering DM decay, as opposed to annihilation, the expected extension can be even larger, making spatial extension a stronger discriminant.
5. *Spectral character:* In some cases, further restrictive cuts have been applied, motivated by some of the spectral properties expected from dark satellites (e.g., hard power-law indices, spectral features, detection above 10 GeV, etc.). A population of dark satellites should have a common spectral shape.

Current simulations of Milky Way-sized halos (e.g., Via Lactea II [188] or Aquarius [151]) are unable to simulate the subhalo hierarchy below a mass  $\sim 10^5 M_\odot$ , while the theoretical minimum DM halo mass can be as low as  $10^{-6} M_\odot$  [193–195]. Thus, extrapolations to lower masses are required to assess the contribution of nearby, low-mass subhalos to the potentially detectable dark satellites.

Understanding the number and distribution of DM subhalos is an important step toward their potential discovery. Previous work has begun to address this issue, e.g., [96–98]. The authors of Refs. [99,191] concluded from a search for DM subhalos in the 2FGL catalog [55] that none of the unidentified sources in the catalog is a clear DM candidate. Ref. [99] found that although many faint sources could not be ruled out as DM candidates, among sources with integral fluxes above 1 GeV,  $\Phi_{1\text{ GeV}} > 10^{-9} \text{ cm}^{-2} \text{ s}^{-1}$  (that is, the brightest ones) all but a handful could be ruled out as DM candidates for almost any combination of annihilation channel and  $m_\chi$ . They used this finding in combination with results from the Aquarius simulation on subhalo abundance and internal structure to demonstrate that this technique could be used to obtain competitive limits on  $\langle \sigma v \rangle$ .



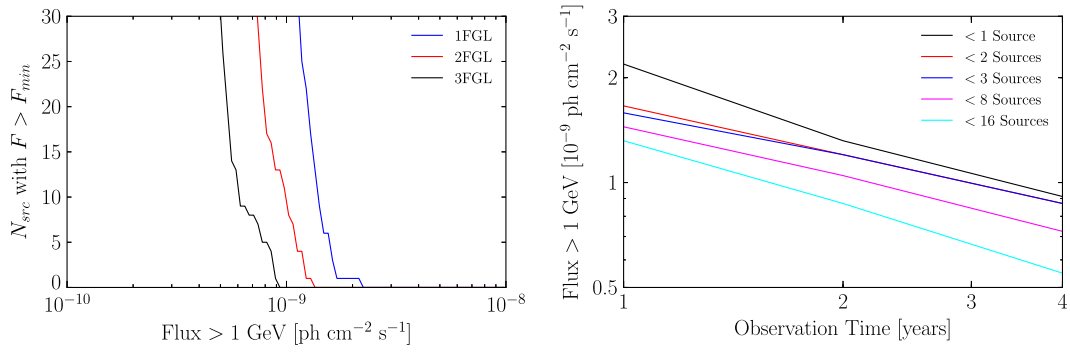


**Fig. 18.** Left: number of potential DM candidate sources in the 1FGL (1 year of LAT data [54]), 2FGL (2 years of data [55]) and 3FGL (4 years of data [53]) catalogs. Right: time-progression of the threshold above which all but  $N_{\text{cand}}$  sources have been excluded as potential DM candidates.

The systematic uncertainties associated with modeling the subhalo population (e.g., different internal structure models, mass functions, radial distributions, sub-substructure) have not been deeply explored. For example, an updated analysis using the 3FGL catalog and a more conservative model to describe the dark satellites' structural properties obtained a factor  $\sim 4$  weaker upper limits on  $\langle \sigma v \rangle$  [95], and in fact identified a set of unassociated catalog sources that is consistent with a DM-interpretation of the Galactic center excess (e.g.,  $\sim 50$  GeV DM annihilation to  $b\bar{b}$ ).

The identification and association of cataloged sources continues after the production of the catalog. In particular, many unassociated LAT sources have been identified as pulsars from radio observations (see e.g., [196] and references therein) and others have been associated with blazars using data from the *WISE* mission and optical spectroscopy [56].

#### 4.6.2. Undiscovered satellites: Sensitivity projections

An extended LAT mission will benefit the search for dark satellites in the following ways:

1. Setting a fainter threshold for source detection. A lower source detection threshold increases the number of faint dark satellites that could be detected as unassociated sources.
2. Providing better localization of sources, which effectively lowers the threshold for source association. The source association procedure assesses the chance false association rate, which scales with the area of the source localization region. Improving the localization reduces this area and hence the chance false association rate, allowing for more associations at a given probability threshold (see, e.g., § 5 of [53] for a discussion of the source association procedure).
3. Providing better spectral characterization of unassociated sources, thus setting a fainter threshold at which highly curved DM-like spectra and power-law spectra can be distinguished.
4. Providing greater sensitivity to spatial extension of unassociated sources.
5. Providing a longer baseline for detecting temporal variability. Temporal variability can be used to associate sources to background blazars, reducing the number of unassociated sources

To project the sensitivity for dark satellite searches, we have performed a study based on Refs. [99] and [95], which examine the unassociated sources for potential DM candidates. To do this we started with all of the sources in each of the LAT published point source catalogs and applied a few simple criteria:

1. We excluded all associated sources.
2. We excluded all sources within  $20^\circ$  of the Galactic plane. This criterion was applied because the source detection threshold is much higher in the plane than at higher Galactic latitudes.
3. We excluded variable sources; specifically we exclude sources with a variability index  $h > 80$ , following [99].
4. Finally, we excluded high-significance sources, i.e., those that were detected with  $TS > 100$ ; the better characterization of these sources makes it much easier to identify multi-wavelength counterparts and to distinguish astrophysical sources from potential dark satellites.

In Fig. 18 we show that each of the LAT source catalogs has an “exclusion threshold” above which very few (i.e.,  $N_{\text{cand}} \lesssim 20$ ) catalog sources pass the above criteria to be viable dark satellite candidates. The right panel of Fig. 18 also indicates that for a given  $N_{\text{cand}}$  the effective threshold scales roughly as  $\sqrt{t}$ .

We can then use estimates of the expected flux distribution of dark satellites from  $N$ -body simulations of Galactic structure. Following Refs. [95] we have adopted the relationship for  $N_{\text{cand}}$  with integral flux above 1 GeV,  $I_{1\text{GeV}}$ , greater than a threshold sensitivity  $S$ :

$$N_{\text{cand}}(S) = \left( \frac{S_0}{S} \right)^{1.5} \frac{\langle \sigma v \rangle}{\langle \sigma v \rangle_0}, \quad (8)$$

where the scaling factors are  $S_0 = 9.83 \times 10^{13} \text{ ph cm}^{-2} \text{ s}^{-1}$  and  $\langle \sigma v \rangle_0 = 6.23 \times 10^{-27} \text{ cm}^3 \text{ s}^{-1}$ .



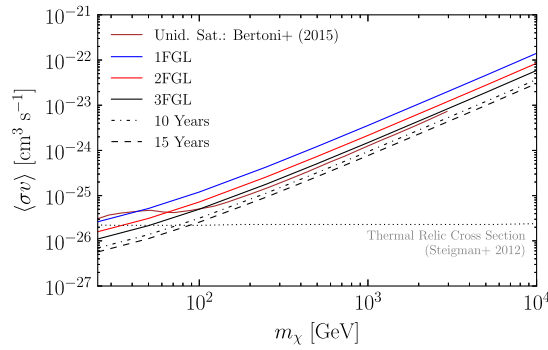


**Fig. 19.** Projected upper limits derived from considering the expected number of dark satellite candidates  $N_{\text{cand}}$  in LAT sources catalogs as a function of  $\langle\sigma v\rangle$ . The extrapolations to 10 and 15 years are based on an assumed  $\sqrt{t}$  scaling of exclusion threshold for  $N_{\text{cand}} < 1$  of the 3FGL shown in Fig. 18.

Using the relationship from Eq. (8) we can project the 95% CL upper limits by solving for the value of  $\langle\sigma v\rangle$  for which  $N_{\text{cand}} > 3$  but no candidates are observed. The results are shown in Fig. 19. We expect this search to be sensitive to annihilation at the thermal relic cross section for masses up to 100 GeV in the  $b\bar{b}$  channel.

#### 4.7. Galaxy clusters

The study of DM in galaxy clusters has a long history, dating back to the first evidence of DM found by F. Zwicky [11]. The systematic uncertainty in the determination of DM density profiles and  $J$  factors in clusters is similar in many ways to the case of dSphs discussed above. The dominant uncertainty in the  $J$  factors for clusters arises from two orthogonal astrophysical considerations. First, the empirically-measured cluster mass profiles, which are derived from a combination of X-ray temperature profiles and gas kinematics, e.g., [197], are uncertain. Second, the predicted  $\gamma$ -ray luminosity that arises from the contribution of DM substructure in the clusters is also uncertain. The role of DM substructure (or subhalos) for the total DM annihilation flux can be conveniently expressed in terms of a boost factor  $b$ . Determining values for  $b$  requires assumptions on the relative abundance of subhalos and of their structural properties. These assumptions are usually inspired by the results from  $N$ -body cosmological simulations. However, even the highest-resolution current simulations fail to resolve the whole subhalo hierarchy. For cluster-sized simulations, this mass resolution limit is  $\sim 10^8 M_\odot$  [198,199], as compared to the smallest subhalos, which may have masses as low as  $10^{-6} M_\odot$  [193–195]. Estimates of the boost to the DM annihilation signal due to subhalos is thus dependent on extrapolations over several orders of magnitude [200].

Another challenge to searching for  $\gamma$  rays from DM interactions in galaxy clusters is that clusters are believed to host relativistic particle populations, most notably cosmic-ray electrons, but possibly protons as well [201]. As such,  $\gamma$  rays may arise from astrophysical processes in the intra-cluster medium (ICM).

##### 4.7.1. Galaxy clusters: Current status

Historically, X-ray observations have been pivotal for the selection of cluster samples. More specifically, the HIFLUCGS catalog [202] has been the basis for several recent analyses. The catalog contains a complete flux-limited sample of the brightest X-ray clusters at low redshift  $z \leq 0.2$ . In most cases, the  $\gamma$ -ray analyses have considered either a subset of the most nearby, most massive clusters (e.g., Coma, Fornax or the Virgo cluster [101–107]) or targeted entire samples [108,203]. The Perseus cluster is another well-motivated target but due to the presence of two bright Active Galactic Nuclei (AGN) in the cluster along with its proximity to the Galactic plane, this target is probably better suited for Cerenkov telescopes [204,205]. At present no cluster-wide emission has been detected in  $\gamma$  rays.<sup>4</sup>

In sample studies, a stacking analysis is often used to reach a greater sensitivity [102,104,108,208–211]. For example, joint likelihood fitting of the sample may provide a factor of 2–3 improvement with respect to the case for which only the cluster with the highest  $J$  factor was used in the analysis [102,212].

One challenge when analyzing nearby galaxy clusters is that both their predicted non-thermal and DM-induced  $\gamma$ -ray emissions are expected to be spatially extended (up to  $\sim 3^\circ$  if the nearest cluster, Virgo, is excluded.<sup>5</sup>) At the same time clusters host AGN. While significant point-like flux can be expected from the central AGN in a cluster, searches have only yielded upper limits [211,213]. A sub-threshold AGN residing in a cluster would manifest itself as diffuse  $\gamma$  ray emission with characteristics similar to that expected from the ICM (e.g., a power-law spectrum with  $\Gamma = 2.3$  or softer). This would result in an additional foreground emission, predominantly toward the center of the cluster, where the DM emission also peaks. However, the DM annihilation flux profile is expected to be shallower and more extended than the non-thermal emission

<sup>4</sup> This is with the exception of a reported excess from Virgo [100,206,207]. However, the recent analysis in [100] indicated that this excess is likely associated with unmodeled Galactic diffuse emission and/or a combination of weak point sources.

<sup>5</sup> The Virgo cluster has a spatial extent of  $\sim 14^\circ$  and analyzing the surrounding region in the sky presents a number of challenges [100].

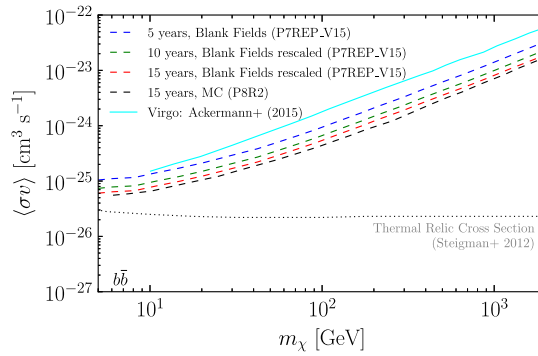


**Fig. 20.** Projected upper limits on the WIMP annihilation cross section from a joint analysis of 32 nearby galaxy clusters as a function of DM mass for DM annihilating into  $b\bar{b}$ . The colored dashed lines correspond to rescaling of the obtained median sensitivity from an analysis of blank fields using Pass 7REP data [215], while the black dashed line corresponds to the expected median sensitivity based on simulations of the  $\gamma$ -ray sky. The limits obtained from the Virgo galaxy cluster in [100] are also shown for comparison. (For interpretation of the references to colour in this figure legend, the reader is referred to the web version of this article.)

profile once DM substructures are taken into account [214]. Hence, the cluster outskirts may be an attractive possibility for DM searches.

#### 4.7.2. Galaxy clusters: Sensitivity projections

For our sensitivity projections we consider a set of 32 clusters, chosen from the HIFLUGCS catalog, maximizing the total  $J$  factor of all targets and minimizing potential overlap between nearby clusters.<sup>6</sup> Spatially, each cluster is modeled under the assumption of an NFW DM density profile. We include DM subhalos down to  $10^{-6}M_\odot$ . For the description of the subhalos (and consequently of the subhalo boost,  $b$ ), we follow the recent work [200], which predicts a flattening of the halo concentration parameter for the smallest halo masses, and consequently, moderate  $b \sim 30$ –40 for galaxy clusters. We adopt the same approach as for the dSphs (see Section 4.5.2), and use the “ROI-specific photon simulations” described in Appendix D. Fig. 20 shows the effect of continued data taking on the upper limits to the DM annihilation cross section. These projections were made by rescaling the projected sensitivity calculated in Ref. [210] by the  $\sqrt{t}$  and accounting for the improved sensitivity with Pass 8 data. Overall, the limits improve by a factor  $\sim 2$  over the whole WIMP mass range considered.

### 4.8. Cosmological WIMP searches

The discussion above has focused on DM annihilation in the Milky Way, Milky Way satellites and galaxy clusters. Searches for DM signals in  $\gamma$ -ray data are also sensitive to the accumulated emission from DM annihilation in all the DM halos that have formed in the Universe [76]. Though this emission is “unresolved”, it can be modeled given a mass function for DM halos and a description of the DM halo structural properties. The latter is usually made by assuming a universal form for the DM density profile, e.g., NFW [141] or Einasto [216] (see also Appendix A). As for the halo mass function, in principle, it could be deduced from the observed luminosity function of galaxies. However, this method is hindered by the current uncertainties in the mapping of galaxy luminosity to DM halo mass. A more robust understanding of the DM halo mass function and its redshift evolution comes from  $N$ -body cosmological simulations [217,218]. Two of the largest-volume cosmological simulations to date, e.g., provide a statistically-complete sample of DM halos down to a maximum circular velocity of about 50 km/s, or a mass of approximately  $10^9 M_\odot$  [219,220]. Based on these and previous  $N$ -body simulation results, different functional forms for the halo mass function and its redshift dependence have been proposed in recent years, e.g., [221,222]. The integrated DM annihilation signal from all halos at all cosmic epochs can then be predicted by combining the information on the halo mass function and the DM density profile of individual halos.

#### 4.8.1. Searches for contributions to the IGRB spectrum: Current status

A possible way to find cosmological DM signatures is by searching for features in the IGRB spectrum [109–111,223–225]. The statistics are good but this method is nonetheless limited by the large systematic uncertainties on the reconstructed IGRB related to the uncertainty of the Galactic diffuse emission (which is a strong foreground to the IGRB). At present these dominate the statistical uncertainties over the entire energy range (see Fig. 7 in Ref. [64] and Appendix A in Ref. [111]). Known astrophysical source populations contributing to the IGRB typically can be modeled starting from the resolved component of the population present in the EGB, or from observations at other wavelengths (radio, IR, X-ray). From

<sup>6</sup> In our analysis we also consider each of the 106 HIFLUGCS clusters as an isolated system. Given the broad point-spread function at the lowest energies, overlaps may occur between neighboring targets, which would introduce a potential bias in a joint analysis [210].

these models, blazars, star-forming galaxies, and radio galaxies are found to be the main contributors, and altogether can make up the total of the measured IGRB intensity although with large uncertainties [77]. DM constraints then can be obtained by comparing the expected cosmological DM signal with the IGRB residual spectrum after subtracting the expected astrophysical contribution, e.g. [77,109–111].

Interestingly, studying the contributions to the IGRB can also shed light on an entirely different class of DM candidate: evaporating primordial black-holes (PBHs, see [226] for a review). The strongest limits on the density of PBHs, in the mass range from  $10^{14}$  to  $10^{16}$  g, come from studies of diffuse  $\gamma$ -ray emission [226–228].

#### 4.8.2. Searches for contributions to the IGRB spectrum: Sensitivity projections

Currently, the dominant uncertainties in the derivation of DM limits from the IGRB energy spectrum are from the large uncertainties associated with the modeling of the Galactic foregrounds [111]. Thus, any IGRB-based DM sensitivity projections will largely depend on how these foregrounds will be understood in the future. However, it is difficult to predict how knowledge of the Galactic diffuse emission will improve in the next few years. For this reason, we considered two scenarios, for which the systematic uncertainties from modeling the Galactic diffuse emission are reduced to 50% and 10% of their current value.

On the other hand, as explained in Section 4.8.1, the majority of the IGRB flux arises from the  $\gamma$ -ray emission of unresolved AGN and star-forming galaxies. Thus, the projected sensitivity of the LAT to extragalactic DM will also depend on the uncertainties in the contribution of (unresolved) point sources to the IGRB. We discuss in detail the evolution of these uncertainties in Appendix G.

Fig. 21 shows the projected upper limits on the DM annihilation cross-section in the  $b\bar{b}$  annihilation channel, evaluated using the same method that was employed in [77]. The estimates and uncertainties of the contributions of different source populations to the IGRB after 15 years of data (“optimized astro” in the figure) are described in Appendix G. We have assumed a reduction of a factor 2 for the size of the statistical errors in the IGRB measurement, based on what is expected from both this larger data set and from the increased LAT acceptance in Pass 8 (see Appendix C for details). In addition, two cases are shown in Fig. 21, corresponding to different assumptions on the future evolution of the systematic errors: a first case in which they will be reduced by a factor 2 with respect to their current values (blue dashed line), and a second, more optimistic case in which a very good control on the systematics has been achieved down to a value of 10% of the present level (red dot-dashed line). For both cases we have the same level of theoretical uncertainties on the strength of the DM annihilation signal (represented by the red shaded region in Fig. 21) as the one derived in [111] for the current DM limits. This is conservative, as future  $N$ -body cosmological simulations with higher particle resolution should help in lowering the main source of these uncertainties, namely the structural properties of low-mass DM halos and subhalos and the exact slope of the subhalo mass function (see, e.g., [199,229] for recent and promising developments). It is however difficult to estimate the evolution of these uncertainties at the moment.

In both cases, it can be seen in Fig. 21 that there is significant improvement of the current DM limits (solid line) over the whole WIMP mass range considered. The improvement is about a factor 2 for the case in which the systematics errors are half of the current ones, and ranges between a factor  $\sim 2$  to 5 for the case of having systematics reduced down to 10% the present values, depending on the WIMP mass. Also, as expected, reducing the systematics uncertainties has a larger impact on the DM sensitivity at low WIMP masses, while increased statistics primarily improves the sensitivity at higher masses.

#### 4.8.3. IGRB anisotropies and cross-correlation measurements: Current status

Integrating the IGRB over the entire sky results in a large loss of information. More information can be recovered and exploited by investigating the anisotropy properties of the measured IGRB. Three measures of anisotropy currently are being studied: (i) the auto-correlation or angular power spectrum (APS) of the IGRB [60,123,123–137], (ii) the cross-correlation with Large Scale Structure (LSS) tracers (galaxy catalogs and lensing surveys) [61,112–122], and (iii) pixel fluctuations (also referred to as one-point statistics) [158,159,230–234].

Relative to spectral analyses, auto-correlation analyses possess the advantage that the background is dominated by astrophysical point sources just below the detection threshold. Thus, masking/removing newly detected point sources greatly reduces the astrophysical background and enhances the DM sensitivity. For example, the anisotropy of the high-latitude  $\gamma$ -ray sky is reduced by about four orders of magnitude when the 3FGL sources are masked with respect to the case in which they are not. In comparison, the intensity of the IGRB when masking the 3FGL sources is reduced by only 20%–30% over most of the energy range (it can be 50%–80% above 100 GeV). Clearly, using a deeper point-source catalog available with many years of data taking can substantially improve the sensitivity to DM via auto-correlation. The auto-correlation of the IGRB was first measured in [60] using 2 years of LAT data. Constraints on DM were derived in [123,131,137]. As with the IGRB energy spectrum (Section 4.8.2), these constraints account for the expected contributions from astrophysical sources and their uncertainties. The expected astrophysical contribution to the APS is dominated by blazars at all energies. In comparison, the expected contribution of blazars to the IGRB energy spectrum is sub-dominant below 50 GeV [124,134].

The LAT has measured the APS of the diffuse emission at Galactic latitudes  $|b| > 30^\circ$  using approximately 2 years of data [60]. The APS, denoted as  $C_p(E)$ , has been measured in four energy bins spanning 1–50 GeV and, at multipoles  $l \geq 155$ , an angular power above the photon noise level is detected in all energy bins. Since the measured angular power is approximately constant at all multipoles, the origin of the APS is attributed to the contribution of one or more un-clustered

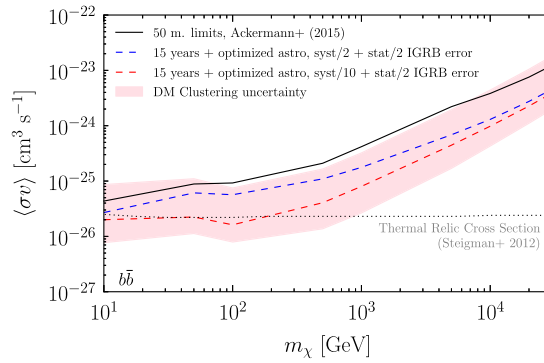


**Fig. 21.** Projected upper limits on the WIMP annihilation cross section derived from the IGRB energy spectrum after 15 years of data taking, compared to the most recent limits derived in [77] using 50 months of data (thin solid line). The dashed blue and red dotted curves correspond to cases in which the systematic uncertainties are reduced by factors of 2 and 10, respectively, relative to their values in the 50-month analysis. In both cases, the statistical uncertainties have been reduced by a factor of 2 (see text for details). The shaded red area corresponds to the uncertainties from the modeling of the cosmological DM annihilation signal (see [111]). (For interpretation of the references to colour in this figure legend, the reader is referred to the web version of this article.)

point-source populations. Ref. [124] finds that measured values of  $C_p$  are compatible with the anisotropy from Radio Loud AGN, namely blazars and mis-aligned AGN (MAGN).

Cross correlations with LSS provide a fundamental advance with respect to the study of the IGRB spectrum only. They, in fact, give access to the redshift dimension, which is integrated out in the energy spectrum and thus cannot be used in an analysis of LAT data by itself. LSS tracers come with redshift information, and a positive correlation with a given tracer is equivalent to isolating the  $\gamma$ -ray emission coming from the redshift range spanned by the tracer itself in the IGRB. Moreover, since different tracers/catalogs are available, each covering a different redshift range, using them in conjunction effectively allows *redshift tomography* of the IGRB, i.e., splitting the emission according to the different redshift ranges where such emission originated. In particular, for DM searches it is useful to isolate the low-redshift part of the IGRB ( $z \lesssim 0.5$ ) where the DM signal peaks, as opposed to standard astrophysical components, which typically peak at  $z \sim 1$ . Constraints on DM from the cross-correlation are stronger than those from the energy spectrum since the DM signal then can be compared with the low- $z$  IGRB (where the DM signal peaks) as opposed to the whole  $z$ -integrated IGRB.

The cross-correlation signal is weak and has been detected only slightly above  $3\sigma$  very recently [61] using 5 years of LAT data. Thus, such cross-correlation studies will greatly benefit from additional data taking. By performing accurate measurements of the cross correlation at different redshifts, distinguishing DM-induced emission from the other astrophysical contributors will be easier owing to the peculiar  $z$ -dependence of the LSS. The measured correlations have been used in [119] to derive conservative constraints on DM neglecting any possible astrophysical contribution, and in [112] to infer more aggressive constraints by fitting a multi-component model with both DM and astrophysical sources. When adopting the same DM annihilation boost factor from DM substructures, the constraints from cross-correlation studies are about a factor of 10 stronger than those derived from the IGRB energy spectrum.

Finally, one-point statistics measurements are also sensitive to DM. These DM signatures in the IGRB have been investigated theoretically in [232–234] but so far there have been no DM searches using 1-point statistics with LAT data (see however [230] for a non-DM oriented work using 11 months of LAT data between 1 and 300 GeV). However, as discussed in Section 4.4.1, this method has also been applied the Galactic center region to test whether the Galactic center excess can be better fitted by a smooth component or as a collection of confused/unresolved point sources [158,159].

These studies have typically started with a low-background event sample (e.g., P7REP\_CLEAN) and then masked both the Galactic plane and some or all of the cataloged sources to increase the signal-to-noise ratio. For example, Ref. [61] used P7REP\_CLEAN data for  $|b| > 30^\circ$ , then masked  $1^\circ$  radius disks around all 3FGL catalog sources, and increased the disk radius to  $2^\circ$  degrees below 1 GeV around the 500 brightest cataloged sources (see §3 of that paper for additional details on the data selection).

#### 4.8.4. IGRB anisotropies and cross-correlation measurements: Sensitivity projections

Rather than deriving projections for each of the methods described in Section 4.8.3, we will consider the specific case of the APS analysis. We expect the sensitivity of the pixel fluctuations to scale similarly with time. The sensitivity of the cross-correlation with LSS tracers depends critically on the details of forthcoming catalogs of LSS tracers, which are difficult to predict.

Following the work in [137,235], we consider in Appendix H two cases for the properties of extragalactic DM halos and subhalos: the LOW case, where halos are relatively poor in subhalos, and the HIGH case, that imply large subhalo boosts to the DM annihilation cosmological signal. The constraints for these scenarios are shown in Fig. 22. According to our sensitivity estimates, 15 years of data improve the current results (which use 2 years of data P7\_CLEAN) by about a factor of 2–3 for the two DM substructure models considered. This prediction suggests that DM searches based on APS measurements are

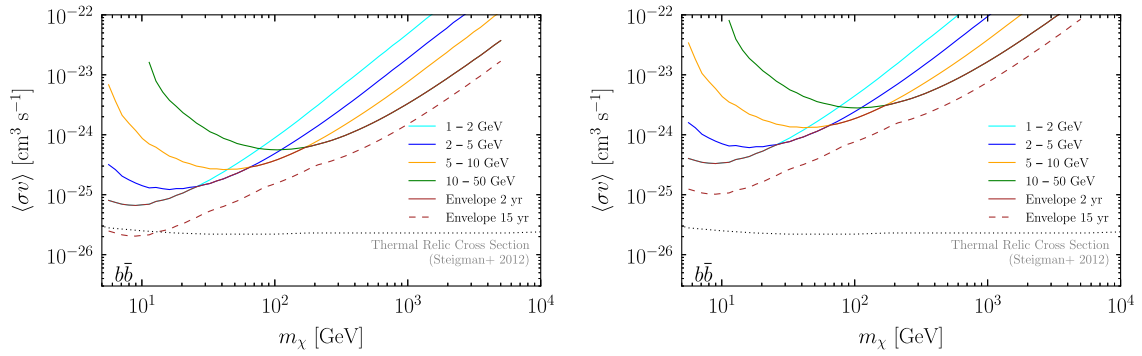


**Fig. 22.** 95% CL limits on the DM annihilation cross section considering two different scenarios for extragalactic DM halos and their substructures (HIGH on left, LOW on right); see [235] for further details. The limits from 2 years of data are shown for the four different energy bins adopted in the analysis of APS data (cyan, blue, orange, and green) and for a convolution of them (solid brown line). The projections for the same energy bins and their convolution is also shown for 15 years of data. (For interpretation of the references to colour in this figure legend, the reader is referred to the web version of this article.)

background limited and scale roughly as  $\sqrt{t}$ . (The increased statistics from using Pass 8 data account for 10%–20% of the improvement.)

#### 4.9. Spectral lines

In many DM models, pairs of DM particles can annihilate into a  $\gamma$  ray and a second particle ( $X$ ), e.g.,  $\gamma\gamma$ ,  $\gamma Z$ , or  $\gamma H$ . Since DM is strongly constrained to be electrically neutral, it has no direct coupling to photons. Thus the process  $\chi\chi \rightarrow \gamma X$  occurs only through higher-order loops, resulting in a branching fraction that is only  $\sim 10^{-4}$ – $10^{-1}$  [236–240]. If a DM particle annihilates to  $\gamma X$  the photons are monochromatic in the rest frame with rest-frame energy

$$E_\gamma = m_\chi \left( 1 - \frac{m_X^2}{4m_\chi^2} \right). \quad (9)$$

This would result in a line-like feature in the  $\gamma$ -ray spectrum. Possible evidence of such a line-like feature at 130 GeV strongly correlated with the Galactic center region was reported [57,241–243], and also seen in nearby galaxy clusters [244], and unassociated LAT sources [245,246]. The feature was not seen in the vicinity of nearby dwarf galaxies [247]. However such a signal is expected to be much fainter than in the Galactic center. Potential instrumental effects and a similar feature detected in the bright  $\gamma$ -ray emission from cosmic-ray interactions in Earth's upper atmosphere (the Limb) have also been discussed [244,248,249]. A systematic investigation of the spatial morphology of the 130 GeV feature and other line-like features in the Galactic plane is presented in [250].

##### 4.9.1. Spectral lines: Current status

Since these reports, the LAT Collaboration has searched for spectral lines using both the Pass 7REP [251] and Pass 8 [80] data sets and found that the original putative signal has faded to less than one standard deviation significance ( $< 1\sigma$ ) once the trials factors associated with scanning in DM particle mass from 1 to 500 GeV and for several different ROIs associated with different DM radial profiles, which are shown in Fig. 23.

It is important to note that almost all of the fitting for spectral lines has been performed in the energy domain only. That is to say, the fitting used the  $\gamma$ -ray spectrum averaged over each of the ROIs, rather than simultaneously fitting spatial and spectral templates. This method greatly reduced the systematic uncertainties associated with modeling the astrophysical backgrounds, as we need only consider the potential biases in modeling the background with relatively simple spectral form rather than all of the potential biases from modeling the complicated spatial distribution of the Galactic diffuse emission. As shown in Fig. 24, by scanning control regions including the Galactic plane away from the Galactic center, the Vela pulsar and the Earth's limb, we have found that the systematic uncertainties are at the level of  $f_{\text{syst}} \sim 0.015$ .

##### 4.9.2. Spectral lines: Sensitivity projections

To project the effect of additional data on searches for spectral lines, we use largely the same methodology as for the DM searches targeting the Galactic center and halo (Section 4.4). The main difference is that instead of calculating the effective background by summing over pixels and energy bins, here we only sum over the energy bins. We model the background with a simple spectral form (typically the product of a power law and the exposure as a function of energy), model the signal with the LAT's energy dispersion function (which has a resolution of  $\Delta E/E < 0.10$  from 1 to 500 GeV), use narrow energy bins (typically 0.01 dex, or  $\Delta E/E = 0.023$ ), and assign  $f_{\text{syst}} = 0.015$ .

From the projections shown in Fig. 25 it is clear that searches for spectral lines are systematics limited up to  $\sim 100$  GeV ( $\sim 10$  GeV) for the R41 (R3) region, and background limited up to hundreds of GeV (i.e., the expected upper limit is  $> 10$  ph).



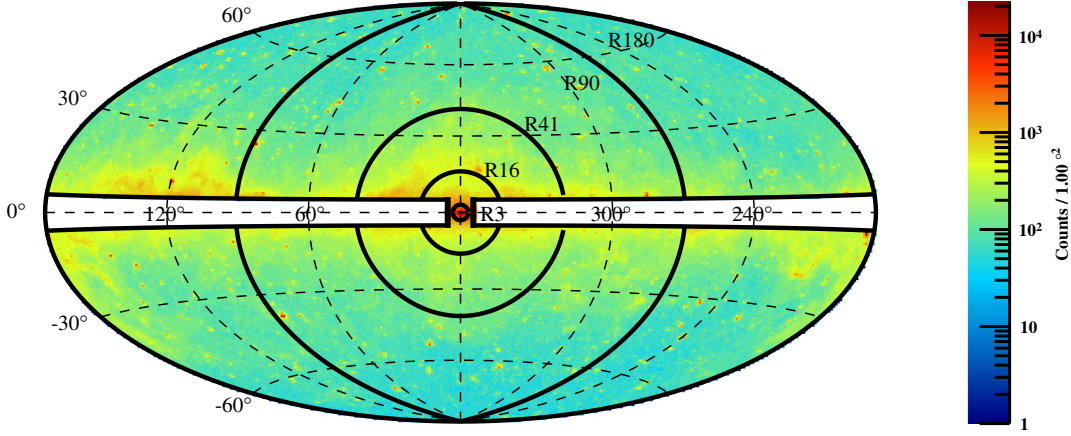


**Fig. 23.** Counts map for six years of P8R2-CLEAN data binned in  $1^\circ \times 1^\circ$  spatial bins plotted in Galactic coordinates in Hammer-Aitoff projection. The energy range is 1–750 GeV. Also shown are the outlines of the ROIs used in Ref. [59]. The Galactic plane region with longitude greater than  $6^\circ$  from the Galactic center and latitude smaller than  $5^\circ$  is removed from all signal ROIs. The R3, R16, R41, and R90 ROIs are optimized for the gNFW ( $\gamma = 1.3$ ), NFW, Einasto, and Isothermal profiles, respectively. Refs. [57,241] used somewhat different ROIs that were created by selecting a set of pixels with the largest expected signal-to-noise given the observed data and a similar set of DM density profiles; however the difference in ROIs does not significantly alter the results.

Source: This figure is from Ref. [59] (reproduced by permission of the APS and the authors).

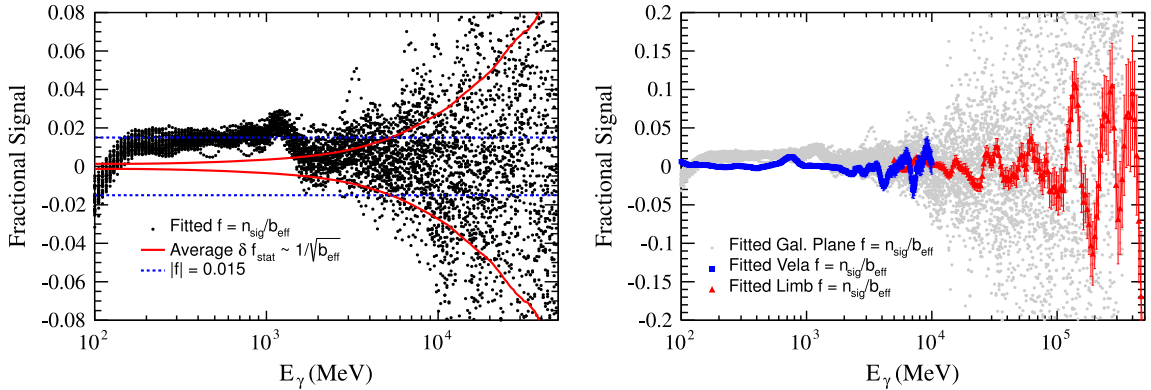


**Fig. 24.** Fractional signals ( $f_{\text{sig}}$ ) in a scan of the Galactic plane. (Left) dots show observed  $f_{\text{sig}}$  in  $31^\circ \times 10^\circ$  boxes along the Galactic plane. The solid red line is the average of the statistical uncertainties of the individual boxes. The blue dashed line is the value we chose to characterize  $f_{\text{sys}}$  modeling biases. (Right) The same, but with values of  $f_{\text{sig}}$  from the Vela pulsar and Earth Limb control samples added and the Galactic plane points shown in gray. (For interpretation of the references to colour in this figure legend, the reader is referred to the web version of this article.)

Source: These figures are from Ref. [59] (reproduced by permission of the APS and the authors); see that reference for additional details.

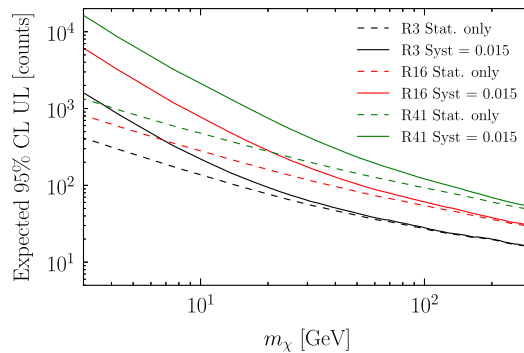


**Fig. 25.** Projected upper limits in signal counts for 15 years of LAT data for three different ROIs. Dashed lines show projected limits from statistical uncertainties only, while the solid lines show projected limits including both statistical and systematic uncertainties, with the level of systematic uncertainty assigned at  $f_{\text{sys}} = 1.5\%$  of the effective background. See text for details.



#### 4.10. Axions and axion-like particles

Axions and ALPs may be detected through either their decay to photons or through spectral signatures in high-energy sources induced by photon-ALP oscillations.

Heavy axions decaying into  $\gamma$  rays would be very similar to decaying DM and could potentially be constrained with observations of the IGRB (see Section 4.8).<sup>7</sup> Decaying light axions and ALPs could be detected at  $\gamma$ -ray energies if they are produced relativistically. This is the case in the production, e.g., through nucleon–nucleon Bremsstrahlung in the interiors of neutron stars [253].

A second approach is to search for signatures of photon-ALP oscillation in the spectra of  $\gamma$ -ray sources. For  $\gamma$  rays propagating through a magnetic field  $B_{\mu G} = B/\mu G$  and a plasma with plasma frequency  $\omega_{\text{neV}} = \omega/\text{neV}$ , the oscillation probability between photons and ALPs is maximal and independent of energy between  $E_{\text{crit}} \lesssim E \lesssim E_{\text{max}}$ , where (e.g. [254,255])

$$E_{\text{crit}} = 2.5 \text{ GeV} \frac{|m_{\text{neV}}^2 - \omega_{\text{neV}}^2|}{g_{11} B_{\mu G}}, \quad (10)$$

$$E_{\text{max}} = 2.12 \times 10^6 \text{ GeV } g_{11} B_{\mu G}^{-1}, \quad (11)$$

for ALP masses  $m_{\text{neV}} = m_a/\text{neV}$  and photon-ALP coupling  $g_{11} = g_{a\gamma}/10^{-11} \text{ GeV}^{-1}$ .<sup>8</sup> The magnetic field strengths in galaxies and clusters of galaxies are found to be of the order of the  $mG$  and  $\mu G$ , respectively (e.g. [257]). For the intergalactic medium, the field strength is constrained to be  $B \lesssim 10^{-9} \text{ G}$  (e.g. [258]). Thus, from these numbers and Eqs. (10)–(11), it is evident that for  $\gamma$  rays propagating in the magnetic fields of galaxies, galaxy clusters and the intergalactic medium, only an oscillation into light ALPs is possible (i.e.,  $m_a \lesssim \mu\text{eV}$ ) whereas the conversion probability to axions is vanishingly small.

The photon-ALP oscillations could manifest themselves in two ways in the spectra of  $\gamma$ -ray sources:

1. Above  $E_{\text{crit}}$ , up to 50% of the photons of an initially un-polarized pure photon beam can convert into ALPs, leading to a decrease of the source photon flux. Depending on the (often turbulent) ambient magnetic field, this decrease is accompanied by chaotic oscillations (irregularities) in the energy spectrum [259–261]. These spectral irregularities are not time dependent; thus, for each target, a particular, stable-in-time spectral pattern is expected.
2. ALPs could enhance the  $\gamma$ -ray fluxes from cosmological objects that are otherwise attenuated in interaction with photons of the extragalactic background light (EBL) (e.g. [262–266]). The EBL spans from UV to far-infrared and is composed of the integrated starlight emitted over the entire history of the Universe and starlight absorbed and re-emitted by dust in galaxies (e.g., [267]). A fraction of the photons converting to ALPs during propagation could lead to a secondary component in the spectrum at high energies given that the ALPs can reconvert into  $\gamma$  rays before reaching Earth.

Photon-ALP oscillations could also be used to search for a  $\gamma$ -ray signal from core-collapse supernovae [268–270]. Axions and ALPs would be produced in such explosions in a burst lasting several seconds, similar to the production of neutrinos. ALPs produced in such a way could subsequently convert into  $\gamma$  rays in the magnetic field of the Milky Way. On the other hand,  $\gamma$  rays produced in the dense core of the supernovae would not escape to the surface, and the  $\gamma$ -ray emission is expected to be delayed with respect to the neutrino emission. Thus, the observation of a pulse of  $\gamma$  rays coincident with the expected neutrino signal from a Galactic supernova would be evidence for the existence of ALPs.

##### 4.10.1. Axions and ALPs: Current status

The current limits on the ALP parameters are summarized in Fig. 26 (red shaded regions). The search for  $\gamma$  rays from axion or ALP decays produced in neutron star interiors lead to the limits labeled “ALPs from NS” (gray hatched region, assuming the model-dependent factor  $\mathcal{N} = 1$ ) [253]. The analysis used five years of Pass 7REP LAT data and combined the results of four nearby neutron stars which are not observed at  $\gamma$ -ray energies. The limits constrain the QCD axion mass (black line and yellow band in Fig. 26) to be below  $7.9 \times 10^{-2} \text{ eV}$ . It should be noted that these limits not only depend on the axion and ALP coupling to photons but also on the axion and ALP production through nucleon–nucleon Bremsstrahlung.

Limits depending only on the coupling between ALPs and photons were derived by searching for spectral irregularities around  $E_{\text{crit}}$  in the  $\gamma$ -ray spectrum of the radio galaxy NGC 1275 [271]. In total, six years of Pass 8 data were analyzed. NGC 1275 is the most viable source for such searches as it is (a) a bright  $\gamma$ -ray emitter leading to high signal-to-noise ratio and a well determined spectrum and (b) it is located at the center of the cool-core Perseus galaxy cluster. Such galaxy clusters have strong magnetic fields of the order of tens of  $\mu G$  at their centers (e.g. [257]). The limits are the strongest reported so far in the mass range  $0.5 \text{ neV} \lesssim m_a \lesssim 20 \text{ neV}$  and surpass the sensitivity of the planned laboratory experiment ALPS II [274] in that mass range. Together with the bounds from the non-observation of a Gamma-Ray Burst (GRB) from the SN 1987A [270] and the non-observations of irregularities with the H.E.S.S. Cerenkov telescopes in the spectrum of the

<sup>7</sup> However, these heavy axions cannot constitute the DM since their lifetime is too short. ALPs in this mass range, on the other hand, could constitute all of the DM, if additional degrees of freedom above the electro-weak scale at high energies are assumed [252]. Otherwise, the ALPs would exceed the critical density of the Universe.

<sup>8</sup> In these equations, we have neglected a possible photon dispersion term [256], since it will not be relevant for the energies and magnetic fields considered in the following.

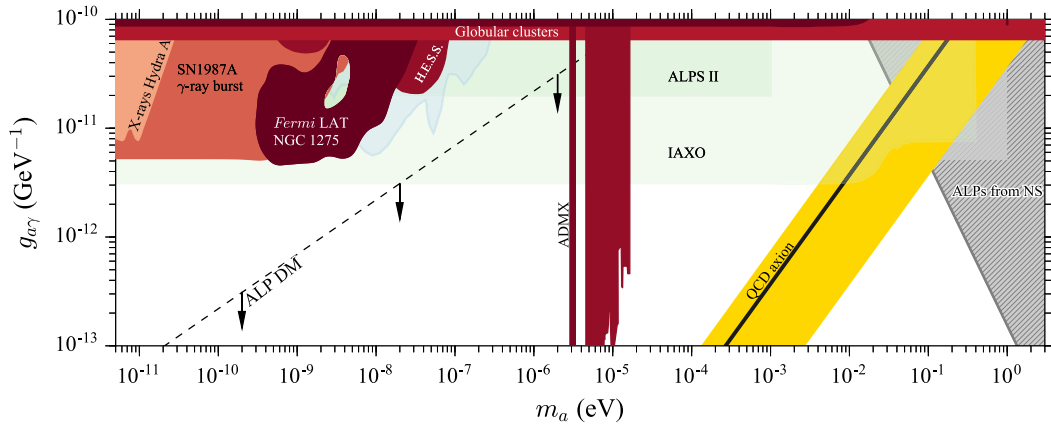


**Fig. 26.** Current status of the limits imposed on the ALP parameter space by different experiments and targets. Limits derived with LAT observations are shown as dark red (NGC 1275 in the Perseus galaxy cluster [271]) and gray hatched (neutron stars [253]) regions. Limits from other experiments are shown in red. The parameter space where ALPs could explain a low  $\gamma$ -ray opacity is shown in light blue. The parameter space where ALPs could explain hints for a low  $\gamma$ -ray opacity is shown in blue. Sensitivity estimates for future laboratory experiments are shown in green. The QCD axion line is shown in yellow. ALP parameters below the dashed line could account for all the DM. See Refs. [272,273] and references therein. (For interpretation of the references to colour in this figure legend, the reader is referred to the web version of this article.)

blazar PKS 2155–304 [275] (see also [276]), ALPs are now almost ruled out as a viable solution for the (now questioned) reported evidence of a reduced opacity of the Universe to  $\gamma$  rays [262] (blue shaded region in Fig. 26). However, the limits do not yet constrain models where ALPs could account for all the DM, indicated by the dashed line labeled  $\theta_1 \mathcal{N} = 1$  in Fig. 26.

#### 4.10.2. Axions and ALPs: Sensitivity projections

The flux limits derived from the observation of neutron stars in [253] depend on the precision of the measurement of the astrophysical backgrounds and are therefore expected to improve with  $\sqrt{t}$ , similarly to the dSphs for lower WIMP masses.

On the whole, the LAT sensitivity to ALPs from the measurement of distortions of the spectrum of NGC 1275 appears to be systematics limited. The major, dominant uncertainties in the limits derived from the spectrum of NGC 1275 in [271] stem from the unknown magnetic field structure in the Perseus galaxy cluster over large spatial scales. Future radio observations with the Square Kilometer Array will provide a wealth of rotation measures [277]. These will improve understanding of the strength and morphology of the cluster magnetic field [278], and thus lower the uncertainties.

On the other hand, the bounds on low-mass ALPs ( $m_a \lesssim 1$  neV) could be significantly improved if a Galactic supernova occurred during the operational lifetime of the LAT: its sensitivity is superior to that of the Gamma-Ray Spectrometer of the *Solar Maximum Mission* that was used to derive the current bounds from the non-detection of  $\gamma$  rays from SN 1987A (light-red shaded region labeled “SN  $\gamma$ -ray burst” in Fig. 26).

Future LAT observations of distant AGNs could also provide an additional step forward to testing ALPs as a possible solution to the suggested reduced opacity of the Universe to  $\gamma$  rays [262,266,279,280]. In particular, a careful statistical study of those  $\gamma$  rays suffering from the strongest EBL attenuation should shed light on the role of ALPs as possible “boosters” of the cosmological  $\gamma$ -ray flux received at Earth. The LAT is the ideal instrument not only because of its point-source sensitivity, which enables observation of high-redshift AGNs up to very high energies, but very especially thanks to its continuous scanning of the entire  $\gamma$ -ray sky. Indeed, any violent and transient cosmological phenomena (such as  $\gamma$ -ray flares from blazars or GRBs) that could be potentially used for these opacity studies will very likely be observed by the LAT (consequently enhancing the chances to detect some of the few photons expected at the highest optical depths). Note that this is less likely for Cerenkov telescopes given their much narrower fields of view and reduced duty cycles.

## 5. Discussion

Here we review the projected limits for the different search targets (Section 5.1), and consider the results in the context of other indirect-detection DM searches (Section 5.2) as well as direct-detection and collider-production searches (Section 5.3). This discussion will be focused on WIMP searches, as the results for Axions and ALPs are summarized in Fig. 26 and Section 4.10.

### 5.1. Summary of projected limits

With the categories of limiting factors presented in Section 4.3 in mind, we can broadly categorize the search targets as follows:

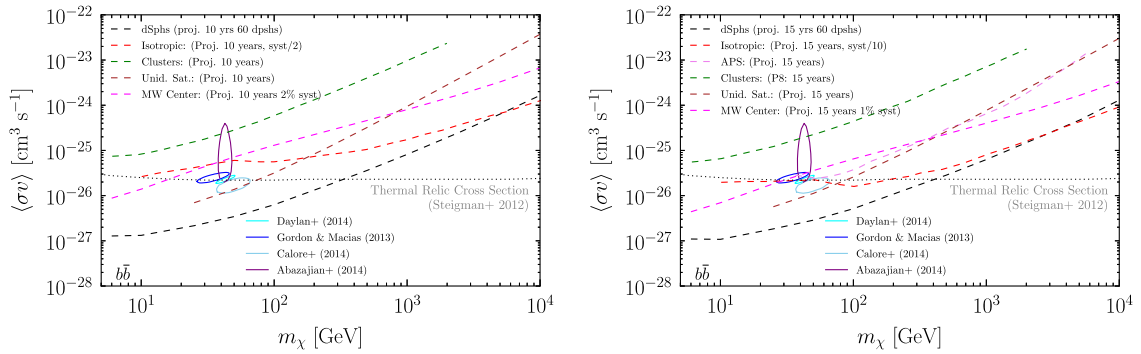


**Fig. 27.** Comparison of projected LAT limits for 10 years (left) and 15 years (right) of data for the search methods described in Section 4. Favored contours for several Galactic center analyses are also included for comparison.

1. Searches targeting objects with substantial astrophysical backgrounds, such as the Galactic center, large Galaxy clusters, and the LMC are systematics limited up to high energies (e.g.,  $m_\chi \lesssim 10$  TeV for the Galactic center,  $m_\chi \lesssim 1$  TeV for the LMC).
2. Searches for spectral lines from the Galactic halo benefit from additional discriminating power in the spectral domain, but are still systematics limited at low energies (e.g.,  $m_\chi \lesssim 100$  GeV for the R16 ROI optimized for the Einasto profile).
3. Searches targeting relatively small objects at high Galactic latitudes, in particular the dSphs, are background limited at lower energies, and signal limited at higher energies. For the combined analysis of dSphs the cross-over point comes at  $m_\chi \sim 500$  GeV (100 GeV) for the  $b\bar{b}$  ( $\tau^+\tau^-$ ) channel.
4. Although the precision of the measurement of the IGRB is systematics limited, statistical analyses of the IGRB, such as fluctuation analysis or cross-correlation analysis, are, for the most part still signal limited in much of the LAT energy range. This is because above a few GeV the combined brightness of the isotropic and Galactic diffuse backgrounds is low enough that on average less than a single background  $\gamma$  ray is expected within the LAT angular resolution.
5. Some searches are limited by our understanding of a source population. This could be a population of background sources, such as the various AGN classes in analyses of the EGB. Or it could be the signal population, such as in the search for the dark satellites among the unassociated cataloged sources. Although the source sensitivity generally scales as  $\sqrt{t}$ , because of the typically steeply falling distribution of fluxes,  $dN/dS \propto S^{3/2}$ , the sensitivity of these searches scales as  $\sim t^{3/4}$ .

In short, the most notable benefits from additional data taking come from the improved sensitivity to signals from dSphs for higher DM masses ( $m_\chi \gtrsim 100$  GeV), from the improved sensitivity of statistical methods of disentangling contributions to the IGRB by virtue of the continued improvement in the point-source sensitivity, and from increased sensitivity to a population of dark satellites whose number rises quickly at decreasing flux thresholds.

Furthermore, searches targeting the dSphs have smaller modeling uncertainties and more robust determinations of the astrophysical  $J$  factors than searches targeting other objects. Additionally these searches have among the best sensitivities across much of the LAT energy band. Overall these considerations suggest that, looking forward, searches targeting the dSphs will continue to have the best sensitivity. This can clearly be seen in Fig. 27.

## 5.2. Relation to other indirect-detection efforts

Several other kinds of experiments can undertake indirect-detection searches for DM: (a) instruments that are sensitive to GeV-to-TeV cosmic rays, (b) imaging atmospheric Cerenkov telescopes (IACTs), (c) water Cerenkov telescopes, (d) cosmic-ray air shower arrays, (e) neutrino telescopes, and (f) instruments sensitive to fluctuations in the cosmic microwave background (CMB). Of these, cosmic-ray detectors, IACTs, and the *Planck* measurements of the CMB are all capable of probing WIMP annihilation at or near the thermal relic cross section in some mass ranges. In this section we compare the sensitivity of DM searches using LAT data with results from these other instruments.

In Fig. 28 we show the most sensitive limits projected for searches using LAT data and compare them with other indirect-detection limits derived from IACTs and *Planck*. The sensitivity of future IACTs, and in particular the Cerenkov Telescope Array (CTA), are somewhat uncertain, owing to uncertainties of the instrument performance and the effects of astrophysical backgrounds. We show projections that include the effects of conservatively estimated systematic uncertainties [281] (see also [282]), as well as projections made with smaller systematic uncertainty and updated instrument performance estimates [283].

In principle, fluxes of cosmic-ray anti-particles (in particular positrons, anti-protons, and also possibly anti-deuterons or anti-helium) could be a signature of DM interactions. Although anti-particles can be produced in astrophysical accelerators, the fluxes and spectra expected from such accelerators are quite different from the expectations for DM interactions. However, comparing results from cosmic-ray measurements from instruments such as PAMELA and AMS-02 with results from  $\gamma$ -ray data is complicated as the constraints on the DM annihilation are dominated by systematic modeling

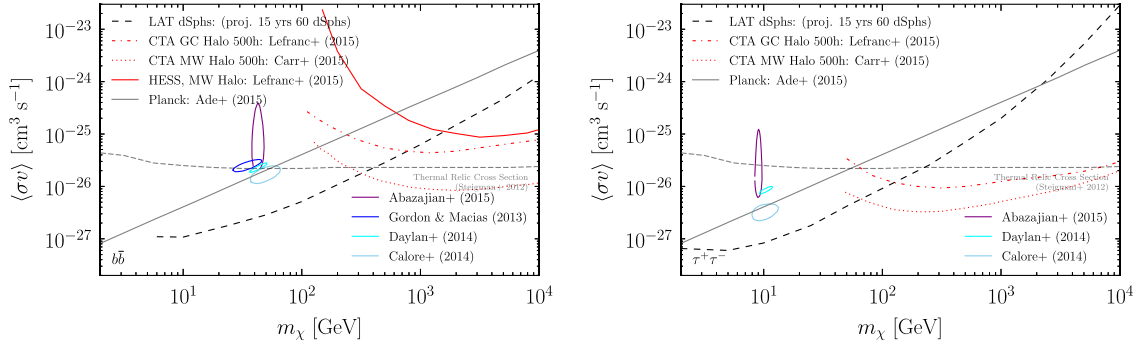


**Fig. 28.** Comparison of projected dSph stacking limits with current and future IACT limits from CTA for the  $b\bar{b}$  (left) and  $\tau^+\tau^-$  (right) channels. The dashed black curve shows the expected limit from the analysis of the artificially expanded target described in Section 4.5.2 for the 15-year data set. IACT limits are in red and taken from [281,283,284]. The limits derived from the *Planck* data [13] are in gray. Finally, favored contours for several Galactic-center analyses are included for comparison. (For interpretation of the references to colour in this figure legend, the reader is referred to the web version of this article.)

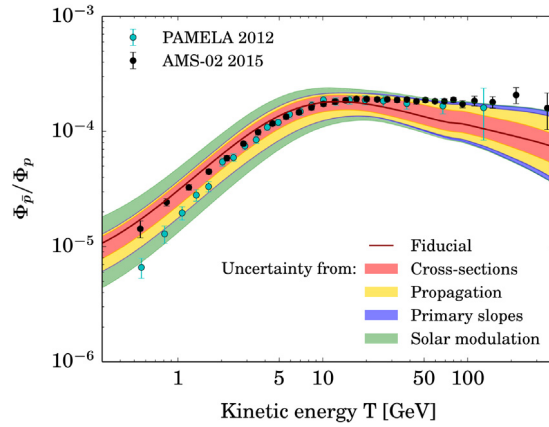


**Fig. 29.** Combined total uncertainty on the predicted secondary  $\bar{p}/p$  ratio, superimposed on the PAMELA [285] and AMS-02 [286,287] data. This figure appeared as Fig. 2 of Ref. [288]; additional details about the uncertainty bands may be found in that work; reproduced under the Creative Commons attribution license.

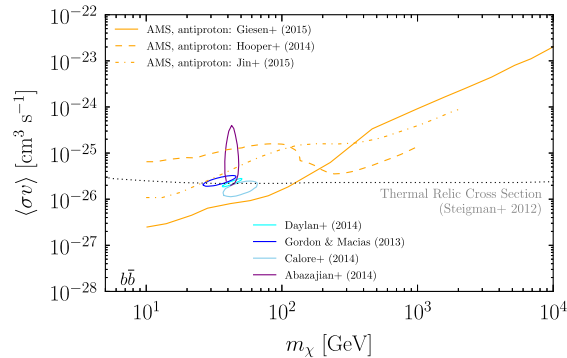


**Fig. 30.** Comparison of three sets of WIMP annihilation cross-section limits derived from the AMS-02 data for  $\Phi(\bar{p})/\Phi(p)$ , but with different assumptions regarding the cosmic-ray behavior [288–290]. Favored contours for several Galactic center analyses are included for comparison.

uncertainties. As an example, the measurement of the ratio of anti-protons to protons,  $\Phi(\bar{p})/\Phi(p)$ , could in principle be used to probe cross sections below the thermal relic level. In practice, however, the constraints based on cosmic-ray data have large modeling uncertainties and are quite model dependent (see Figs. 29 and 30).

Similarly, the ratio of positron to electron fluxes has been measured by the LAT [28], AMS-02 [291,292] and PAMELA [293] and is potentially sensitive to DM interactions. The observed positron to electron flux ratio rises steadily from  $\sim 5\%$  at 1 GeV to  $\sim 15\%$  above 100 GeV, suggesting the injection of high-energy positrons into the interstellar medium. Similarly to the situation with anti-protons, the interpretation of the rising positron fraction and implied constraints on DM annihilation

are dominated by systematic modeling uncertainties, see, e.g., Refs. [294–297] for discussion of the interpretation of the positron excess.

In summary, the LAT data, and in particular the analysis of the dSphs provide the best current constraints on the indirect detection of WIMP annihilation over a wide range of masses and channels,  $\sim 15$  GeV–1.6 TeV ( $\sim 10$ –400 GeV) for the  $b\bar{b}$  ( $\tau^+\tau^-$ ) channel. Furthermore, the constraints will continue to improve with additional data taking.

No instruments currently under development will improve markedly on the LAT sensitivity to  $\gamma$  rays in the 1–50 GeV energy band that effectively sets the sensitivity to WIMP annihilation in the  $\sim 10$ –500 GeV mass range. For 15 years of LAT data taking and estimates of the CTA sensitivity that include systematic uncertainties, we project that the LAT would set the deepest constraints on  $\langle\sigma v\rangle$  up between 300 and 700 GeV (between 80 and 120 GeV) in the  $b\bar{b}$  ( $\tau^+\tau^-$ ) channel for the foreseeable future.

### 5.3. Role of indirect-detection searches for dark matter

Indirect-detection, direct-detection, and production (i.e., collider) searches for DM have different advantages. The complementarity between the methods has been reviewed in a number of recent works (e.g., [298–300]). As discussed in Section 2, indirect-detection searches measure the rate of DM annihilation (or decay) into Standard Model particles. When combined with estimates of the DM density, these observations can be used to estimate or constrain the DM annihilation cross-section averaged over the velocity distribution,  $\langle\sigma v\rangle$ , (or decay lifetime,  $\tau_\chi$ ).

Direct-detection searches measure the rate of scattering of DM particles with Standard Model target particles, typically by measuring the recoil of nuclei (although some experiments are also sensitive to electron recoil, e.g., [301,302]). With knowledge of the scattering target, and estimates of the DM density and velocity distribution, these measurements can be used to estimate or constrain the scattering cross-section of DM particles with Standard Model particles,  $\sigma_{\text{SM},\chi}$ . Direct-detection searches are typically  $10^3$  to  $10^4$  times more sensitive to spin-independent couplings (where the DM particle coherently interacts with the entire nucleus) than to spin-dependent couplings (where the DM particle effectively scatters off a single unpaired nucleon).

Collider searches look for the missing energy and momentum carried away by stable DM particles that were produced in the collisions, but escape the detector volume without interacting. Because stable DM particles are not seen in the detectors, most searches at colliders do not directly measure the cross-section to produce the DM particles by colliding Standard Model particles,  $\sigma_{\text{SM}\rightarrow\chi\chi}$ , but rather the cross-section to produce heavier exotic particles that then cascade down to stable DM final state particles before reaching the detector,  $\sigma_{\text{SM}\rightarrow\text{exotic}}$ .

Additionally, the flux of ultra high-energy neutrinos from the Sun is sensitive to the DM–proton scattering cross-section (also  $\sigma_{\text{SM},\chi}$ , which determines the rate at which DM is captured by the Sun). For values of DM annihilation cross-sections near  $\langle\sigma v\rangle = 3 \times 10^{-26} \text{ cm}^3 \text{ s}^{-1}$  the DM capture rate would be in equilibrium with the DM annihilation rate. The density of DM in the sun would be dependent on  $\langle\sigma v\rangle$ , but the observable neutrino flux would not. The limits on the spin-dependent scattering cross-sections inferred from limits on ultra high-energy neutrino fluxes from the sun are competitive with the best direct-detection measurements [303–305].

There is broad consensus that the three approaches probe different and complementary regions of the DM parameter space [298–300]. Because they measure very different observables, direct comparisons between them depend on a number of assumptions about the nature of DM particles and their interactions. These kinds of comparisons are most often presented in the  $m_\chi$ ,  $\sigma_{\text{SM},\chi}$  space, which is most appropriate for discussing direct-detection results. In Fig. 31 we present a comparison in  $m_\chi$ ,  $\langle\sigma v\rangle$  space using a representative set of assumptions to convert the direct-detection and collider observables into constraints on  $\langle\sigma v\rangle$ .

Conversions from  $\sigma_{\text{SM},\chi}$  and  $\sigma_{\text{SM}\rightarrow\text{exotic}}$  to  $\langle\sigma v\rangle$  (i.e., direct-detection and collider results to indirect detection results respectively) require assumptions about the particle interactions. In Fig. 31 we show results derived using an Effective Field Theory (EFT) framework developed for the Community Summer Study (Snowmass) 2013 by the Cosmic Frontier Working Groups [300]. The EFT framework is a simple and fairly model independent assumption; however, it implies that the dark matter interacts with the Standard Model via a four-particle contact interaction. The interaction particle mass must be much larger than the transfer of momentum of the physical process of interest. Additional details on the representative operators and the model parameter space can also be found in [309,311].

In the context of searches for particle DM, we summarize key points regarding indirect detection.

- Indirect-detection searches look for DM where it has already been determined to exist, i.e., in large-scale astrophysical objects. A discovery of a new particle at the LHC would require follow-on studies of astrophysical data to confirm that it does in fact account for the observed properties of DM. Furthermore, if the mass and cross-section of the DM particle were to be measured at the LHC, indirect searches could be used to directly measure the distribution of the DM particle in astrophysical objects. The results from indirect-detection experiments, given a potential candidate from direct-detection experiments, would measure the distribution in the cosmos.
- The canonical thermal relic cross-section of  $\langle\sigma v\rangle \sim 3 \times 10^{-26} \text{ cm}^3 \text{ s}^{-1}$  applies to an entire class of DM particle candidates. Testing for signals at that cross section tests the entire class of models that predict such candidates.

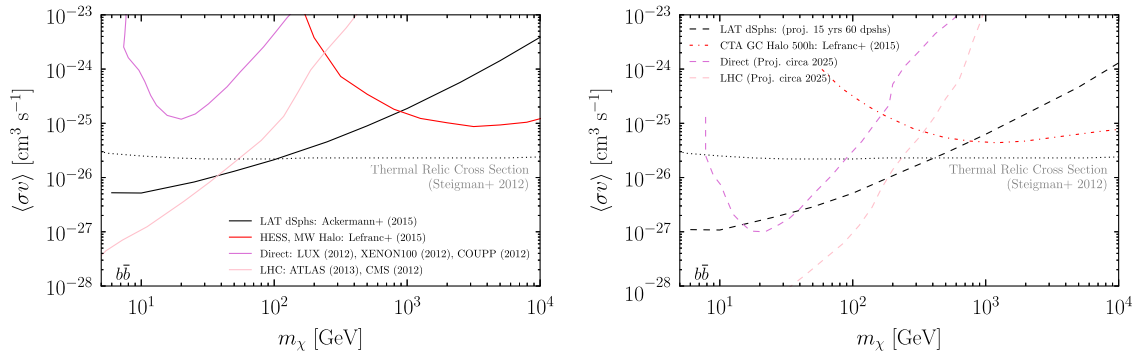


**Fig. 31.** Comparison of best current (left) and projected (right) indirect-detection, direct-detection (spin-dependent) and collider-production limits on  $\langle\sigma v\rangle$  in the  $b\bar{b}$  channel. Conversion of direct-detection and collider limits to the  $\langle\sigma v\rangle$  scale is based on the assumption of four particle contact interactions for the production/annihilation of DM. As noted in the text, this assumption is *quite uncertain* (potentially by orders of magnitude) and the comparisons shown here should be considered schematic. The current IACT limits are taken from Ref. [284]. Following Ref. [298], the direct-detection limits are taken from Ref. [306], and the projection was made using the expected LZ sensitivity. The collider-production limits are taken from Refs. [307,308], and the projection was made for 300 fb $^{-1}$  of data at 13 TeV [309].

- Indirect-detection searches generally have better sensitivity for high DM particle masses, (see, e.g., Fig. 31). Compared to collider searches, which must use the beam energy to produce exotic particles that then decay to DM particles, indirect-detection searches target final state particles with masses  $\sim 0.1 m_\chi$  from the interactions of already existing DM particles. Similarly, direct-detection searches lose sensitivity when the mass of the DM particle is larger than the mass of the target nuclei.
- Indirect-detection searches have the additional benefit that, in the event of a detection, they measure the mass of the DM candidate. If the DM mass is large, an indirect-detection measurement could determine the energy reach needed for the next collider, or influence the choice of the best nuclear target for direct detection.
- LHC limits on new physics do not translate directly to limits on  $\langle\sigma v\rangle$  (Fig. 31). Inferred cross-section limits vary by orders of magnitude depending on assumptions about the coupling and the mediator of the DM annihilations. For example, unless a specific model is imposed (e.g., Supersymmetry), the collider limits are based on an effective field theory. This requires the total energy of the event to be much lighter than the mediator for the field theory to be valid [310].
- Relative to direct-detection and collider searches, indirect-detection searches generally have better sensitivity for DM particles coupling to leptons. Direct-detection searches are typically more sensitive to nuclear recoil than electron recoil (though see, e.g., [301,302]), and the highest-energy lepton collider (LEP2) had a maximum center of mass energy of  $\sim 200$  GeV.
- Direct and indirect searches probe complementary DM interactions with the Standard Model. In some models, the scattering cross section is velocity suppressed while the annihilation cross section is not, making indirect searches more sensitive for those models [311].

## 6. Summary

In this paper we have examined current strategies for searching for DM signals in the LAT data, presenting existing search results and projecting how their sensitivities will improve with additional LAT data.

Although many LAT search targets are becoming systematics- or background-limited with the several years of LAT data already obtained, the most promising targets are still signal limited in much of the LAT energy range and for these cases the LAT sensitivity scales as better than  $\sqrt{t}$ .

1. The most promising target, the dSphs (Section 4.5.1), are signal-limited above  $\sim 500$  GeV ( $\sim 100$  GeV) in the  $b\bar{b}$  ( $\tau^+\tau^-$ ) channel. Furthermore, the searches targeting the dSphs have already set the most constraining limits on DM signals. Thus we are in the fortunate situation that the best target will also provide the most improvement as additional data are analyzed.
  - (a) Ongoing and planned deep, optical surveys are expected to discover numerous additional dSphs in the coming years, possibly by the hundreds once LSST is operational.
  - (b) With 15 years of data the LAT sensitivity for the dSph search would allow excluding the thermal relic cross section for masses up to  $>400$  GeV ( $>200$  GeV) in the  $b\bar{b}$  ( $\tau^+\tau^-$ ) channels.
  - (c) Projections also indicate that with 15 years of data the sensitivity for the dSphs would reach below  $2 \times 10^{-27} \text{ cm}^3 \text{ s}^{-1}$  for masses around 50 GeV in the  $b\bar{b}$  channel, allowing the DM interpretation of the Galactic center excess to be confirmed or refuted.
  - (d) With 15 years of data the volume over which the LAT would be able to detect 100 GeV DM annihilation to  $b\bar{b}$  from a typical dwarf galaxy at  $5\sigma$  significance would approximately double from  $\sim 2100 \text{ kpc}^3$  presently to  $>4200 \text{ kpc}^3$ .



2. The second approach for which the LAT sensitivity will continue to improve faster than  $\sqrt{t}$  is in constraining the population of the highest  $J$  factor Galactic DM subhalos (Section 4.6). Although the source detection sensitivity will improve only as  $\sqrt{t}$ , combined with an estimated  $J$  factor distribution that scales as  $dN/dJ \propto J^{-3/2}$ , the sensitivity to Galactic DM subhalos scales as  $t^{3/4}$ .
3. The third approach for which the LAT is, in effect, signal limited is in characterizing the populations of sources that are currently below the detection threshold. By reducing the uncertainties on estimates of the contributions of unresolved sources to the EGB, and thus reducing the uncertainty on what fraction of the EGB can be accounted for from the known  $\gamma$ -ray emitting source populations, limits on cosmological DM annihilation will tighten accordingly. We estimate that both the fraction of the EGB not attributable to detected sources and the uncertainties of the total contribution of known source classes will decrease as  $t^{3/4}$  or better.
4. A fourth search strategy for which the LAT results are largely signal limited is the measurement of the attenuation of emission from high-energy AGN. Observation of even a few  $\gamma$  rays from these sources with energies above the optical depth limit for  $\gamma\gamma$  attenuation on the EBL could be evidence of photon–axion oscillations.
5. A fifth approach for which the LAT is purely signal limited is in the observation of spectacular transient phenomena (such as Galactic supernovae, or bright, ultra-distant GRBs) that can also be used to search for signals from photon–axion oscillations.

Indirect detection is the only approach that searches for DM in the astrophysical targets where it is known to exist. The LAT is uniquely exploring an important range of cross-section-WIMP mass space, with a cross section sensitivity that is commensurate with constraining theories, or indirectly detecting dark matter at theoretically motivated cross sections. The advances expected with continued LAT data taking will be significant and will not be superseded by another experiment in the foreseeable future. Furthermore, the variety of search strategies possible with LAT data allows consistency cross checks, which are important, e.g., for interpreting the GeV excess near the Galactic center.

## Acknowledgments

The *Fermi* LAT Collaboration acknowledges generous ongoing support from a number of agencies and institutes that have supported both the development and the operation of the LAT as well as scientific data analysis. These include the National Aeronautics and Space Administration and the Department of Energy in the United States, the Commissariat à l’Energie Atomique and the Centre National de la Recherche Scientifique/Institut National de Physique Nucléaire et de Physique des Particules in France, the Agenzia Spaziale Italiana and the Istituto Nazionale di Fisica Nucleare in Italy, the Ministry of Education, Culture, Sports, Science and Technology (MEXT), High Energy Accelerator Research Organization (KEK) and Japan Aerospace Exploration Agency (JAXA) in Japan, and the K.A. Wallenberg Foundation, the Swedish Research Council and the Swedish National Space Board in Sweden.

Additional support for science analysis during the operations phase is gratefully acknowledged from the Istituto Nazionale di Astrofisica in Italy and the Centre National d’Études Spatiales in France.

Brandon Anderson and Manuel Meyer have been supported by a grant of the Knut and Alice Wallenberg foundation, PI : Jan Conrad. Miguel Sánchez-Cond is a Wenner-Gren Fellow and acknowledges the support of the Wenner-Gren Foundations to develop his research.

Massimiliano Razzano was funded by contract FIRB-2012-RBFR12PM1F from the Italian Ministry of Education, University and Research (MIUR).

We thank Daniel Hooper and Bridget Bertoni for useful discussions about projecting the sensitivity for searches targeting potential dark satellites among the LAT unassociated sources.

We thank Leslie Rosenberg and Gray Rybka for providing the contours from the ADMX axion search used in preparing Fig. 26.

We thank Tim Tait and William Shepherd for their discussions on dark matter complementarity with direct-detection experiments and collider searches.

We thank David Williams and Emmanuel Moulin for discussions on the CTA sensitivity and for providing data used in Fig. 28.

Finally, we thank Francesca Calore and Matthieu Schaller for preparing Fig. 12 based on Fig. 4 in [160].

## Appendix A. Dark matter density profiles

In the studies described in this paper we used several models of the spatial distribution of the DM. A generalized Navarro–Frenk–White (gNFW) profile [142], given by

$$\rho(r) = \frac{\rho_0}{(r/r_s)^\gamma (1 + r/r_s)^{3-\gamma}} \quad (\text{A.1})$$

models adiabatic contraction in the core of the distribution, i.e., within the scale radius  $r_s$ . Typical values of  $\gamma$  for the gNFW profile are in the range 1.0–1.4. The  $\gamma = 1$  case gives the canonical NFW profile [141]. The Einasto profile [143] is defined as:

$$\rho(r) = \rho_0 \exp\{-(2/\alpha)[(r/r_s)^\alpha - 1]\}, \quad (\text{A.2})$$

(we typically set  $\alpha = 0.17$ ), and is similar to gNFW profiles. The Burkert profile [140] is defined as

$$\rho(r) = \frac{\rho_0}{[r/r_s + 1][(r/r_s)^2 + 1]}, \quad (\text{A.3})$$

and is much flatter inside the scale radius, and is similar to a cored, isothermal profile given by

$$\rho(r) = \frac{\rho_0}{1 + (r/r_s)^2}. \quad (\text{A.4})$$

For practicality, we typically terminate the profile at some distance  $r_{\text{max}}$  that is several times larger than  $r_s$ . The values of  $(r_s, r_{\text{max}}, \rho_0)$  depend on the target in question. For the Milky Way halo we set  $\rho_0$  such that the local DM density (at 8.5 kpc from the Galactic Center) is  $0.4 \text{ GeV cm}^{-3}$ .

## Appendix B. Calculating gamma-ray spectra from WIMP annihilation

Owing to the cascade of particles produced as unstable DM annihilation products decay or hadronize, the  $\gamma$  rays from DM annihilation in most channels do not feature a sharp line at  $E_\gamma = m_\chi$ , but rather a continuous spectrum with characteristic energies significantly lower than the DM mass. Indeed, most indirect searches for DM do not involve searches for  $\gamma$ -ray spectral lines from DM annihilating directly into  $\gamma$  rays, but rather consider the DM annihilation channels:

$$\chi\chi \rightarrow s\bar{s}, b\bar{b}, t\bar{t}, gg, W^-W^+, e^+e^-, \mu^+\mu^-, \text{ and } \tau^+\tau^-. \quad (\text{B.1})$$

Annihilation into pairs of  $u$  or  $d$  quarks produces a similar spectrum as annihilation into gluon pairs,  $c\bar{c}$  is similar to  $s\bar{s}$ , and  $ZZ$  to  $W^-W^+$ , so bounds on such channels can be extrapolated approximately from the subset of channels we analyze in detail. Channels of DM annihilating to massive particles are open only above the mass threshold, i.e., when the DM particle mass is equal to that of the heavy Standard Model particle in the final state. In our searches we typically scan over DM masses between 5 GeV and 10 TeV, though the range depends somewhat on the search target (e.g., for spectral lines we have scanned from 100 MeV to 500 GeV).

For each final state, we calculate the spectrum of  $\gamma$  rays per annihilation as a function of DM mass (i.e.,  $dN_\gamma/dE_\gamma$ ) using the DMFIT software package [40]. We note that this formulation does not yet include electroweak corrections [312–316]. The electroweak corrections are expected to be important (assuming s-wave annihilation) when the DM mass is heavier than 1 TeV, and for this mass range would alter the spectra substantially for the  $W^+W^-$ ,  $e^+e^-$ ,  $\mu^+\mu^-$  and  $\tau^+\tau^-$  channels, increasing the number of expected  $\gamma$  rays per DM annihilation below  $\sim 10$  GeV [316,317]. However, the bounds on DM annihilation fluxes in the high-mass regime come primarily from the highest-energy  $\gamma$  rays, which are statistics-limited. Even for 10 TeV dark matter masses in the most-affected channels, including the electroweak corrections improves the limits on  $\langle\sigma v\rangle$  by  $\lesssim 20\%$  for typical analyses (see e.g., [36,138,317]).

## Appendix C. The *Fermi* LAT and LAT data

The LAT is a pair-conversion telescope that converts  $\gamma$  rays to  $e^+e^-$  pairs that are tracked in the instrument. The data analysis is event-based; individual pair conversion events are reconstructed and their energies and directions are estimated from the reconstructed data. Rates of charged-particle backgrounds exceed the  $\gamma$ -ray rates by factors of up to  $10^4$ , requiring powerful event selection criteria to obtain relatively pure  $\gamma$ -ray samples.

The LAT consists of three detector subsystems: a tracker/converter to promote pair conversion and measure the directions of the resulting particles, a calorimeter composed of 8.6 radiation lengths of CsI(Tl) scintillation crystals that provides an energy resolution of  $\Delta E/E \sim 10\%$  at 100 GeV, and an anti-coincidence detector of plastic scintillator tiles that surrounds the tracker and is key in charged-particle background rejection. The tracker comprises 18 x-y layers of silicon-strip detectors; the front 12 layers are interleaved with thin (3% radiation length) tungsten converter foils and the next four layers are interleaved with thick (18% radiation length) foils, and the final two layers have no converter foils. Detailed descriptions of the LAT and of its performance can be found elsewhere [1,79].

Iterations of the LAT event reconstruction and classification algorithms have been grouped into so called “Passes”. A number of iterations occurred before launch and were informed by simulations and beam test data of prototypes. For the first three years of the *Fermi* mission, data were processed with the last pre-launch versions (“Pass 6”). Since then, the data have been reprocessed three times. The first was with “Pass 7” [79], which consists of the same event reconstruction algorithms, but updated event classification criteria to account for knowledge gained about the LAT performance and charged-particle backgrounds since launch. The second reprocessing, designated “Pass 7 Reprocessed” or “Pass 7Rep”, used almost exactly the same algorithms as Pass 7 but incorporated updated calibration constants. The most recent reprocessing has been with “Pass 8”, which included entirely new reconstruction algorithms that were designed to account for effects observed in on-orbit data that had not been anticipated in simulations and affected the performance of the LAT, in particular the pile-up of out-of-time signals into event readouts [80]. Pass 8 also included new reconstruction algorithms that had not been fully implemented prior to launch, such as improved pattern recognition in all three sub-systems [80], and improvements to the energy fitting algorithm that push the upper edge of the LAT energy range up to 3 TeV [318].

Each reprocessing has included all of the data from the entire mission to date. The LAT Collaboration released the entire  $\gamma$ -ray data sets, and corresponding analysis files (see below), for each, to present a single, coherent, data set.

Each Pass of the algorithms implements several different event selection criteria that are optimized for different types of analyses. For Pass 8, the LAT Collaboration redeveloped the nested event selections that provide varying levels of cosmic-ray background rejection [80]. The nomenclature convention for the various event selections is to provide the Pass version and the name of the event selection criteria (e.g., P8R2\_SOURCE). Associated with each event selection are instrument response functions (IRFs) that parametrize the LAT performance. As our understanding of the instrument improves, from time to time the LAT Collaboration updates the IRFs for the various event selections. The IRF names indicate the analysis Pass they are associated with, as well as a version number (e.g., P8R2\_SOURCE\_V6). More details about the event reconstruction, event selection criteria, and IRFs can be found in Refs. [79] and [80].<sup>9</sup>

At the time of writing, the most recent published versions of many LAT analyses were performed with approximately six years of data, running from 2008 August to 2014 August. Throughout this paper we will specify both the Pass version and data interval used for the LAT results we discuss. Most of the current results presented in this paper were obtained with either the Pass 7 Rep or Pass 8 data sets. Unless stated otherwise, all of projections that we present were made with simulations of the Pass 8 data using the corresponding IRFs.

## Appendix D. Monte Carlo simulations

We performed three types of Monte Carlo simulations to make the data realizations we used to project the expected sensitivity of the DM searches described in this paper. In practice, all three types of simulations give results that agree to better than a few percent and to well within the analysis uncertainties. The choice of simulation method is primarily dictated by convenience and technical details such as available computer processing time and data storage.

1. *All-sky photon simulations*: we used the `gtobssim`<sup>10</sup> tool to simulate a total of 15 years of LAT data taking over the entire sky. The `gtobssim` tool generates individual  $\gamma$  rays from each source in the model, applies accept–reject sampling to simulate the instrumental acceptance, and finally convolves each  $\gamma$  ray with parametrized representations of the LAT spatial and spectral resolution. We simulated data for most of the DM targets described in Section 4, as well as for models of all of the astrophysical backgrounds described in Section 3.
2. *ROI-specific photon simulations*: we also used the `gtobssim` tool to simulate a total of 15 years of *Fermi* LAT data for much smaller regions covering specific targets, such as the individual dwarf spheroidal galaxies. These simulations included the “baseline” astrophysical background model described in Section 3, and in some cases also included the specific model of the unresolved source populations.
3. *Binned model map simulations*: we used the `gtmodel` tool to make predicted counts maps (i.e., maps of the expected number of photons in each pixel) of small regions of the sky. We then simulated Poisson fluctuations with respect to the predicted counts maps. These simulations generally included only the “baseline” astrophysical background model described in Section 3.

## Appendix E. Modeling the Galactic diffuse emission

The construction of the Galactic diffuse emission model used for these projections is described in considerably more detail in Ref. [319]. Here we will briefly summarize some key points, and discuss the uncertainties that most directly affect DM searches.

Determination of the distribution of interstellar gas relies mostly on the 21-cm line of atomic hydrogen, which traces neutral atomic hydrogen, and on the 2.6-mm line of carbon monoxide, which is a surrogate tracer of neutral molecular hydrogen. The Doppler shifts of the lines due to the motion of gas around the center of the Galaxy enables building quasi three-dimensional models of the gas distribution (e.g., [62, App. B]). This method suffers from limitations due to pile up along the line of sight of many structures, internal velocity dispersions of gas clouds, systematic deviations from circular motion about the Galactic center, and from kinematic ambiguity (for each velocity there are two possible positions) for the region of the Galaxy within the orbit of the solar system. For directions within about 10° longitude of the Galactic center or anti-center, the Doppler shifts due to Galactic rotation are smaller than the internal velocity dispersions and the distribution of gas cannot be determined via this method.

Additional interstellar gas components are the dark neutral medium, neutral gas that is not traced properly by the combination of the 21-cm and CO lines, and ionized gas. The dark neutral medium can be traced by infrared emission from interstellar dust grains, since they are sufficiently well mixed with neutral gas [320,321]. Thermal emission from dust, however, does not provide information on the location along the line of sight of the emitting gas. The distribution of ionized gas can be evaluated approximately using tracers like dispersion measures of pulsar emission, radio recombination lines

<sup>9</sup> Performance details for each of the iterations of the event reconstruction and classification algorithms used since launch are available at [http://www.slac.stanford.edu/exp/glast/groups/canda/lat\\_Performance.htm](http://www.slac.stanford.edu/exp/glast/groups/canda/lat_Performance.htm).

<sup>10</sup> See, e.g., [http://fermi.gsfc.nasa.gov/ssc/data/analysis/scitools/obssim\\_tutorial.html](http://fermi.gsfc.nasa.gov/ssc/data/analysis/scitools/obssim_tutorial.html) for more details about the `gtobssim` tool.

(observations are available only in limited regions of the sky), and free-free emission in the microwave band (which does not carry distance information).

Target radiation fields span wavelengths from radio to optical/UV. Aside from the CMB, the radiation field is often estimated using numerical codes to calculate the radiation transfer of stellar radiation (e.g., [62, App. C]). The distribution of optical/UV light is taken from simplified yet realistic models of the stellar populations in the Milky Way informed by observations. From these stellar radiation fields, combined with models of the dust distribution and properties in the Milky Way (built similarly to gas models described above), the numerical codes are used to derive the spectrum and spatial distribution of the reprocessed light in the IR domain.

The distribution of cosmic rays for the purpose of modeling interstellar  $\gamma$ -ray emission has been determined mainly with two complementary strategies. On one hand, it can be calculated using numerical codes that solve the cosmic-ray transport equations given a distribution of sources, injection spectra and transport parameters that are informed by direct cosmic-ray measurements and observations of their putative sources at various wavelengths [62]. On the other hand, it is reasonable to assume that variations in the cosmic-ray nuclei spectra are mild on the characteristic scale of interstellar gas complexes due to the moderate energy losses in propagation, so that the  $\gamma$ -ray emission from their mutual interactions can be assumed to be proportional to gas column densities derived as discussed above, and appropriately split into regions along the line of sight using the Doppler shift information [319,322].

An unexpected facet of Galactic interstellar emission that was highlighted by the LAT data is the presence of localized enhancements of cosmic-ray densities; i.e., of diffuse  $\gamma$ -ray emission on top of the large-scale, relatively smooth distributions of cosmic rays in the Milky Way that are evaluated by the propagation codes or by the fit of gas templates to LAT data. The most important example is the *Fermi* bubbles, two lobe-like structures seen on opposite sides of the Galactic center and extending up to Galactic latitudes  $\sim 50^\circ$  [323–325]. Other excesses were seen along the Galactic plane, for example one that was characterized as a cocoon of freshly-accelerated cosmic rays in the cavities of the interstellar medium in the massive-star forming region of Cygnus X [326]. Such excesses are not completely understood yet; thus their modeling is only purely phenomenological based on the LAT data themselves.

## Appendix F. Likelihood formalism and effective background

In LAT analysis we typically optimize our models to maximize the binned Poisson likelihood, defined as:

$$\mathcal{L}(\boldsymbol{\mu}, \boldsymbol{\theta} | \mathcal{D}) = \prod_k \frac{\lambda_k^{n_k} e^{-\lambda_k}}{n_k!}, \quad (\text{F.1})$$

which depends on the  $\gamma$ -ray data  $\mathcal{D}$ , signal parameters  $\boldsymbol{\mu}$ , and nuisance (i.e., background) parameters  $\boldsymbol{\theta}$ . The number of observed counts in each energy and spatial bin, indexed by  $k$ , depends on the data  $n_k(\mathcal{D})$ , while the model-predicted counts depend on the input parameters  $\lambda_k(\boldsymbol{\mu}, \boldsymbol{\theta})$ . The likelihood function includes information about the observed counts, instrument response, exposure and model components. The nuisance parameters are the scaling coefficients and spectral parameters of the astrophysical backgrounds discussed in Section 3.

When projecting the performance of future searches it is important to consider both statistical and systematic uncertainties. It is also important to distinguish between a search parameter space that is background limited (i.e., where the sensitivity is dominated by either statistical or systematic uncertainties of the astrophysical backgrounds) from parameter space that is signal limited (i.e., where the sensitivity is dominated by the small expected signals).

A useful concept that addresses both these considerations is the “effective background”, i.e., the background that is correlated with the signal, or is, so to say, “under” the signal.

For a binned analysis, given normalized models of the signal and background components:  $P_{\text{sig},i}(\boldsymbol{\mu})$  and  $P_{\text{bkg},i}(\boldsymbol{\theta})$ , we can estimate the effective background by calculating the likelihood fit covariance matrix element for the signal size (e.g., starting from Eq. 28 in Ref. [327]) in the approximation that the background is much larger than the signal, giving:

$$b_{\text{eff}} = \frac{N}{\left( \sum_k \frac{P_{\text{sig},k}^2(\boldsymbol{\mu})}{P_{\text{bkg},k}(\boldsymbol{\theta})} \right) - 1}, \quad (\text{F.2})$$

where the summation runs over all pixels in the ROI and all the energy bins and  $N$  is the total number of events in the ROI and energy range. This definition has a few useful properties. First, if the only free parameters in the fit are the overall normalizations of the signal and background components, then in the limit that the signal is much smaller than the background the statistical uncertainty on the number of signal counts will be  $\delta n_{\text{sig}} \simeq \sqrt{b_{\text{eff}}}$ . Second, if the signal and background models are totally degenerated ( $P_{\text{sig},k}(\boldsymbol{\mu}) = P_{\text{bkg},k}(\boldsymbol{\theta})$  for all  $k$ ), then the term in the summation will be equal to 1 and  $b_{\text{eff}}$  will diverge, indicating that we have little power to distinguish signal from background. If this were the case, the statistical errors for the likelihood fit would be extremely large, corresponding to an upper limit on the cross section sufficient to generate all of the observed events through DM annihilation. Finally, if the signal and background models differ significantly the term in the summation will be much greater than 1 and  $b_{\text{eff}}$  will be proportionally less than  $N$ . That is, the statistical uncertainty on the signal will correspond to an effective background that is much less than the total number of

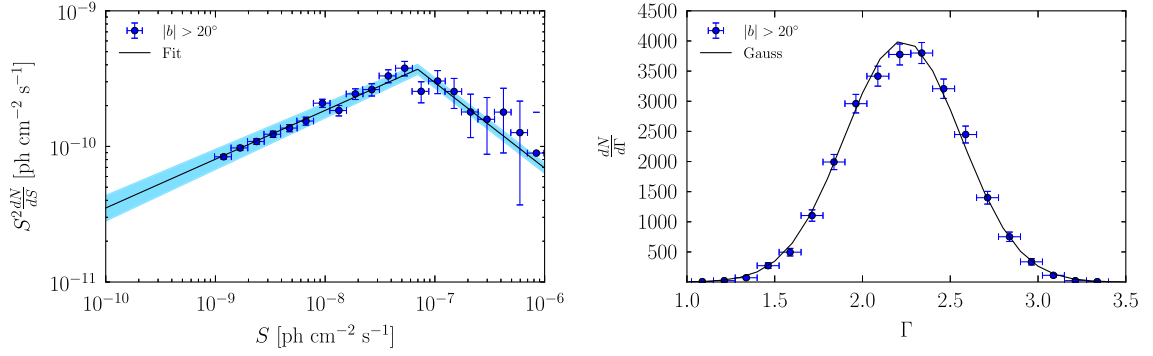


**Fig. G.32.** Left: Flux distribution of simulated blazars using the intrinsic  $dN/dS$  of the 1FGL catalog [328] (blue points) together with a fit (black solid line) and the  $1\sigma$  uncertainty band (cyan). Right: photon index distribution of simulated blazars from the observed distribution of sources in the 3FGL catalog [329]. The black curve is the best-fit Gaussian distribution, with an average of 2.23 and a standard deviation of 0.33. (For interpretation of the references to colour in this figure legend, the reader is referred to the web version of this article.)

background events in the ROI. The LAT Collaboration has found empirically that by quantifying the systematic uncertainties of the astrophysical background modeling as a percentage of  $b_{\text{eff}}$ , we are often able to account for those uncertainties in the likelihood fitting procedure and include them in DM constraints.

In the best-case scenario, where the background is well modeled, the expected uncertainty of the number of signal events is simply  $\delta n_{\text{sig}} = b_{\text{eff}}^{1/2}$ . We can then define the ratio of the signal to the effective background as  $f_{\text{sig}}$ , and the estimate of the statistical uncertainty  $\delta f_{\text{stat}}$  in terms of the effective background:

$$f_{\text{sig}} = \frac{n_{\text{sig}}}{b_{\text{eff}}}, \quad (\text{F.3})$$

$$\delta f_{\text{stat}} = \frac{\delta n_{\text{sig}}}{b_{\text{eff}}} \simeq b_{\text{eff}}^{-1/2}. \quad (\text{F.4})$$

Using the exposure,  $J$  factor, and the per-annihilation  $\gamma$ -ray spectra we can convert from  $\delta n_{\text{sig}}$  to the uncertainty on the thermally averaged annihilation cross section  $\delta\langle\sigma v\rangle$ . Furthermore, when the number of background events is large and well into the Gaussian regime, we can estimate the median upper limits ( $1.645\delta\langle\sigma v\rangle$ ), the 68% containment band ( $0.925\delta\langle\sigma v\rangle$ – $2.645\delta\langle\sigma v\rangle$ ) and the 95% containment band ( $0.590\delta\langle\sigma v\rangle$ – $3.645\delta\langle\sigma v\rangle$ ) in terms of  $\delta\langle\sigma v\rangle$ .

In practical terms, we note that in many cases systematic biases could either induce a fake signal or mask a true signal much larger than the expected statistical uncertainties. From the width of the distribution of  $f_{\text{sig}}$  for the trials in control regions, where we do not expect to detect any signal, we can estimate the total (statistical + systematic) uncertainty. When  $f_{\text{stat}} < f_{\text{sig}}$ , the total error is dominated by systematic uncertainties. When our fitting procedure allows for negative signals (such as in the searches for spectral lines) we can take a simple measure of the width such as the root-mean-square of the distribution. However, in many cases our fitting procedure only allows for positive signals and approximately half of the trials have  $f_{\text{sig}} = 0$ . In those cases we assign as our estimate of the systematic error the difference (taken in quadrature) of the  $1\sigma$  (84% CL) enclosure of the total error estimate and the statistical error estimate from the control region:

$$\delta f_{\text{syst}}^2 = f_{\text{sig}}^2(84\%) - \delta f_{\text{stat}}^2(84\%). \quad (\text{F.5})$$

## Appendix G. Projecting the uncertainty of contributions to the extragalactic gamma-ray background

We have estimated the point source sensitivity map for 15 years of observations by following the procedure described in the 2FGL catalog [55]. A four year sensitivity map is shown in Fig. 4.

For 15 years of data, the average high latitude ( $|b| > 20^\circ$ ) integrated energy flux detection threshold for a source with a photon index of  $\Gamma = 2.2$  is  $\sim 1.1 \times 10^{-9} \text{ ph cm}^{-2} \text{ s}^{-1}$  ( $> 100 \text{ MeV}$ ).

We have modeled the intrinsic source count distribution of blazars (i.e., distribution of the true fluxes),  $dN/dS$ , where  $S$  is the photon flux for  $E > 100 \text{ MeV}$ , of the 1FGL catalog [328] as a broken power law with a flux break at  $7 \times 10^{-8} \text{ ph cm}^{-2} \text{ s}^{-1}$  and a slope above (below) the break equal to 2.63 (1.64). We modeled the fluxes of the individual blazars with single power laws with index  $\Gamma$ . Given this flux distribution the predicted number of detected blazars with 15 years of data is about 3300.

In Fig. G.32 we show the distributions of  $S^2 dN/dS$  and photon index,  $dN/d\Gamma$ , for this sample of simulated blazars.

We can then estimate the contribution of blazars, which are the most numerous source population in  $\gamma$ -ray catalogs (see, e.g., [329]), to the EGB. Specifically, for each source (indexed by  $i$ ), the flux  $S_i$  and index  $\Gamma_i$  are sampled from the distributions shown in Fig. G.32 and the energy spectrum  $dN/dE_i$  is derived from the definition of the photon flux ( $S = \int dN/dE dE$ ). Finally, we sum all of the simulated spectra and average over the solid angle,  $|b| > 20^\circ$ , to obtain the contribution of blazars



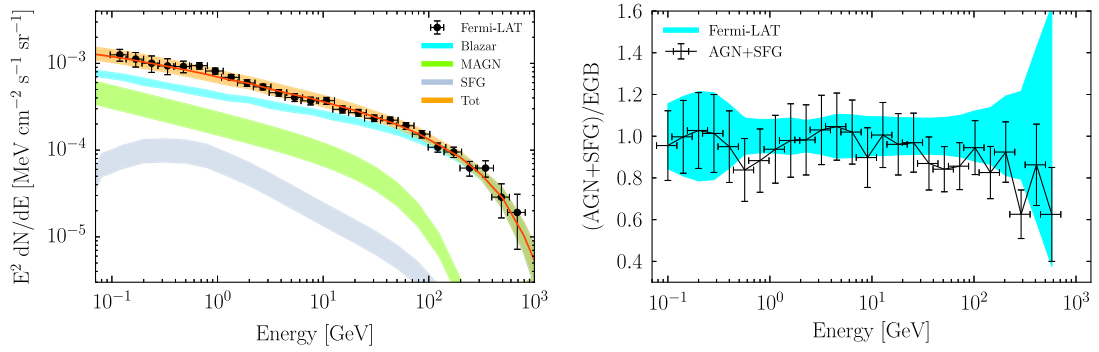


**Fig. G.33.** Left: contribution of blazars (cyan band), MAGN (green band) and SFGs (gray band) to the *Fermi*-LAT EGB data (black points). The total best fit of the summed contributions from AGN (blazars and MAGN) and SFG is depicted with a solid red line, with the orange uncertainties given by the orange band. Right: fraction of the AGN plus SFG contribution relative to the EGB (black points) together with the statistical EGB errors (cyan band). (For interpretation of the references to colour in this figure legend, the reader is referred to the web version of this article.)

to the EGB. The result for blazars is displayed in the left-hand panel of Fig. G.33 where their average contribution to the EGB is 65% with an uncertainty of about 10%.

We have followed the same procedure to estimate the uncertainty for the MAGN contribution to the EGB. We used the same intrinsic source count distribution, but rescaling the number of sources with a factor of 1/50, to match the ratio of MAGN to blazars observed in the 3FGL catalog. We predict a total of  $\sim 70$  MAGN detectable in 15 years and we predict an uncertainty of the order of 30% for the contribution of this source population to the EGB. We consider the same level of uncertainty to apply to the contribution of Star-Forming Galaxies (SFG) as well.

The contributions of blazars, MAGN, and SFG populations to the EGB are shown in Fig. G.33 (left panel). The total  $\gamma$ -ray emission from these source populations is consistent with the EGB measurement derived with 50 months of data [64] (see right panel of Fig. G.33). The uncertainties of the contributions of MAGN and SFG are a factor of  $\sim 4$  smaller than the uncertainties of their contributions from the analyses of the current LAT catalog [77,110] due to the increased number of detected sources with 15 years of data.

## Appendix H. Projecting the sensitivity of the angular power spectrum analysis

In order predict to the sensitivity of the LAT to DM signals in the APS we have used the same formalism as in Ref. [124]. That work considered the APS produced by the unresolved flux of populations of unclustered point sources, which is given by:

$$C_P(E_0 \leq E \leq E_1) = \int_{\Gamma_{\min}}^{\Gamma_{\max}} d\Gamma \int_0^{S_t(\Gamma)} S^2 \frac{d^2 N}{dS d\Gamma} dS, \quad (\text{H.1})$$

where  $S$  is the photon flux of the source integrated in the range  $E_0 \leq E \leq E_1$ ,  $S_t(\Gamma)$  denotes the flux detection threshold as a function of  $\Gamma$  and  $d^2 N/(dS d\Gamma)$  is the differential number of sources per unit flux  $S$ , unit photon index  $\Gamma$  and unit solid angle. We take  $S_t(\Gamma)$  to be constant in  $\Gamma$  because we restrict the analysis to energies  $> 1$  GeV where the bias for the source detection with respect to the photon index is small. We evaluate  $S_t(\Gamma)$  as the average value of the point source sensitivity for 15 years of exposure at  $|b| > 30^\circ$  and  $E > 1$  GeV:  $S_t \approx 1 \times 10^{-10}$  ph cm $^{-2}$  s $^{-1}$ . Using this model we have derived the  $C_P(E)$  in the same energy bins as in Ref. [60]. The results are displayed in Fig. H.34. With 15 years of data the threshold flux is lower by about a factor of 5 with respect to the threshold from two years of data, therefore the APS from unresolved AGN is also lower. However, different source populations have different intrinsic flux distribution, resulting in different scaling behaviors for  $C_P(E)$ . The  $C_P(E)$  for MAGN, for example, decreases by about a factor of 3, while for Flat Spectrum Radio Quasars (FSRQ) it decreases by a factor of 7. MAGN and low-intermediate synchrotron peak BL Lac objects (LISP) have steeper source count distributions, below the flux threshold, than High-Synchrotron Peak BL Lacertae objects (HSP) and FSRQ. Therefore, with lower flux thresholds the angular power for unresolved MAGN and LISP are reduced by a smaller factor than for HSP and FSRQ sources. Since the  $C_P(E)$  of astrophysical sources are lower we have rescaled the LAT data by a factor of 1/5 in Fig. H.34 so as to match the theoretical predictions from AGN.

We used the results shown in Fig. H.34 to project the LAT sensitivity to a DM contribution of extragalactic subhalos in the case of a  $b\bar{b}$  annihilation channel. We used the APS data in four energy bins [60] independently, and derived 95% CL limits on  $\langle \sigma v \rangle$  by requiring that the sum of the DM-induced intensity APS averaged in the multipole range  $155 < l < 204$  and our prediction for the Radio Loud AGN contribution to  $C_P$  not exceeding the measured  $C_P$  in the  $155 < l < 504$  multipole range plus 1.64 times the uncertainty. We show the projected limits for each energy bin as well as the envelope produced by the limits for all four energy bins in Fig. 22 in Section 4.8.4.

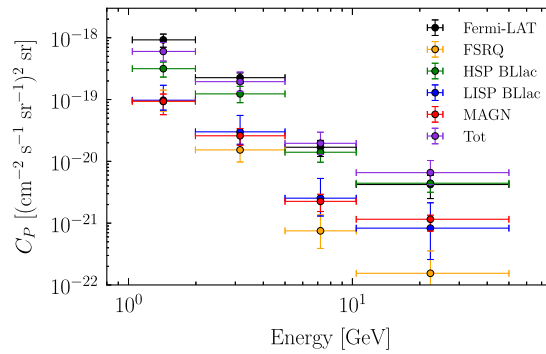


**Fig. H.34.** Angular power  $C_P(E)$  for MAGN (red long-dashed points), LISP (blue short-dashed), HSP (green dotted), FSRQ (yellow dot-dashed), and the total anisotropy (violet solid) from all the radio-loud AGNs. The data are a rescaled version, with a factor 1/5, of the measured APS in Ref. [60] (black solid points). (For interpretation of the references to colour in this figure legend, the reader is referred to the web version of this article.)

## Appendix I. List of acronyms and abbreviations

1FGL	First <i>Fermi</i> -LAT Source Catalog
2FGL	Second <i>Fermi</i> -LAT Source Catalog
3FGL	Third <i>Fermi</i> -LAT Source Catalog
AGN	Active Galactic Nucleus
ALP	Axion-Like Particle
APS	Angular Power Spectrum
CMB	Cosmic Microwave Background
DES	Dark Energy Survey
DM	Dark Matter
dSph	Dwarf Spheroidal Galaxy
EBL	Extragalactic Background Light
EGB	Extragalactic Gamma-ray Background
EFT	Effective Field Theory
FSRQ	Flat-Spectrum Radio Quasar
GRB	Gamma-Ray Burst
IACT	Imaging Atmospheric Cerenkov Telescope
ICM	Intra-Cluster Medium
IGRB	Isotropic Gamma-Ray Background
IRF	Instrument Response Function
LAT	Large Area Telescope
LHC	Large Hadron Collider
LMC	Large Magellanic Cloud
l.o.s.	line-of-sight
LSS	Large-Scale Structure
MAGN	Misaligned AGN
PBH	Primordial Black Hole
pNGB	pseudo-Nambu–Goldstone Boson
ROI	Region of Interest
SDSS	Sloan Digital Sky Survey
SFG	Star-Forming Galaxy
SMC	Small Magellanic Cloud
WIMP	Weakly Interacting Massive Particle

## References

- [1] W. Atwood, et al., The large area telescope on the *Fermi* gamma-ray space telescope mission, *Astrophys. J.* 697 (2009) 1071–1102. <http://dx.doi.org/10.1088/0004-637X/697/2/1071>. [arXiv:0902.1089](https://arxiv.org/abs/0902.1089).
- [2] D. Hooper, L. Goodenough, Dark matter annihilation in the Galactic center as seen by the *Fermi* gamma ray space telescope, *Phys. Lett. B* 697 (2011) 412–428. <http://dx.doi.org/10.1016/j.physletb.2011.02.029>. [arXiv:1010.2752](https://arxiv.org/abs/1010.2752).
- [3] K.N. Abazajian, et al., A astrophysical and dark matter interpretations of extended gamma-ray emission from the Galactic center, *Phys. Rev. D* 90 (2) (2014) 023526. <http://dx.doi.org/10.1103/PhysRevD.90.023526>. [arXiv:1402.4090](https://arxiv.org/abs/1402.4090).

- [4] T. Daylan, et al., The characterization of the gamma-ray signal from the central Milky Way: A case for annihilating dark matter, *Phys. Dark Universe* 12 (2016) 1–23. <http://dx.doi.org/10.1016/j.dark.2015.12.005>. arXiv:1402.6703.
- [5] M. Ackermann, et al., Searching for dark matter annihilation from Milky Way Dwarf spheroidal galaxies with six years of Fermi large area telescope data, *Phys. Rev. Lett.* 115 (23) (2015) 231301. <http://dx.doi.org/10.1103/PhysRevLett.115.231301>. arXiv:1503.02641.
- [6] J.L. Feng, Dark matter candidates from particle physics and methods of detection, *Annu. Rev. Astron. Astrophys.* 48 (2010) 495–545. <http://dx.doi.org/10.1146/annurev-astro-082708-101659>. arXiv:1003.0904.
- [7] T.A. Porter, R.P. Johnson, P.W. Graham, Dark matter searches with astroparticle data, *Annu. Rev. Astron. Astrophys.* 49 (2011) 155–194. <http://dx.doi.org/10.1146/annurev-astro-081710-102528>. arXiv:1104.2836.
- [8] J. Conrad, J. Cohen-Tanugi, L.E. Strigari, Wimp searches with gamma rays in the Fermi era: Challenges, methods and results, *Sov. J. Exp. Theor. Phys.* 121 (2015) 1104–1135. <http://dx.doi.org/10.1134/S1063776115130099>. arXiv:1503.06348.
- [9] G. Bertone, D. Hooper, J. Silk, Particle dark matter: evidence, candidates and constraints, *Phys. Rep.* 405 (2005) 279–390. <http://dx.doi.org/10.1016/j.physrep.2004.08.031>. arXiv:hep-ph/0404175.
- [10] V. Rubin, N. Thonnard, J. Ford, W. K., Rotational properties of 21 SC galaxies with a large range of luminosities and radii, from NGC 4605/R = 4kpc/ to UGC 2885/R = 122 kpc/, *Astrophys. J.* 238 (1980) 471. <http://dx.doi.org/10.1086/158003>.
- [11] F. Zwicky, Die Rotverschiebung von extragalaktischen Nebeln, *Helv. Phys. Acta* 6 (1933) 110–127.
- [12] P. Ade, et al., Planck 2013 results. XVI. Cosmological parameters, *Astron. Astrophys.* 571 (2014) A16. <http://dx.doi.org/10.1051/0004-6361/201321591>. arXiv:1303.5076.
- [13] P.A.R. Ade, et al., Planck 2015 results. XIII. Cosmological parameters, ArXiv e-prints arXiv:1502.01589.
- [14] K.A. Olive, TASI lectures on dark matter, ArXiv e-prints arXiv:astro-ph/0301505.
- [15] C.S. Frenk, S.D.M. White, Dark matter and cosmic structure, *Ann. Phys.* 524 (2012) 507–534. <http://dx.doi.org/10.1002/andp.201200212>. arXiv:1210.0544.
- [16] M. Markevitch, et al., Direct constraints on the dark matter self-interaction cross-section from the merging galaxy cluster 1E0657-56, *Astrophys. J.* 606 (2004) 819–824. <http://dx.doi.org/10.1086/383178>. arXiv:astro-ph/0309303.
- [17] D. Akerib, et al., First results from the LUX dark matter experiment at the Sanford underground research facility, *Phys. Rev. Lett.* 112 (9) (2014) 091303. <http://dx.doi.org/10.1103/PhysRevLett.112.091303>. arXiv:1310.8214.
- [18] G. Steigman, B. Dasgupta, J.F. Beacom, Precise relic WIMP abundance and its impact on searches for dark matter annihilation, *Phys. Rev. D* 86 (2) (2012) 023506. <http://dx.doi.org/10.1103/PhysRevD.86.023506>. arXiv:1204.3622.
- [19] S. Campbell, B. Dutta, E. Komatsu, Effects of velocity-dependent dark matter annihilation on the energy spectrum of the extragalactic gamma-ray background, *Phys. Rev. D* 82 (9) (2010) 095007. <http://dx.doi.org/10.1103/PhysRevD.82.095007>. arXiv:1009.3530.
- [20] H. Baer, et al., Dark matter production in the early Universe: Beyond the thermal WIMP paradigm, *Phys. Rep.* 555 (2015) 1–60. <http://dx.doi.org/10.1016/j.physrep.2014.10.002>. arXiv:1407.0017.
- [21] L. Bergström, Dark matter evidence, particle physics candidates and detection methods, *Ann. Phys.* 524 (2012) 479–496. <http://dx.doi.org/10.1002/andp.201200116>. arXiv:1205.4882.
- [22] J.L. Feng, J. Kumar, The WIMPless miracle: dark-matter particles without weak-scale masses or weak interactions, *Phys. Rev. Lett.* 101 (2008) 231301. <http://dx.doi.org/10.1103/PhysRevLett.101.231301>. arXiv:0803.4196.
- [23] N. Arkani-Hamed, et al., A theory of dark matter, *Phys. Rev. D* 79 (2009) 015014. <http://dx.doi.org/10.1103/PhysRevD.79.015014>. arXiv:0810.0713.
- [24] A. Ibarra, D. Tran, C. Weniger, Indirect searches for decaying dark matter, *International J. Modern Phys. A* 28 (2013) 1330040. <http://dx.doi.org/10.1142/S0217751X13300408>. arXiv:1307.6434.
- [25] A.A. Abdo, et al., Measurement of the cosmic ray  $e^+ + e^-$  spectrum from 20 GeV to 1 TeV with the Fermi large area telescope, *Phys. Rev. Lett.* 102 (18) (2009) 181101. <http://dx.doi.org/10.1103/PhysRevLett.102.181101>. arXiv:0905.0025.
- [26] M. Ackermann, et al., Fermi LAT observations of cosmic-ray electrons from 7 GeV to 1 TeV, *Phys. Rev. D* 82 (9) (2010) 092004. <http://dx.doi.org/10.1103/PhysRevD.82.092004>. arXiv:1008.3999.
- [27] M. Ackermann, et al., Searches for cosmic-ray electron anisotropies with the Fermi large area telescope, *Phys. Rev. D* 82 (9) (2010) 092003. <http://dx.doi.org/10.1103/PhysRevD.82.092003>. arXiv:1008.5119.
- [28] M. Ackermann, et al., Measurement of separate cosmic-ray electron and positron spectra with the Fermi large area telescope, *Phys. Rev. Lett.* 108 (1) (2012) 011103. <http://dx.doi.org/10.1103/PhysRevLett.108.011103>. arXiv:1109.0521.
- [29] P. Ullio, et al., Cosmological dark matter annihilations into gamma-rays—a closer look, *Phys. Rev. D* 66 (2002) 123502. <http://dx.doi.org/10.1103/PhysRevD.66.123502>. arXiv:astro-ph/0207125.
- [30] R. Catena, P. Ullio, A novel determination of the local dark matter density, *J. Cosmol. Astropart. Phys.* 8 (2010) 004. <http://dx.doi.org/10.1088/1475-7516/2010/08/004>. arXiv:0907.0018.
- [31] J. Bovy, S. Tremaine, On the local dark matter density, *Astrophys. J.* 756 (2012) 89. <http://dx.doi.org/10.1088/0004-637X/756/1/89>. arXiv:1205.4033.
- [32] M. Pato, F. Iocco, G. Bertone, Dynamical constraints on the dark matter distribution in the Milky Way, *J. Cosmol. Astropart. Phys.* 12 (2015) 001. <http://dx.doi.org/10.1088/1475-7516/2015/12/001>. arXiv:1504.06324.
- [33] F. Nesti, P. Salucci, The dark matter halo of the Milky Way, *AD 2013, J. Cosmol. Astropart. Phys.* 7 (2013) 16. <http://dx.doi.org/10.1088/1475-7516/2013/07/016>. arXiv:1304.5127.
- [34] Y. Sofue, Grand rotation curve and dark matter halo in the Milky Way galaxy, *Publ. Astron. Soc. Japan* 64 (2012) 75. <http://dx.doi.org/10.1093/pasj/64.4.75>. arXiv:1110.4431.
- [35] M. Weber, W. de Boer, Determination of the local dark matter density in our galaxy, *Astron. Astrophys.* 509 (2010) A25. <http://dx.doi.org/10.1051/0004-6361/200913381>. arXiv:0910.4272.
- [36] J. Buch, et al., PPPC 4 DM secondary: a Poor particle physicist cookbook for secondary radiation from dark matter, *J. Cosmol. Astropart. Phys.* 9 (2015) 037. <http://dx.doi.org/10.1088/1475-7516/2015/09/037>. arXiv:1505.01049.
- [37] M. Kaplinghat, T. Linden, H.-B. Yu, Galactic center excess in  $\gamma$  rays from annihilation of self-interacting dark matter, *Phys. Rev. Lett.* 114 (21) (2015) 211303. <http://dx.doi.org/10.1103/PhysRevLett.114.211303>. arXiv:1501.03507.
- [38] T. Lacroix, et al., The Spatial Morphology of the Secondary Emission in the Galactic Center Gamma-Ray Excess, ArXiv e-prints arXiv:1512.01846.
- [39] G.A. Gómez-Vargas, et al., Constraints on WIMP annihilation for contracted dark matter in the inner galaxy with the Fermi-LAT, *J. Cosmol. Astropart. Phys.* 10 (2013) 29. <http://dx.doi.org/10.1088/1475-7516/2013/10/029>. arXiv:1308.3515.
- [40] T.E. Jeltema, S. Profumo, Fitting the gamma-ray spectrum from dark matter with DMFIT: GLAST and the Galactic center region, *J. Cosmol. Astropart. Phys.* 0811 (2008) 003. <http://dx.doi.org/10.1088/1475-7516/2008/11/003>. arXiv:0808.2641.
- [41] S. Weinberg, A new light boson? *Phys. Rev. Lett.* 40 (1978) 223–226. <http://dx.doi.org/10.1103/PhysRevLett.40.223>.
- [42] F. Wilczek, Problem of strong P and T invariance in the presence of instantons, *Phys. Rev. Lett.* 40 (1978) 279–282. <http://dx.doi.org/10.1103/PhysRevLett.40.279>.
- [43] R.D. Peccei, H.R. Quinn, CP conservation in the presence of pseudoparticles, *Phys. Rev. Lett.* 38 (1977) 1440–1443. <http://dx.doi.org/10.1103/PhysRevLett.38.1440>.
- [44] J. Jaeckel, A. Ringwald, The low-energy frontier of particle physics, *Annu. Rev. Nucl. Part. Sci.* 60 (2010) 405–437. <http://dx.doi.org/10.1146/annurev.nucl.012809.104433>. arXiv:1002.0329.
- [45] E. Witten, Some properties of O(32) superstrings, *Phys. Lett. B* 149 (1984) 351–356. [http://dx.doi.org/10.1016/0370-2693\(84\)90422-2](http://dx.doi.org/10.1016/0370-2693(84)90422-2).
- [46] A. Ringwald, Axions and Axion-Like Particles, ArXiv e-prints arXiv:1407.0546.
- [47] L.F. Abbott, P. Sikivie, A cosmological bound on the invisible axion, *Phys. Lett. B* 120 (1983) 133–136. [http://dx.doi.org/10.1016/0370-2693\(83\)90638-X](http://dx.doi.org/10.1016/0370-2693(83)90638-X).

- [48] J. Preskill, M.B. Wise, F. Wilczek, Cosmology of the invisible axion, *Phys. Lett. B* 120 (1983) 127–132. [http://dx.doi.org/10.1016/0370-2693\(83\)90637-8](http://dx.doi.org/10.1016/0370-2693(83)90637-8).
- [49] M. Dine, W. Fischler, The not-so-harmless axion, *Phys. Lett. B* 120 (1983) 137–141. [http://dx.doi.org/10.1016/0370-2693\(83\)90639-1](http://dx.doi.org/10.1016/0370-2693(83)90639-1).
- [50] D.J.E. Marsh, Axiverse extended: Vacuum destabilization, early dark energy, and cosmological collapse, *Phys. Rev. D* 83 (12) (2011) 123526. <http://dx.doi.org/10.1103/PhysRevD.83.123526>. arXiv:1102.4851.
- [51] P. Arias, et al., WISPy cold dark matter, *J. Cosmol. Astropart. Phys.* 6 (2012) 13. <http://dx.doi.org/10.1088/1475-7516/2012/06/013>. arXiv:1201.5902.
- [52] G. Raffelt, L. Stodolsky, Mixing of the photon with low-mass particles, *Phys. Rev. D* 37 (1988) 1237–1249. <http://dx.doi.org/10.1103/PhysRevD.37.1237>.
- [53] F. Acero, et al., Fermi large area telescope third source catalog, *Astrophys. J. Suppl.* 218 (2015) 23. <http://dx.doi.org/10.1088/0067-0049/218/2/23>. arXiv:1501.02003.
- [54] A.A. Abdo, et al., Fermi large area telescope first source catalog, *Astrophys. J. Suppl.* 188 (2010) 405–436. <http://dx.doi.org/10.1088/0067-0049/188/2/405>. arXiv:1002.2280.
- [55] P.L. Nolan, et al., Fermi large area telescope second source catalog, *Astrophys. J. Suppl.* 199 (2012) 31. <http://dx.doi.org/10.1088/0067-0049/199/2/31>. arXiv:1108.1435.
- [56] F. Massaro, et al., Refining the associations of the Fermi large area telescope source catalogs, *Astrophys. J. Suppl.* 217 (2015) 2. <http://dx.doi.org/10.1088/0067-0049/217/1/2>. arXiv:1503.05556.
- [57] C. Weniger, A tentative gamma-ray line from dark matter annihilation at the Fermi large area telescope, *J. Cosmol. Astropart. Phys.* 1208 (2012) 007. <http://dx.doi.org/10.1088/1475-7516/2012/08/007>. arXiv:1204.2797.
- [58] M. Ackermann, et al., Search for gamma-ray spectral lines with the Fermi large area telescope and dark matter implications, *Phys. Rev. D* 88 (8) (2013) 082002. <http://dx.doi.org/10.1103/PhysRevD.88.082002>.
- [59] M. Ackermann, et al., Updated search for spectral lines from Galactic dark matter interactions with pass 8 data from the Fermi large area telescope, *Phys. Rev. D* 91 (12) (2015) 122002. <http://dx.doi.org/10.1103/PhysRevD.91.122002>.
- [60] M. Ackermann, et al., Anisotropies in the diffuse gamma-ray background measured by the Fermi LAT, *Phys. Rev. D* 85 (8) (2012) 083007. <http://dx.doi.org/10.1103/PhysRevD.85.083007>. arXiv:1202.2856.
- [61] J.-Q. Xia, et al., Tomography of the Fermi-lat  $\gamma$ -ray diffuse extragalactic signal via cross correlations with galaxy catalogs, *Astrophys. J. Suppl.* 217 (1) (2015) 15. <http://dx.doi.org/10.1088/0067-0049/217/1/15>. arXiv:1503.05918.
- [62] M. Ackermann, et al., Fermi-LAT Observations of the diffuse  $\gamma$ -ray emission: Implications for cosmic rays and the interstellar medium, *Astrophys. J.* 750 (2012) 3. <http://dx.doi.org/10.1088/0004-637X/750/1/3>. arXiv:1202.4039.
- [63] T. Delahaye, et al., The GeV–TeV Galactic gamma-ray diffuse emission. I. Uncertainties in the predictions of the hadronic component, *Astron. Astrophys.* 531 (2011) A37. <http://dx.doi.org/10.1051/0004-6361/201116647>. arXiv:1102.0744.
- [64] M. Ackermann, et al., The spectrum of isotropic diffuse gamma-ray emission between 100 MeV and 820 GeV, *Astrophys. J.* 799 (2015) 86. <http://dx.doi.org/10.1088/0004-637X/799/1/86>. arXiv:1410.3696.
- [65] M. Ackermann, et al., Constraints on the Galactic halo dark matter from Fermi-LAT diffuse measurements, *Astrophys. J.* 761 (2012) 91. <http://dx.doi.org/10.1088/0004-637X/761/2/91>. arXiv:1205.6474.
- [66] F. Calore, I. Cholis, C. Weniger, Background model systematics for the Fermi GeV excess, *J. Cosmol. Astropart. Phys.* 3 (2015) 38. <http://dx.doi.org/10.1088/1475-7516/2015/03/038>. arXiv:1409.0042.
- [67] M. Ajello, et al., Fermi-LAT observations of high-energy gamma-ray emission toward the Galactic center, *Astrophys. J.* 819 (2016) 44. <http://dx.doi.org/10.3847/0004-637X/819/1/44>. arXiv:1511.02938.
- [68] P.M.W. Kalberla, U. Haud, GASS: The Parkes Galactic all-sky survey. Update: improved correction for instrumental effects and new data release, *Astron. Astrophys.* 578 (2015) A78. <http://dx.doi.org/10.1051/0004-6361/201525859>. arXiv:1505.01011.
- [69] B. Winkel, et al., The Effelsberg-Bonn H I survey: Milky Way gas. First data release, *Astron. Astrophys.* 585 (2016) A41. <http://dx.doi.org/10.1051/0004-6361/201527007>. arXiv:1512.05348.
- [70] D. Malyshev, I. Cholis, J.D. Gelfand, Fermi Gamma-ray Haze via dark matter and millisecond pulsars, *Astrophys. J.* 722 (2010) 1939–1945. <http://dx.doi.org/10.1088/0004-637X/722/2/1939>. arXiv:1002.0587.
- [71] N. Mirabal, Dark matter versus pulsars: catching the impostor, *Mon. Not. R. Astron. Soc.* 436 (2013) 2461–2464. <http://dx.doi.org/10.1093/mnras/stt1740>. arXiv:1309.3428.
- [72] D. Hooper, et al., Millisecond pulsars cannot account for the inner Galaxy's GeV excess, *Phys. Rev. D* 88 (8) (2013) 083009. <http://dx.doi.org/10.1103/PhysRevD.88.083009>. arXiv:1305.0830.
- [73] R.M. O'Leary, et al., Young Pulsars and the Galactic Center GeV Gamma-ray Excess, ArXiv e-prints arXiv:1504.02477.
- [74] J. Petrović, P.D. Serpico, G. Zaharijas, Millisecond pulsars and the Galactic center gamma-ray excess: the importance of luminosity function and secondary emission, *J. Cosmol. Astropart. Phys.* 2 (2015) 23. <http://dx.doi.org/10.1088/1475-7516/2015/02/023>. arXiv:1411.2980.
- [75] I. Cholis, D. Hooper, T. Linden, Challenges in explaining the Galactic center gamma-ray excess with millisecond pulsars, *J. Cosmol. Astropart. Phys.* 6 (2015) 43. <http://dx.doi.org/10.1088/1475-7516/2015/06/043>. arXiv:1407.5625.
- [76] M. Fornasa, M.A. Sánchez-Conde, The nature of the diffuse gamma-ray background, *Phys. Rep.* 598 (2015) 1–58. <http://dx.doi.org/10.1016/j.physrep.2015.09.002>. arXiv:1502.02866.
- [77] M. Ajello, et al., The origin of the extragalactic gamma-ray background and implications for dark-matter annihilation, *Astrophys. J.* 800 (2) (2015) L27. <http://dx.doi.org/10.1088/2041-8205/800/2/L27>. arXiv:1501.05301.
- [78] T. Mizuno, et al., Cosmic-ray background flux model based on a gamma-ray large area space telescope balloon flight engineering model, *Astrophys. J.* 614 (2004) 1113–1123. <http://dx.doi.org/10.1086/423801>. arXiv:astro-ph/0406684.
- [79] M. Ackermann, et al., The Fermi large area telescope on orbit: Event classification, instrument response functions, and calibration, *Astrophys. J. Suppl.* 203 (2012) 4. <http://dx.doi.org/10.1088/0067-0049/203/1/4>. arXiv:1206.1896.
- [80] W. Atwood, et al., Pass 8: Toward the Full Realization of the Fermi-LAT Scientific Potential, ArXiv e-prints arXiv:1303.3514.
- [81] F. Calore, et al., A tale of tails: Dark matter interpretations of the Fermi GeV excess in light of background model systematics, *Phys. Rev. D* 91 (6) (2015) 063003. <http://dx.doi.org/10.1103/PhysRevD.91.063003>. arXiv:1411.4647.
- [82] C. Gordon, O. Macías, Dark matter and pulsar model constraints from Galactic center Fermi-LAT gamma-ray observations, *Phys. Rev. D* 88 (8) (2013) 083521. <http://dx.doi.org/10.1103/PhysRevD.88.083521>. arXiv:1306.5725.
- [83] K.N. Abazajian, R.E. Keeley, Bright gamma-ray Galactic Center excess and dark dwarfs: Strong tension for dark matter annihilation despite Milky Way halo profile and diffuse emission uncertainties, *Phys. Rev. D* 93 (8) (2016) 083514. <http://dx.doi.org/10.1103/PhysRevD.93.083514>. arXiv:1510.06424.
- [84] X. Huang, T. Enßlin, M. Selig, Galactic dark matter search via phenomenological astrophysics modeling, *J. Cosmol. Astropart. Phys.* 4 (2016) 030. <http://dx.doi.org/10.1088/1475-7516/2016/04/030>. arXiv:1511.02621.
- [85] B. Zhou, et al., GeV excess in the Milky Way: The role of diffuse Galactic gamma-ray emission templates, *Phys. Rev. D* 91 (12) (2015) 123010. <http://dx.doi.org/10.1103/PhysRevD.91.123010>. arXiv:1406.6948.
- [86] A. Drlica-Wagner, et al., Search for gamma-ray emission from DES dwarf spheroidal galaxy candidates with Fermi-LAT data, *Astrophys. J.* 809 (2015) L4. <http://dx.doi.org/10.1088/2041-8205/809/1/L4>. arXiv:1503.02632.
- [87] A. Geringer-Sameth, S.M. Koushiappas, M.G. Walker, Comprehensive search for dark matter annihilation in dwarf galaxies, *Phys. Rev. D* 91 (8) (2015) 083535. <http://dx.doi.org/10.1103/PhysRevD.91.083535>. arXiv:1410.2242.
- [88] M. Ackermann, et al., Search for dark matter satellites using Fermi-LAT, *Astrophys. J.* 747 (2012) 121. <http://dx.doi.org/10.1088/0004-637X/747/2/121>. arXiv:1201.2691.



- [89] M.N. Mazziotta, et al., A model-independent analysis of the Fermi large area telescope gamma-ray data from the Milky Way dwarf galaxies and halo to constrain dark matter scenarios, *Astropart. Phys.* 37 (2012) 26–39. <http://dx.doi.org/10.1016/j.astropartphys.2012.07.005>. arXiv:1203.6731.
- [90] A. Geringer-Sameth, S.M. Koushiappas, Exclusion of canonical weakly interacting massive particles by joint analysis of Milky Way dwarf galaxies with data from the Fermi gamma-ray space telescope, *Phys. Rev. Lett.* 107 (24) (2011) 241303. <http://dx.doi.org/10.1103/PhysRevLett.107.241303>. arXiv:1108.2914.
- [91] M. Ackermann, et al., Constraining dark matter models from a combined analysis of Milky Way satellites with the Fermi large area telescope, *Phys. Rev. Lett.* 107 (24) (2011) 241302. <http://dx.doi.org/10.1103/PhysRevLett.107.241302>. arXiv:1108.3546.
- [92] A.A. Abdo, et al., Observations of Milky Way dwarf spheroidal galaxies with the Fermi-large area telescope detector and constraints on dark matter models, *Astrophys. J.* 712 (2010) 147–158. <http://dx.doi.org/10.1088/0004-637X/712/1/147>. arXiv:1001.4531.
- [93] S. Li, et al., Search for gamma-ray emission from eight dwarf spheroidal galaxy candidates discovered in year two of dark energy survey with Fermi-LAT data, *Phys. Rev. D* 93 (4) (2016) 043518. <http://dx.doi.org/10.1103/PhysRevD.93.043518>. arXiv:1511.09252.
- [94] Y.-L. Sming Tsai, Q. Yuan, X. Huang, A generic method to constrain the dark matter model parameters from Fermi observations of dwarf spheroids, *J. Cosmol. Astropart. Phys.* 3 (2013) 018. <http://dx.doi.org/10.1088/1475-7516/2013/03/018>. arXiv:1212.3990.
- [95] B. Bertoni, D. Hooper, T. Linden, Examining the Fermi-LAT third source catalog in search of dark matter subhalos, *J. Cosmol. Astropart. Phys.* 12 (2015) 035. <http://dx.doi.org/10.1088/1475-7516/2015/12/035>. arXiv:1504.02087.
- [96] B. Anderson, et al., Fermi-LAT sensitivity to dark matter annihilation in via Lactea II substructure, *Astrophys. J.* 718 (2010) 899–904. <http://dx.doi.org/10.1088/0004-637X/718/2/899>. arXiv:1006.1628.
- [97] L. Pieri, et al., Implications of high-resolution simulations on indirect dark matter searches, *Phys. Rev. D* 83 (2) (2011) 023518. <http://dx.doi.org/10.1103/PhysRevD.83.023518>. arXiv:0908.0195.
- [98] A.V. Belikov, et al., Searching for dark matter subhalos in the Fermi-LAT second source catalog, *Phys. Rev. D* 86 (4) (2012) 043504. <http://dx.doi.org/10.1103/PhysRevD.86.043504>. arXiv:1111.2613.
- [99] A. Berlin, D. Hooper, Stringent constraints on the dark matter annihilation cross section from subhalo searches with the Fermi gamma-ray space telescope, *Phys. Rev. D* 89 (1) (2014) 016014. <http://dx.doi.org/10.1103/PhysRevD.89.016014>. arXiv:1309.0525.
- [100] M. Ackermann, et al., Search for extended gamma-ray emission from the virgo galaxy cluster with FERMI-LAT, *Astrophys. J.* 812 (2015) 159. <http://dx.doi.org/10.1088/0004-637X/812/2/159>. arXiv:1510.00004.
- [101] M. Ackermann, et al., Constraints on dark matter annihilation in clusters of galaxies with the Fermi large area telescope, *J. Cosmol. Astropart. Phys.* 5 (2010) <http://dx.doi.org/10.1088/1475-7516/2010/05/025>. arXiv:1002.2239.
- [102] X. Huang, G. Vertongen, C. Weniger, Galaxy clusters and gamma-ray lines: Probing gravitino dark matter with the Fermi lat, *ArXiv e-prints* arXiv:1110.6236.
- [103] T. Arlen, et al., Constraints on cosmic rays, magnetic fields, and dark matter from gamma-ray observations of the coma cluster of galaxies with VERITAS and Fermi, *Astrophys. J.* 757 (2012) 123. <http://dx.doi.org/10.1088/0004-637X/757/2/123>. arXiv:1208.0676.
- [104] S. Ando, D. Nagai, Fermi-LAT constraints on dark matter annihilation cross section from observations of the Fornax cluster, *J. Cosmol. Astropart. Phys.* 7 (2012) 17. <http://dx.doi.org/10.1088/1475-7516/2012/07/017>. arXiv:1201.0753.
- [105] X. Huang, G. Vertongen, C. Weniger, Probing dark matter decay and annihilation with Fermi LAT observations of nearby galaxy clusters, *J. Cosmol. Astropart. Phys.* 1 (2012) 42. <http://dx.doi.org/10.1088/1475-7516/2012/01/042>. arXiv:1110.1529.
- [106] D.A. Prokhorov, An analysis of Fermi-LAT observations of the outskirts of the Coma cluster of galaxies, *Mon. Not. R. Astron. Soc.* 441 (2014) 2309–2315. <http://dx.doi.org/10.1093/mnras/stu707>.
- [107] M. Ackermann, et al., Search for gamma-ray emission from the coma cluster with six years of Fermi-LAT data, *Astrophys. J.* 819 (2016) 149. <http://dx.doi.org/10.3847/0004-637X/819/2/149>. arXiv:1507.08995.
- [108] Y.-F. Liang, et al., Search for Gamma-ray Line Feature from a Group of Nearby Galaxy Clusters with Fermi LAT Pass 8 Data, *ArXiv e-prints* arXiv:1602.06527.
- [109] S. Ando, K. Ishiwata, Constraints on decaying dark matter from the extragalactic gamma-ray background, *J. Cosmol. Astropart. Phys.* 1505 (05) (2015) 024. <http://dx.doi.org/10.1088/1475-7516/2015/05/024>. arXiv:1502.02007.
- [110] M. Di Mauro, F. Donato, Composition of the Fermi-LAT isotropic gamma-ray background intensity: Emission from extragalactic point sources and dark matter annihilations, *Phys. Rev. D* 91 (12) (2015) 123001. <http://dx.doi.org/10.1103/PhysRevD.91.123001>. arXiv:1501.05316.
- [111] M. Ackermann, et al., Limits on dark matter annihilation signals from the Fermi LAT 4-year measurement of the isotropic gamma-ray background, *J. Cosmol. Astropart. Phys.* 9 (2015) 008. <http://dx.doi.org/10.1088/1475-7516/2015/09/008>. arXiv:1501.05464.
- [112] A. Cuoco, et al., Dark matter searches in the gamma-ray extragalactic background via cross-correlations with galaxy catalogs, *Astrophys. J. Suppl.* 221 (2015) 29. <http://dx.doi.org/10.1088/0067-0049/221/2/29>. arXiv:1506.01030.
- [113] J.-Q. Xia, et al., A cross-correlation study of the Fermi-LAT  $\gamma$ -ray diffuse extragalactic signal, *Mon. Not. R. Astron. Soc.* 416 (2011) 2247–2264. arXiv:1103.4861.
- [114] A. Cuoco, et al., Angular signatures of annihilating dark matter in the cosmic gamma-ray background, *Phys. Rev. D* 77 (2008) 123518. <http://dx.doi.org/10.1103/PhysRevD.77.123518>. arXiv:0710.4136.
- [115] S. Ando, V. Pavlidou, Imprint of galaxy clustering in the cosmic gamma-ray background, *Mon. Not. R. Astron. Soc.* 400 (2009) 2122. <http://dx.doi.org/10.1111/j.1365-2966.2009.15605.x>. arXiv:0908.3890.
- [116] S. Ando, Power spectrum tomography of dark matter annihilation with local galaxy distribution, *J. Cosmol. Astropart. Phys.* 1410 (10) (2014) 061. <http://dx.doi.org/10.1088/1475-7516/2014/10/061>. arXiv:1407.8502.
- [117] N. Fornengo, et al., Evidence of cross-correlation between the CMB lensing and the  $\Gamma$ -ray sky, *Astrophys. J.* 802 (1) (2015) L1. <http://dx.doi.org/10.1088/2041-8205/802/1/L1>. arXiv:1410.4997.
- [118] S. Camera, et al., Tomographic-spectral approach for dark matter detection in the cross-correlation between cosmic shear and diffuse  $\gamma$ -ray emission, *J. Cosmol. Astropart. Phys.* 1506 (06) (2015) 029. <http://dx.doi.org/10.1088/1475-7516/2015/06/029>. arXiv:1411.4651.
- [119] M. Regis, et al., Particle dark matter searches outside the local group, *Phys. Rev. Lett.* 114 (24) (2015) 241301. <http://dx.doi.org/10.1103/PhysRevLett.114.241301>. arXiv:1503.05922.
- [120] S. Ando, A. Benoit-Lévy, E. Komatsu, Mapping dark matter in the gamma-ray sky with galaxy catalogs, *Phys. Rev. D* 90 (2) (2014) 023514. <http://dx.doi.org/10.1103/PhysRevD.90.023514>. arXiv:1312.4403.
- [121] M. Shirasaki, S. Horiuchi, N. Yoshida, Cross-correlation of cosmic shear and extragalactic gamma-ray background: Constraints on the dark matter annihilation cross-section, *Phys. Rev. D* 90 (6) (2014) 063502. <http://dx.doi.org/10.1103/PhysRevD.90.063502>. arXiv:1404.5503.
- [122] S. Camera, et al., A novel approach in the weakly interacting massive particle quest: Cross-correlation of gamma-ray anisotropies and cosmic shear, *Astrophys. J.* 771 (2013) L5. <http://dx.doi.org/10.1088/2041-8205/771/1/L5>. arXiv:1212.5018.
- [123] G.A. Gomez-Vargas, et al., Dark matter implications of Fermi-LAT measurement of anisotropies in the diffuse gamma-ray background, *Nucl. Instrum. Meth. A* 742 (2014) 149–153. <http://dx.doi.org/10.1016/j.nima.2013.11.009>.
- [124] M. Di Mauro, et al., Fermi-LAT  $\gamma$ -ray anisotropy and intensity explained by unresolved radio-loud active Galactic nuclei, *J. Cosmol. Astropart. Phys.* 1411 (11) (2014) 021. <http://dx.doi.org/10.1088/1475-7516/2014/11/021>. arXiv:1407.3275.
- [125] S.S. Campbell, Angular power spectra with finite counts, *Mon. Not. R. Astron. Soc.* 448 (3) (2015) 2854–2878. <http://dx.doi.org/10.1093/mnras/stv135>. arXiv:1411.4031.
- [126] F. Calore, et al.,  $\gamma$ -ray anisotropies from dark matter in the Milky Way: the role of the radial distribution, *Mon. Not. R. Astron. Soc.* 442 (2) (2014) 1151–1156. <http://dx.doi.org/10.1093/mnras/stu912>. arXiv:1402.0512.
- [127] N. Fornengo, M. Regis, Particle dark matter searches in the anisotropic sky, *Front. Phys.* 2 (2014) 6. <http://dx.doi.org/10.3389/fphys.2014.00006>. arXiv:1312.4835.



- [128] S.S. Campbell, J.F. Beacom, Combined Flux and Anisotropy Searches Improve Sensitivity to Gamma Rays from Dark Matter, ArXiv e-prints [arXiv:1312.3945](#).
- [129] Y. Inoue, et al., Probing the cosmic X-ray and MeV gamma-ray background radiation through the anisotropy, *Astrophys. J.* 776 (2013) 33. [http://dx.doi.org/10.1088/0004-637X/776/1/33](#). [arXiv:1308.1951](#).
- [130] A.E. Broderick, et al., Lower limits upon the anisotropy of the extragalactic gamma-ray background implied by the 2FGL and 1FHL catalogs, *Astrophys. J.* 796 (1) (2014) 12. [http://dx.doi.org/10.1088/0004-637X/796/1/12](#). [arXiv:1308.0015](#).
- [131] S. Ando, E. Komatsu, Constraints on the annihilation cross section of dark matter particles from anisotropies in the diffuse gamma-ray background measured with Fermi-LAT, *Phys. Rev. D* 87 (12) (2013) 123539. [http://dx.doi.org/10.1103/PhysRevD.87.123539](#). [arXiv:1301.5901](#).
- [132] J. Ripken, et al., The sensitivity of Cherenkov telescopes to dark matter and astrophysical anisotropies in the diffuse gamma-ray background, *J. Cosmol. Astropart. Phys.* 1401 (01) (2014) 049. [http://dx.doi.org/10.1088/1475-7516/2014/01/049](#). [arXiv:1211.6922](#).
- [133] J.P. Harding, K.N. Abazajian, Models of the contribution of blazars to the anisotropy of the extragalactic diffuse gamma-ray background, *J. Cosmol. Astropart. Phys.* 1211 (2012) 026. [http://dx.doi.org/10.1088/1475-7516/2012/11/026](#). [arXiv:1206.4734](#).
- [134] A. Cuoco, E. Komatsu, J.M. Siegal-Gaskins, Joint anisotropy and source count constraints on the contribution of blazars to the diffuse gamma-ray background, *Phys. Rev. D* 86 (2012) 063004. [http://dx.doi.org/10.1103/PhysRevD.86.063004](#). [arXiv:1202.5309](#).
- [135] S. Ando, E. Komatsu, Anisotropy of the cosmic gamma-ray background from dark matter annihilation, *Phys. Rev. D* 73 (2006) 023521. [http://dx.doi.org/10.1103/PhysRevD.73.023521](#). [arXiv:astro-ph/0512217](#).
- [136] S. Ando, et al., Dark matter annihilation or unresolved astrophysical sources? Anisotropy probe of the origin of cosmic gamma-ray background, *Phys. Rev. D* 75 (2007) 063519. [http://dx.doi.org/10.1103/PhysRevD.75.063519](#). [arXiv:astro-ph/0612467](#).
- [137] M. Fornasa, et al., Characterization of dark-matter-induced anisotropies in the diffuse gamma-ray background, *Mon. Not. R. Astron. Soc.* 429 (2013) 1529–1553. [http://dx.doi.org/10.1093/mnras/sts444](#). [arXiv:1207.0502](#).
- [138] M.R. Buckley, et al., Search for gamma-ray emission from dark matter annihilation in the large magellanic cloud with the Fermi large area telescope, *Phys. Rev. D* 91 (2015) 102001. [http://dx.doi.org/10.1103/PhysRevD.91.102001](#). [arXiv:1502.01020](#).
- [139] A. Albert, et al., Search for 100 MeV to 10 GeV  $\gamma$ -ray lines in the Fermi-LAT data and implications for gravitino dark matter in the  $\mu$ VSSM, *J. Cosmol. Astropart. Phys.* 10 (2014) 23. [http://dx.doi.org/10.1088/1475-7516/2014/10/023](#). [arXiv:1406.3430](#).
- [140] A. Burkert, The structure of dark matter halos in dwarf galaxies, *Astrophys. J.* 447 (1995) L25. [http://dx.doi.org/10.1086/309560](#). [arXiv:astro-ph/9504041](#).
- [141] J.F. Navarro, C.S. Frenk, S.D.M. White, The structure of cold dark matter halos, *Astrophys. J.* 462 (1996) 563. [http://dx.doi.org/10.1086/177173](#). [arXiv:arXiv:astro-ph/9508025](#).
- [142] A.V. Kravtsov, et al., The cores of dark matter-dominated galaxies: Theory versus observations, *Astrophys. J.* 502 (1998) 48–58. [http://dx.doi.org/10.1086/305884](#). [arXiv:astro-ph/9708176](#).
- [143] J.F. Navarro, et al., The diversity and similarity of simulated cold dark matter haloes, *Mon. Not. R. Astron. Soc.* 402 (2010) 21–34. [http://dx.doi.org/10.1111/j.1365-2966.2009.15878.x](#). [arXiv:0810.1522](#).
- [144] F. Iocco, M. Pato, G. Bertone, Evidence for dark matter in the inner Milky Way, *Nat. Phys.* 11 (2015) 245–248. [http://dx.doi.org/10.1038/nphys3237](#). [arXiv:1502.03821](#).
- [145] R. Durazo, X. Hernandez, S. Mendoza, Evidence for Dark Matter in the Inner Milky Way...Really? ArXiv e-prints [arXiv:1503.07501](#).
- [146] S. Garbari, et al., A new determination of the local dark matter density from the kinematics of K dwarfs, *Mon. Not. R. Astron. Soc.* 425 (2012) 1445–1458. [http://dx.doi.org/10.1111/j.1365-2966.2012.21608.x](#). [arXiv:1206.0015](#).
- [147] C. Moni Bidin, et al., No evidence of dark matter in the solar neighborhood, *Bol. Asoc. Argentina Astron. Plata Argentina* (2011) 289–292. [arXiv:1204.3919](#).
- [148] C. Moni Bidin, et al., Kinematical and chemical vertical structure of the Galactic thick disk. II. A lack of dark matter in the solar neighborhood, *Astrophys. J.* 751 (2012) 30. [http://dx.doi.org/10.1088/0004-637X/751/1/30](#). [arXiv:1204.3924](#).
- [149] C. Moni Bidin, et al., On the local dark matter density, in: *Revista Mexicana de Astronomia y Astrofisica Conference Series*, in: *Revista Mexicana de Astronomia y Astrofisica*, vol. 46, 2015, p. 105. [arXiv:1411.2625](#).
- [150] J. Stadel, et al., Quantifying the heart of darkness with GALAH—a multibillion particle simulation of a Galactic halo, *Mon. Not. R. Astron. Soc.* 398 (2009) L21–L25. [http://dx.doi.org/10.1111/j.1745-3933.2009.00699.x](#). [arXiv:0808.2981](#).
- [151] V. Springel, et al., The aquarius project: the subhaloes of Galactic haloes, *Mon. Not. R. Astron. Soc.* 391 (2008) 1685–1711. [http://dx.doi.org/10.1111/j.1365-2966.2008.14066.x](#). [arXiv:0809.0898](#).
- [152] P. Colin, O. Valenzuela, A. Klypin, Bars and cold dark matter halos, *Astrophys. J.* 644 (2006) 687–700. [http://dx.doi.org/10.1086/503791](#). [arXiv:astro-ph/0506627](#).
- [153] M. Gustafsson, M. Fairbairn, J. Sommer-Larsen, Baryonic pinching of galactic dark matter halos, *Phys. Rev. D* 74 (12) (2006) 123522. [http://dx.doi.org/10.1103/PhysRevD.74.123522](#). [arXiv:astro-ph/0608634](#).
- [154] P.B. Tissera, et al., Dark matter response to galaxy formation, *Mon. Not. R. Astron. Soc.* 406 (2010) 922–935. [http://dx.doi.org/10.1111/j.1365-2966.2010.16777.x](#). [arXiv:0911.2316](#).
- [155] O.Y. Gnedin, et al., Halo Contraction Effect in Hydrodynamic Simulations of Galaxy Formation, ArXiv e-prints [arXiv:1108.5736](#).
- [156] K.N. Abazajian, M. Kaplinghat, Detection of a gamma-ray source in the Galactic center consistent with extended emission from dark matter annihilation and concentrated astrophysical emission, *Phys. Rev. D* 86 (8) (2012) 083511. [http://dx.doi.org/10.1103/PhysRevD.86.083511](#). [arXiv:1207.6047](#).
- [157] Q. Yuan, B. Zhang, Millisecond pulsar interpretation of the Galactic center gamma-ray excess, *J. High Energy Phys.* 3 (2014) 1–8. [http://dx.doi.org/10.1016/j.jhep.2014.06.001](#). [arXiv:1404.2318](#).
- [158] R. Bartels, S. Krishnamurthy, C. Weniger, Strong support for the millisecond pulsar origin of the Galactic center GeV excess, *Phys. Rev. Lett.* 116 (2016) 051102. [arXiv:1506.05104](#).
- [159] S.K. Lee, et al., Evidence for unresolved gamma-ray point sources in the inner galaxy, *Phys. Rev. Lett.* 116 (2016) 051103. [arXiv:1506.05124](#).
- [160] M. Schaller, et al., Dark matter annihilation radiation in hydrodynamic simulations of Milky Way haloes, *Mon. Not. R. Astron. Soc.* 455 (2016) 4442–4451. [http://dx.doi.org/10.1093/mnras/stv2667](#). [arXiv:1509.02166](#).
- [161] F. Calore, et al., Simulated Milky Way analogues: implications for dark matter indirect searches, *J. Cosmol. Astropart. Phys.* 12 (2015) 053. [http://dx.doi.org/10.1088/1475-7516/2015/12/053](#). [arXiv:1509.02164](#).
- [162] I. Cholis, D. Hooper, T. Linden, A New Determination of the Spectra and Luminosity Function of Gamma-Ray Millisecond Pulsars, ArXiv e-prints [arXiv:1407.5583](#).
- [163] A.W. McConnachie, The observed properties of dwarf galaxies in and around the local group, *Astron. J.* 144 (2012) 4. [http://dx.doi.org/10.1088/0004-6256/144/1/4](#). [arXiv:1204.1562](#).
- [164] M. Mateo, Dwarf galaxies of the local group, *Ann. Rev. Astron. Astrophys.* 36 (1998) 435–506. [http://dx.doi.org/10.1146/annurev.astro.36.1.435](#). [arXiv:astro-ph/9810070](#).
- [165] J. Greveich, M.E. Putman, HI in local group dwarf galaxies and stripping by the Galactic halo, *Astrophys. J.* 696 (2009) 385–395; *Astrophys. J.* 721 (2010) 922 (erratum). [http://dx.doi.org/10.1088/0004-637X/721/1/922](#), [http://dx.doi.org/10.1088/0004-637X/696/1/385](#). [arXiv:0901.4975](#).
- [166] K. Spekkens, et al., The dearth of neutral hydrogen in Galactic dwarf spheroidal galaxies, *Astrophys. J.* 795 (2014) L5. [http://dx.doi.org/10.1088/2041-8205/795/1/L5](#). [arXiv:1410.0028](#).
- [167] N.W. Evans, F. Ferrer, S. Sarkar, A travel guide to the dark matter annihilation signal, *Phys. Rev. D* 69 (12) (2004) 123501. [http://dx.doi.org/10.1103/PhysRevD.69.123501](#). [arXiv:astro-ph/0311145](#).
- [168] I. Cholis, P. Salucci, Extracting limits on dark matter annihilation from gamma ray observations towards dwarf spheroidal galaxies, *Phys. Rev. D* 86 (2) (2012) 023528. [http://dx.doi.org/10.1103/PhysRevD.86.023528](#). [arXiv:1203.2954](#).

- [169] V. Bonnavard, et al., Dark matter annihilation and decay profiles for the reticulum II dwarf spheroidal galaxy, *Astrophys. J.* 808 (2015) L36. <http://dx.doi.org/10.1088/2041-8205/808/2/L36>. arXiv:1504.03309.
- [170] P. Ullio, M. Valli, A Critical Reassessment of Particle Dark Matter Limits from Dwarf Satellites, ArXiv e-prints arXiv:1603.07721.
- [171] P. Scott, et al., Direct constraints on minimal supersymmetry from Fermi-LAT observations of the dwarf galaxy segue 1, *J. Cosmol. Astropart. Phys.* 1 (2010) 31. <http://dx.doi.org/10.1088/1475-7516/2010/01/031>. arXiv:0909.3300.
- [172] D.G. York, et al., The sloan digital sky survey: Technical summary, *Astron. J.* 120 (2000) 1579–1587. <http://dx.doi.org/10.1086/301513>. arXiv:astro-ph/0006396.
- [173] T. Abbott, et al., The Dark Energy Survey, ArXiv e-prints arXiv:astro-ph/0510346.
- [174] K. Bechtol, et al., Eight New Milky Way companions discovered in first-year dark energy survey data, *Astrophys. J.* 807 (2015) 50. arXiv:1503.02584.
- [175] S.E. Kposov, et al., Beasts of the southern wild: Discovery of nine ultra faint satellites in the vicinity of the magellanic clouds, *Astrophys. J.* 805 (2015) 130. <http://dx.doi.org/10.1088/0004-637X/805/2/130>. arXiv:1503.02079.
- [176] D. Kim, H. Jerjen, Horologium II: A second ultra-faint Milky Way satellite in the horologium constellation, *Astrophys. J.* 808 (2015) L39. <http://dx.doi.org/10.1088/2041-8205/808/2/L39>. arXiv:1505.04948.
- [177] A. Drlica-Wagner, et al., Eight ultra-faint galaxy candidates discovered in year two of the dark energy survey, *Astrophys. J.* 813 (2015) 109. <http://dx.doi.org/10.1088/0004-637X/813/2/109>. arXiv:1508.03622.
- [178] N. Kaiser, et al., Pan-STARRS: A large synoptic survey telescope array, *Proc. SPIE Int. Soc. Opt. Eng.* 4836 (2002) 154–164. <http://dx.doi.org/10.1117/12.457365>.
- [179] B.P.M. Laevens, et al., A new faint Milky Way satellite discovered in the Pan-STARRS1  $3\pi$  survey, *Astrophys. J.* 802 (2015) L18. <http://dx.doi.org/10.1088/2041-8205/802/2/L18>. arXiv:1503.05554.
- [180] B.P.M. Laevens, et al., Sagittarius II, Draco II and Laevens 3: Three new Milky Way satellites discovered in the Pan-STARRS 1  $3\pi$  survey, *Astrophys. J.* 813 (2015) 44. <http://dx.doi.org/10.1088/0004-637X/813/1/44>. arXiv:1507.07564.
- [181] A. Albert, et al., Searching for dark matter annihilation in recently discovered Milky Way satellites with Fermi-lat, *Astrophys. J.* (2016) submitted for publication.
- [182] R. Caputo, et al., Search for gamma-ray emission from dark matter annihilation in the small magellanic cloud with the Fermi large area telescope, *Phys. Rev. D* 93 (6) (2016) 062004. <http://dx.doi.org/10.1103/PhysRevD.93.062004>. arXiv:1603.00965.
- [183] A. Drlica-Wagner, et al., Searching for dark matter annihilation in the smith high-velocity cloud, *Astrophys. J.* 790 (2014) 24. <http://dx.doi.org/10.1088/0004-637X/790/1/24>. arXiv:1405.1030.
- [184] Z. Ivezic, et al., LSST: From Science Drivers to Reference Design and Anticipated Data Products, ArXiv e-prints arXiv:0805.2366.
- [185] E. Tollerud, et al., Hundreds of Milky Way satellites? Luminosity bias in the satellite luminosity function, *Astrophys. J.* 688 (2008) 277–289. <http://dx.doi.org/10.1086/592102>. arXiv:0806.4381.
- [186] J.R. Hargis, B. Willman, A.H.G. Peter, Too many, too few, or just right? The predicted number and distribution of Milky Way dwarf galaxies, *Astrophys. J.* 795 (2014) L13. <http://dx.doi.org/10.1088/2041-8205/795/1/L13>. arXiv:1407.4470.
- [187] C. He, et al., Prospects for detecting gamma rays from annihilating dark matter in dwarf galaxies in the era of the dark energy survey and large synoptic survey telescope, *Phys. Rev. D* 91 (6) (2015) 063515. <http://dx.doi.org/10.1103/PhysRevD.91.063515>.
- [188] M. Kuhlen, P. Madau, J. Silk, Exploring dark matter with Milky Way substructure, *Science* 325 (2009) 970. <http://dx.doi.org/10.1126/science.1174881>. arXiv:0907.0005.
- [189] L.E. Strigari, R.H. Wechsler, The cosmic abundance of classical Milky Way satellites, *Astrophys. J.* 749 (2012) 75. <http://dx.doi.org/10.1088/0004-637X/749/1/75>. arXiv:1111.2611.
- [190] J. Diemand, P. Madau, B. Moore, The distribution and kinematics of early high- $\sigma$  peaks in present-day haloes: implications for rare objects and old stellar populations, *Mon. Not. R. Astron. Soc.* 364 (2005) 367–383. <http://dx.doi.org/10.1111/j.1365-2966.2005.09604.x>. arXiv:astro-ph/0506615.
- [191] H.-S. Zechlin, D. Horns, Unidentified sources in the Fermi-LAT second source catalog: the case for DM subhalos, *J. Cosmol. Astropart. Phys.* 11 (2012) 50. <http://dx.doi.org/10.1088/1475-7516/2012/11/050>. arXiv:1210.3852.
- [192] B. Bertoni, D. Hooper, T. Linden, Is The Gamma-Ray Source 3FGL J2212.5 + 0703 A Dark Matter Subhalo? ArXiv e-prints arXiv:1602.07303.
- [193] S. Profumo, et al., A running spectral index in supersymmetric dark-matter models with quasi-stable charged particles, *Phys. Rev. D* 71 (2005) 023518. <http://dx.doi.org/10.1103/PhysRevD.71.023518>. arXiv:astro-ph/0410714.
- [194] T. Bringmann, Particle models and the small-scale structure of dark matter, *New J. Phys.* 11 (2009) 105027. <http://dx.doi.org/10.1088/1367-2630/11/10/105027>. arXiv:0903.0189.
- [195] J.M. Cornell, S. Profumo, W. Shepherd, Kinetic decoupling and small-scale structure in effective theories of dark matter, *Phys. Rev. D* 88 (1) (2013) 015027. <http://dx.doi.org/10.1103/PhysRevD.88.015027>. arXiv:1305.4676.
- [196] A.A. Abdo, et al., The second Fermi large area telescope catalog of gamma-ray pulsars, *Astrophys. J. Suppl.* 208 (2013) 17. <http://dx.doi.org/10.1088/0067-0049/208/2/17>. arXiv:1305.4385.
- [197] C.L. Sarazin, X-ray emission from clusters of galaxies, *Rev. Modern Phys.* 58 (1986) 1–115. <http://dx.doi.org/10.1103/RevModPhys.58.1>.
- [198] L. Gao, et al., The phoenix project: the dark side of rich galaxy clusters, *Mon. Not. R. Astron. Soc.* 425 (2012) 2169. arXiv:1201.1940.
- [199] W.A. Hellwing, et al., The Copernicus Complexio: a high-resolution view of the small-scale Universe, *Mon. Not. R. Astron. Soc.* <http://dx.doi.org/10.1093/mnras/stw214>. arXiv:1505.06436.
- [200] M.A. Sánchez-Conde, F. Prada, The flattening of the concentration-mass relation towards low halo masses and its implications for the annihilation signal boost, *Mon. Not. R. Astron. Soc.* 442 (2014) 2271–2277. <http://dx.doi.org/10.1093/mnras/stu1014>. arXiv:1312.1729.
- [201] G. Brunetti, T.W. Jones, Cosmic rays in galaxy clusters and their nonthermal emission, *Internat. J. Modern Phys. D* 23 (2014) 30007. <http://dx.doi.org/10.1142/S0218271814300079>. arXiv:1401.7519.
- [202] T.H. Reiprich, H. Böhringer, The mass function of an X-ray flux-limited sample of galaxy clusters, *Astrophys. J.* 567 (2002) 716–740. <http://dx.doi.org/10.1086/338753>. arXiv:astro-ph/0111285.
- [203] M. Ackermann, et al., GeV gamma-ray flux upper limits from clusters of galaxies, *Astrophys. J.* 717 (2010) L71–L78. <http://dx.doi.org/10.1088/2041-8205/717/1/L71>. arXiv:1006.0748.
- [204] J. Aleksić, et al., Detection of very high energy  $\gamma$ -ray emission from the perseus cluster head-tail galaxy IC 310 by the MAGIC telescopes, *Astrophys. J.* 723 (2010) L207–L212. <http://dx.doi.org/10.1088/2041-8205/723/2/L207>. arXiv:1009.2155.
- [205] J. Aleksić, et al., Detection of very-high energy  $\gamma$ -ray emission from NGC 1275 by the MAGIC telescopes, *Astron. Astrophys.* 539 (2012) L2. <http://dx.doi.org/10.1051/0004-6361/201118668>. arXiv:1112.3917.
- [206] J. Han, et al., Constraining extended gamma-ray emission from galaxy clusters, *Mon. Not. R. Astron. Soc.* 427 (2012) 1651–1665. <http://dx.doi.org/10.1111/j.1365-2966.2012.22080.x>. arXiv:1207.6749.
- [207] O. Macías-Ramírez, et al., Evaluating the gamma-ray evidence for self-annihilating dark matter from the Virgo cluster, *Phys. Rev. D* 86 (7) (2012) 076004. <http://dx.doi.org/10.1103/PhysRevD.86.076004>. arXiv:1207.6257.
- [208] O. Reimer, et al., EGRET upper limits on the high-energy gamma-ray emission of galaxy clusters, *Astrophys. J.* 588 (2003) 155–164. <http://dx.doi.org/10.1086/374046>. arXiv:astro-ph/0301362.
- [209] B. Huber, et al., Probing the cosmic-ray content of galaxy clusters by stacking Fermi-LAT count maps, *Astron. Astrophys.* 560 (2013) A64. <http://dx.doi.org/10.1051/0004-6361/201321947>. arXiv:1308.6278.
- [210] M. Ackermann, et al., Search for cosmic-ray-induced gamma-ray emission in galaxy clusters, *Astrophys. J.* 787 (2014) 18. <http://dx.doi.org/10.1088/0004-637X/787/1/18>. arXiv:1308.5654.
- [211] D.A. Prokhorov, E.M. Churazov, Counting gamma rays in the directions of galaxy clusters, *Astron. Astrophys.* 567 (2014) A93. <http://dx.doi.org/10.1051/0004-6361/201322454>. arXiv:1309.0197.

- [212] S. Zimmer, et al., A Combined Analysis of Clusters of Galaxies—Gamma Ray Emission from Cosmic Rays and Dark Matter, ArXiv e-prints [arXiv:1110.6863](#).
- [213] K.L. Dutton, et al., A stacked analysis of brightest cluster galaxies observed with the Fermi large area telescope, *Mon. Not. R. Astron. Soc.* 429 (2013) 2069–2079. [http://dx.doi.org/10.1093/mnras/sts477](#). [arXiv:1211.6344](#).
- [214] M.A. Sánchez-Conde, et al., Dark matter searches with Cherenkov telescopes: nearby dwarf galaxies or local galaxy clusters? *J. Cosmol. Astropart. Phys.* 12 (2011) 11. [http://dx.doi.org/10.1088/1475-7516/2011/12/011](#). [arXiv:1104.3530](#).
- [215] S. Zimmer, et al., Galaxy Clusters with the Fermi-LAT: Status and Implications for Cosmic Rays and Dark Matter Physics, ArXiv e-prints [arXiv:1502.02653](#).
- [216] J. Einasto, On the construction of a composite model for the Galaxy and on the determination of the system of Galactic parameters, *Trudy Inst. Astroz. Alma-Ata* 51.
- [217] A. Jenkins, et al., The mass function of dark matter halos, *Mon. Not. R. Astron. Soc.* 321 (2001) 372. [http://dx.doi.org/10.1046/j.1365-8711.2001.04029.x](#). [arXiv:astro-ph/0005260](#).
- [218] V. Springel, et al., Simulating the joint evolution of quasars, galaxies and their large-scale distribution, *Nature* 435 (2005) 629–636. [http://dx.doi.org/10.1038/nature03597](#). [arXiv:astro-ph/0504097](#).
- [219] M. Boylan-Kolchin, et al., Resolving cosmic structure formation with the Millennium-II simulation, *Mon. Not. R. Astron. Soc.* 398 (2009) 1150–1164. [http://dx.doi.org/10.1111/j.1365-2966.2009.15191.x](#). [arXiv:0903.3041](#).
- [220] A.A. Klypin, S. Trujillo-Gomez, J. Primack, Dark matter halos in the standard cosmological model: Results from the Bolshoi simulation, *Astrophys. J.* 740 (2011) 102. [http://dx.doi.org/10.1088/0004-637X/740/2/102](#). [arXiv:1002.3660](#).
- [221] R.K. Sheth, G. Tormen, An excursion set model of hierarchical clustering: Ellipsoidal collapse and the moving barrier, *Mon. Not. R. Astron. Soc.* 329 (2002) 61. [http://dx.doi.org/10.1046/j.1365-8711.2002.04950.x](#). [arXiv:astro-ph/0105113](#).
- [222] J.L. Tinker, et al., Toward a halo mass function for precision cosmology: The Limits of universality, *Astrophys. J.* 688 (2008) 709–728. [http://dx.doi.org/10.1086/591439](#). [arXiv:0803.2706](#).
- [223] F. Calore, V. de Romeri, F. Donato, Conservative upper limits on WIMP annihilation cross section from Fermi-LAT  $\gamma$  rays, *Phys. Rev. D* 85 (2) (2012) 023004. [http://dx.doi.org/10.1103/PhysRevD.85.023004](#). [arXiv:1105.4230](#).
- [224] K.N. Abazajian, et al., Conservative constraints on dark matter from the Fermi-LAT isotropic diffuse gamma-ray background spectrum, *J. Cosmol. Astropart. Phys.* 11 (2010) 41. [http://dx.doi.org/10.1088/1475-7516/2010/11/041](#). [arXiv:1002.3820](#).
- [225] A.A. Abdo, et al., Constraints on cosmological dark matter annihilation from the Fermi-LAT isotropic diffuse gamma-ray measurement, *J. Cosmol. Astropart. Phys.* 4 (2010) 14. [http://dx.doi.org/10.1088/1475-7516/2010/04/014](#). [arXiv:1002.4415](#).
- [226] B.J. Carr, et al., New cosmological constraints on primordial black holes, *Phys. Rev. D* 81 (10) (2010) 104019. [http://dx.doi.org/10.1103/PhysRevD.81.104019](#). [arXiv:0912.5297](#).
- [227] B.J. Carr, J.H. MacGibbon, Cosmic rays from primordial black holes and constraints on the early universe, *Phys. Rep.* 307 (1998) 141. [http://dx.doi.org/10.1016/S0370-1573\(98\)00039-8](#).
- [228] A. Barrau, et al., Galactic cosmic rays from PBHs and primordial spectra with a scale, *Phys. Lett. B* 551 (2003) 218–225. [http://dx.doi.org/10.1016/S0370-2693\(02\)03060-5](#). [arXiv:astro-ph/0210149](#).
- [229] T. Ishiyama, Hierarchical formation of dark matter halos and the free streaming scale, *Astrophys. J.* 788 (2014) 27. [http://dx.doi.org/10.1088/0004-637X/788/1/27](#). [arXiv:1404.1650](#).
- [230] D. Malyshev, D.W. Hogg, Statistics of gamma-ray point sources below the Fermi detection limit, *Astrophys. J.* 738 (2011) 181. [http://dx.doi.org/10.1088/0004-637X/738/2/181](#). [arXiv:1104.0010](#).
- [231] S.K. Lee, M. Lisanti, B.R. Safdi, Distinguishing dark matter from unresolved point sources in the inner galaxy with photon statistics, *J. Cosmol. Astropart. Phys.* 1505 (05) (2015) 056. [http://dx.doi.org/10.1088/1475-7516/2015/05/056](#). [arXiv:1412.6099](#).
- [232] M.R. Feyereisen, S. Ando, S.K. Lee, Modelling the flux distribution function of the extragalactic gamma-ray background from dark matter annihilation, *J. Cosmol. Astropart. Phys.* 1509 (09) (2015) 027. [http://dx.doi.org/10.1088/1475-7516/2015/09/027](#). [arXiv:1506.05118](#).
- [233] S.K. Lee, S. Ando, M. Kamionkowski, The gamma-ray-flux probability distribution function from Galactic halo substructure, *J. Cosmol. Astropart. Phys.* 0907 (2009) 007. [http://dx.doi.org/10.1088/1475-7516/2009/07/007](#). [arXiv:0810.1284](#).
- [234] S. Dodelson, et al., Identifying dark matter annihilation products in the diffuse gamma ray background, *Phys. Rev. D* 80 (2009) 083504. [http://dx.doi.org/10.1103/PhysRevD.80.083504](#). [arXiv:0903.2829](#).
- [235] G.A. Gomez-Vargas, et al., Dark matter implications of Fermi-LAT measurement of anisotropies in the diffuse gamma-ray background in: 4th International Fermi Symposium Monterey, California, USA, October 28–November 2, 2012, 2013. [arXiv:1303.2154](#).
- [236] L. Bergstrom, P. Ullio, Full one loop calculation of neutralino annihilation into two photons, *Nuclear Phys. B* 504 (1997) 27–44. [http://dx.doi.org/10.1016/S0550-3213\(97\)00530-0](#). [arXiv:hep-ph/9706232](#).
- [237] S. Matsumoto, J. Sato, Y. Sato, Enhancement of Line Gamma Ray Signature from Bino-like Dark Matter Annihilation Due to CP Violation, ArXiv e-prints [arXiv:hep-ph/0505160](#).
- [238] F. Ferrer, L.M. Krauss, S. Profumo, Indirect detection of light neutralino dark matter in the NMSSM, *Phys. Rev. D* 74 (2006) 115007. [http://dx.doi.org/10.1103/PhysRevD.74.115007](#). [arXiv:hep-ph/0609257](#).
- [239] M. Gustafsson, et al., Significant gamma lines from inert Higgs dark matter, *Phys. Rev. Lett.* 99 (2007) 041301. [http://dx.doi.org/10.1103/PhysRevLett.99.041301](#). [arXiv:astro-ph/0703512](#).
- [240] S. Profumo, Hunting the lightest lightest neutralinos, *Phys. Rev. D* 78 (2008) 023507. [http://dx.doi.org/10.1103/PhysRevD.78.023507](#). [arXiv:0806.2150](#).
- [241] T. Bringmann, et al., Fermi LAT search for internal Bremsstrahlung signatures from dark matter annihilation, *J. Cosmol. Astropart. Phys.* 1207 (2012) 054. [http://dx.doi.org/10.1088/1475-7516/2012/07/054](#). [arXiv:1203.1312](#).
- [242] E. Tempel, A. Hektor, M. Raidal, Fermi 130 GeV gamma-ray excess and dark matter annihilation in sub-haloes and in the Galactic centre, *J. Cosmol. Astropart. Phys.* 1209 (2012) 032. [http://dx.doi.org/10.1088/1475-7516/2012/09/032](#), [http://dx.doi.org/10.1088/1475-7516/2012/11/A01](#). [arXiv:1205.1045](#).
- [243] M. Su, D.P. Finkbeiner, Strong Evidence for Gamma-ray Line Emission from the Inner Galaxy, ArXiv e-prints [arXiv:1206.1616](#).
- [244] A. Hektor, M. Raidal, E. Tempel, Fermi-LAT gamma-ray signal from Earth limb, systematic detector effects and their implications for the 130 GeV gamma-ray excess, *Eur. Phys. J. J* 73 (2013) 2578. [http://dx.doi.org/10.1140/epjc/s10052-013-2578-4](#). [arXiv:1209.4548](#).
- [245] M. Su, D.P. Finkbeiner, Double Gamma-Ray Lines from Unassociated Fermi-LAT Sources, ArXiv e-prints [arXiv:1207.7060](#).
- [246] A. Hektor, M. Raidal, E. Tempel, Double Gamma-ray Lines from Unassociated Fermi-LAT Sources Revisited, ArXiv e-prints [arXiv:1208.1996](#).
- [247] A. Geringer-Sameth, S.M. Koushiappas, Dark matter line search using a joint analysis of dwarf galaxies with the fermi gamma-ray space telescope, *Phys. Rev. D* 86 (2012) 021302. [http://dx.doi.org/10.1103/PhysRevD.86.021302](#). [arXiv:1206.0796](#).
- [248] D. Whiteson, Disentangling instrumental features of the 130 GeV Fermi line, *J. Cosmol. Astropart. Phys.* 1211 (2012) 008. [http://dx.doi.org/10.1088/1475-7516/2012/11/008](#). [arXiv:1208.3677](#).
- [249] D.P. Finkbeiner, M. Su, C. Weniger, Is the 130 GeV line real? A search for systematics in the Fermi-LAT data, *J. Cosmol. Astropart. Phys.* 1301 (2013) 029. [http://dx.doi.org/10.1088/1475-7516/2013/01/029](#). [arXiv:1209.4562](#).
- [250] A. Boyarsky, D. Malyshev, O. Ruchayskiy, Spectral and spatial variations of the diffuse  $\gamma$ -ray background in the vicinity of the Galactic plane and possible nature of the feature at 130 GeV, *Phys. Dark Universe* 2 (2013) 90–96. [http://dx.doi.org/10.1016/j.dark.2013.04.001](#). [arXiv:1205.4700](#).
- [251] J. Bregeon, et al., Fermi-LAT Data Reprocessed with Updated Calibration Constants, ArXiv e-prints [arXiv:1304.5456](#).
- [252] D. Cadamuro, J. Redondo, Cosmological bounds on pseudo Nambu–Goldstone bosons, *J. Cosmol. Astropart. Phys.* 2 (2012) 32. [http://dx.doi.org/10.1088/1475-7516/2012/02/032](#). [arXiv:1110.2895](#).



- [253] B. Berenji, J. Gaskins, M. Meyer, Constraints on axions and axionlike particles from fermi large area telescope observations of neutron stars, *Phys. Rev. D* 93 (2016) 045019. <http://dx.doi.org/10.1103/PhysRevD.93.045019>. arXiv:1602.00091.
- [254] D. Hooper, P.D. Serpico, Detecting axionlike particles with gamma ray telescopes, *Phys. Rev. Lett.* 99 (23) (2007) 231102. <http://dx.doi.org/10.1103/PhysRevLett.99.231102>. arXiv:0706.3203.
- [255] N. Bassan, A. Mirizzi, M. Roncadelli, Axion-like particle effects on the polarization of cosmic high-energy gamma sources, *J. Cosmol. Astropart. Phys.* 5 (2010) 10. <http://dx.doi.org/10.1088/1475-7516/2010/05/010>. arXiv:1001.5267.
- [256] A. Dobrynina, A. Kartavtsev, G. Raffelt, Photon–photon dispersion of TeV gamma rays and its role for photon-ALP conversion, *Phys. Rev. D* 91 (8) (2015) 083003. <http://dx.doi.org/10.1103/PhysRevD.91.083003>. arXiv:1412.4777.
- [257] F. Govoni, L. Feretti, Magnetic fields in clusters of galaxies, *Internat. J. Modern Phys. D* 13 (2004) 1549–1594. <http://dx.doi.org/10.1142/S0218271804005080>. arXiv:astro-ph/0410182.
- [258] L.M. Widrow, Origin of Galactic and extragalactic magnetic fields, *Rev. Modern Phys.* 74 (2002) 775–823. <http://dx.doi.org/10.1103/RevModPhys.74.775>. arXiv:astro-ph/0207240.
- [259] L. Östman, E. Mörtzell, Limiting the dimming of distant type Ia supernovae, *J. Cosmol. Astropart. Phys.* 2 (2005) 5. <http://dx.doi.org/10.1088/1475-7516/2005/02/005>. arXiv:astro-ph/0410501.
- [260] D. Wouters, P. Brun, Irregularity in gamma ray source spectra as a signature of axionlike particles, *Phys. Rev. D* 86 (4) (2012) 043005. <http://dx.doi.org/10.1103/PhysRevD.86.043005>. arXiv:1205.6428.
- [261] D. Wouters, P. Brun, Constraints on axion-like particles from X-ray observations of the hydra galaxy cluster, *Astrophys. J.* 772 (2013) 44. <http://dx.doi.org/10.1088/0004-637X/772/1/44>. arXiv:1304.0989.
- [262] M. Meyer, D. Horns, M. Raue, First lower limits on the photon-axion-like particle coupling from very high energy gamma-ray observations, *Phys. Rev. D* 87 (3) (2013) 035027. <http://dx.doi.org/10.1103/PhysRevD.87.035027>. arXiv:1302.1208.
- [263] M. Simet, D. Hooper, P.D. Serpico, The Milky Way as a kiloparsec-scale axionscope, *Phys. Rev. D* 77 (2008) 063001. <http://dx.doi.org/10.1103/PhysRevD.77.063001>. arXiv:0712.2825.
- [264] A. de Angelis, M. Roncadelli, O. Mansutti, Evidence for a new light spin-zero boson from cosmological gamma-ray propagation? *Phys. Rev. D* 76 (12) (2007) 121301. <http://dx.doi.org/10.1103/PhysRevD.76.121301>. arXiv:0707.4312.
- [265] M.A. Sánchez-Conde, et al., Hints of the existence of axionlike particles from the gamma-ray spectra of cosmological sources, *Phys. Rev. D* 79 (12) (2009) 123511. <http://dx.doi.org/10.1103/PhysRevD.79.123511>. arXiv:0905.3270.
- [266] A. Domínguez, M.A. Sánchez-Conde, F. Prada, Axion-like particle imprint in cosmological very-high-energy sources, *J. Cosmol. Astropart. Phys.* 11 (2011) 20. <http://dx.doi.org/10.1088/1475-7516/2011/11/020>. arXiv:1106.1860.
- [267] M.G. Hauser, E. Dwek, The cosmic infrared background: Measurements and implications, *Annu. Rev. Astron. Astrophys.* 39 (2001) 249–307. <http://dx.doi.org/10.1146/annurev.astro.39.1.249>. arXiv:astro-ph/0105539.
- [268] J.W. Brockway, E.D. Carlson, G.G. Raffelt, SN 1987A gamma-ray limits on the conversion of pseudoscalars, *Phys. Lett. B* 383 (1996) 439–443. [http://dx.doi.org/10.1016/0370-2693\(96\)00778-2](http://dx.doi.org/10.1016/0370-2693(96)00778-2). arXiv:astro-ph/9605197.
- [269] J.A. Grifols, E. Massó, R. Toldrà, Gamma rays from SN 1987A due to pseudoscalar conversion, *Phys. Rev. Lett.* 77 (1996) 2372–2375. <http://dx.doi.org/10.1103/PhysRevLett.77.2372>. arXiv:astro-ph/9606028.
- [270] A. Payez, et al., Revisiting the SN1987A gamma-ray limit on ultralight axion-like particles, *J. Cosmol. Astropart. Phys.* 2 (2015) 6. <http://dx.doi.org/10.1088/1475-7516/2015/02/006>. arXiv:1410.3747.
- [271] M. Ajello, et al., Search for spectral irregularities due to photon-axionlike-particle oscillations with the Fermi large area telescope, *Phys. Rev. Lett.* 116 (16) (2016) 161101. <http://dx.doi.org/10.1103/PhysRevLett.116.161101>. arXiv:1603.06978.
- [272] R. Essig, et al., Dark Sectors and New, Light, Weakly-Coupled Particles, ArXiv e-prints arXiv:1311.0029.
- [273] M. Meyer, J. Conrad, Sensitivity of the Cherenkov telescope array to the detection of axion-like particles at high gamma-ray opacities, *J. Cosmol. Astropart. Phys.* 12 (2014) 16. <http://dx.doi.org/10.1088/1475-7516/2014/12/016>. arXiv:1410.1556.
- [274] R. Bähre, et al., Any light particle search II—technical design report, *J. Instrum.* 8 (2013) 9001. <http://dx.doi.org/10.1088/1748-0221/8/09/T09001>. arXiv:1302.5647.
- [275] A. Abramowski, et al., Constraints on axionlike particles with H.E.S.S. from the irregularity of the PKS 2155–304 energy spectrum, *Phys. Rev. D* 88 (10) (2013) 102003. <http://dx.doi.org/10.1103/PhysRevD.88.102003>. arXiv:1311.3148.
- [276] A. Domínguez, M. Ajello, Spectral analysis of Fermi-LAT blazars above 50 GeV, *Astrophys. J.* 813 (2015) L34. <http://dx.doi.org/10.1088/2041-8205/813/2/L34>. arXiv:1510.07913.
- [277] B.M. Gaensler, R. Beck, L. Feretti, The origin and evolution of cosmic magnetism, *New Rev.* 48 (2004) 1003–1012. <http://dx.doi.org/10.1016/j.newar.2004.09.003>. arXiv:astro-ph/0409100.
- [278] A. Bonafede, et al., Unravelling the origin of large-scale magnetic fields in galaxy clusters and beyond through Faraday rotation measures with the SKA, *PoS AASKA 14* (2015) 095. arXiv:1501.00321.
- [279] A. de Angelis, G. Galanti, M. Roncadelli, Relevance of axionlike particles for very-high-energy astrophysics, *Phys. Rev. D* 84 (10) (2011) 105030. <http://dx.doi.org/10.1103/PhysRevD.84.105030>. arXiv:1106.1132.
- [280] G.I. Rubtsov, S.V. Troitsky, Breaks in gamma-ray spectra of distant blazars and transparency of the universe, *Sov. J. Exp. Theor. Phys. Lett.* 100 (2014) 355–359. <http://dx.doi.org/10.1134/S0021364014180088>. arXiv:1406.0239.
- [281] V. Lefranc, et al., Prospects for annihilating dark matter in the inner galactic halo by the Cherenkov Telescope Array, *Phys. Rev. D* 91 (12) (2015) 122003. <http://dx.doi.org/10.1103/PhysRevD.91.122003>. arXiv:1502.05064.
- [282] H. Silverwood, et al., A realistic assessment of the CTA sensitivity to dark matter annihilation, *J. Cosmol. Astropart. Phys.* 3 (2015) 55. <http://dx.doi.org/10.1088/1475-7516/2015/03/055>. arXiv:1408.4131.
- [283] J. Carr, et al., Prospects for indirect dark matter searches with the Cherenkov Telescope Array (CTA) 2015 arXiv: 1508.06128.
- [284] V. Lefranc, et al., Dark Matter Search in the Inner Galactic Halo with H.E.S.S. I and H.E.S.S. II, ArXiv e-prints arXiv:1509.04123.
- [285] O. Adriani, et al., PAMELA results on the cosmic-ray antiproton flux from 60 MeV to 180 GeV in kinetic energy, *Phys. Rev. Lett.* (12) (2010) 121101. <http://dx.doi.org/10.1103/PhysRevLett.105.121101>. arXiv:1007.0821.
- [286] AMS-02 Collaboration, Talks at the ‘AMS Days at CERN’, April, 2015.
- [287] M. Aguilar, et al., Precision measurement of the proton flux in primary cosmic rays from rigidity 1 GV to 1.8 TV with the alpha magnetic spectrometer on the international space station, *Phys. Rev. Lett.* 114 (17) (2015) 171103. <http://dx.doi.org/10.1103/PhysRevLett.114.171103>.
- [288] G. Giesen, et al., AMS-02 antiprotons, at last! Secondary astrophysical component and immediate implications for dark matter, *J. Cosmol. Astropart. Phys.* 9 (2015) 23. <http://dx.doi.org/10.1088/1475-7516/2015/09/023>. arXiv:1504.04276.
- [289] D. Hooper, T. Linden, P. Mertsch, What does the PAMELA antiproton spectrum tell us about dark matter? *J. Cosmol. Astropart. Phys.* 3 (2015) 21. <http://dx.doi.org/10.1088/1475-7516/2015/03/021>. arXiv:1410.1527.
- [290] H.-B. Jin, Y.-L. Wu, Y.-F. Zhou, Upper limits on dark matter annihilation cross sections from the first AMS-02 antiproton data, *Phys. Rev. D* 92 (5) (2015) 055027. <http://dx.doi.org/10.1103/PhysRevD.92.055027>. arXiv:1504.04604.
- [291] M. Aguilar, et al., First result from the alpha magnetic spectrometer on the international space station: Precision measurement of the positron fraction in primary cosmic rays of 0.5–350 GeV, *Phys. Rev. Lett.* 110 (2013) 141102. <http://dx.doi.org/10.1103/PhysRevLett.110.141102>.
- [292] L. Accardo, et al., High statistics measurement of the positron fraction in primary cosmic rays of 0.5–500 GeV with the alpha magnetic spectrometer on the international space station, *Phys. Rev. Lett.* 113 (2014) 121101. <http://dx.doi.org/10.1103/PhysRevLett.113.121101>.
- [293] O. Adriani, et al., Cosmic-ray positron energy spectrum measured by PAMELA, *Phys. Rev. Lett.* 111 (8) (2013) 081102. <http://dx.doi.org/10.1103/PhysRevLett.111.081102>. arXiv:1308.0133.
- [294] P.D. Serpico, Possible causes of a rise with energy of the cosmic ray positron fraction, *Phys. Rev. D* 79 (2) (2009) 021302. <http://dx.doi.org/10.1103/PhysRevD.79.021302>. arXiv:0810.4846.

- [295] T. Linden, S. Profumo, Probing the pulsar origin of the anomalous positron fraction with AMS-02 and atmospheric Cherenkov telescopes, *Astrophys. J.* 772 (2013) 18. <http://dx.doi.org/10.1088/0004-637X/772/1/18>. arXiv:1304.1791.
- [296] I. Cholis, D. Hooper, Dark matter and pulsar origins of the rising cosmic ray positron fraction in light of new data from the AMS, *Phys. Rev. D* 88 (2) (2013) 023013. <http://dx.doi.org/10.1103/PhysRevD.88.023013>. arXiv:1304.1840.
- [297] A. Ibarra, A.S. Lamperstorfer, J. Silk, Dark matter annihilations and decays after the AMS-02 positron measurements, *Phys. Rev. D* 89 (6) (2014) 063539. <http://dx.doi.org/10.1103/PhysRevD.89.063539>. arXiv:1309.2570.
- [298] S. Arrenberg, et al., Dark Matter in the Coming Decade: Complementary Paths to Discovery and Beyond, ArXiv e-prints [arXiv:1310.8621](https://arxiv.org/abs/1310.8621).
- [299] Y. Gershtein, et al., New Particles Working Group Report of the Snowmass 2013 Community Summer Study, ArXiv e-prints [arXiv:1311.0299](https://arxiv.org/abs/1311.0299).
- [300] D. Bauer, et al., Dark matter in the coming decade: Complementary paths to discovery and beyond, *Phys. Dark Universe* 7 (2015) 16–23. <http://dx.doi.org/10.1016/j.dark.2015.04.001>. arXiv:1305.1605.
- [301] E. Aprile, et al., Exclusion of leptophilic dark matter models using XENON100 electronic recoil data, *Science* 349 (6250) (2015) 851–854. arXiv:1507.07747.
- [302] E. Aprile, et al., Search for event rate modulation in XENON100 electronic recoil data, *Phys. Rev. Lett.* 115 091302. arXiv:1507.07748.
- [303] K. Choi, et al., Search for neutrinos from annihilation of captured low-mass dark matter particles in the sun by super-kamiokande, *Phys. Rev. Lett.* 114 (14) (2015) 141301. <http://dx.doi.org/10.1103/PhysRevLett.114.141301>.
- [304] A.D. Avrorin, et al., Search for neutrino emission from relic dark matter in the sun with the Baikal NT200 detector, *Astropart. Phys.* 62 (2015) 12–20. <http://dx.doi.org/10.1016/j.astropartphys.2014.07.006>. arXiv:1405.3551.
- [305] M.G. Aartsen, et al., Improved limits on dark matter annihilation in the sun with the 79-string icecube detector and implications for supersymmetry, *J. Cosmol. Astropart. Phys.* 4 (2016) 022. <http://dx.doi.org/10.1088/1475-7516/2016/04/022>. arXiv:1601.00653.
- [306] E. Behnke, et al., First dark matter search results from a 4-kg CF<sub>3</sub>I bubble chamber operated in a deep underground site, *Phys. Rev. D* 86 (5) (2012) 052001. <http://dx.doi.org/10.1103/PhysRevD.86.052001>. arXiv:1204.3094.
- [307] G. Aad, et al., Search for dark matter candidates and large extra dimensions in events with a jet and missing transverse momentum with the ATLAS detector, *J. High Energy Phys.* 4 (2013) 75. [http://dx.doi.org/10.1007/JHEP04\(2013\)075](http://dx.doi.org/10.1007/JHEP04(2013)075). arXiv:1210.4491.
- [308] S. Chatrchyan, et al., Search for dark matter and large extra dimensions in monojet events in pp collisions at  $\sqrt{s} = \{7\}$  TeV, *J. High Energy Phys.* 9 (2012) 94. [http://dx.doi.org/10.1007/JHEP09\(2012\)094](http://dx.doi.org/10.1007/JHEP09(2012)094). arXiv:1206.5663.
- [309] J. Goodman, et al., Constraints on dark matter from colliders, *Phys. Rev. D* 82 (11) (2010) 116010. arXiv:arXiv:1008.1783 [hep-ph].
- [310] M. Beltrán, et al., Maverick dark matter at colliders, *J. High Energy Phys.* 9 (2010) 37. arXiv:arXiv:1002.4137 [hep-ph].
- [311] J. Goodman, et al., Constraints on light majorana dark matter from colliders, *Phys. Lett. B* 695 (2011) 185–188. arXiv:arXiv:1005.1286 [hep-ph].
- [312] M. Kachelrieß, P.D. Serpico, Model-independent dark matter annihilation bound from the diffuse gamma ray flux, *Phys. Rev. D* 76 (6) (2007) 063516. <http://dx.doi.org/10.1103/PhysRevD.76.063516>. arXiv:0707.0209.
- [313] V. Berezhinsky, M. Kachelrieß, S. Ostapchenko, Electroweak jet cascading in the decay of superheavy particles, *Phys. Rev. Lett.* 89 (17) (2002) 171802. <http://dx.doi.org/10.1103/PhysRevLett.89.171802>. arXiv:hep-ph/0205218.
- [314] M. Kachelrieß, P.D. Serpico, M.A. Solberg, Role of electroweak Bremsstrahlung for indirect dark matter signatures, *Phys. Rev. D* 80 (12) (2009) 123533. <http://dx.doi.org/10.1103/PhysRevD.80.123533>. arXiv:0911.0001.
- [315] P. Ciafaloni, A. Urbano, TeV scale dark matter and electroweak radiative corrections, *Phys. Rev. D* 82 (4) (2010) 043512. <http://dx.doi.org/10.1103/PhysRevD.82.043512>. arXiv:1001.3950.
- [316] P. Ciafaloni, et al., Weak corrections are relevant for dark matter indirect detection, *J. Cosmol. Astropart. Phys.* 1103 (2011) 019. <http://dx.doi.org/10.1088/1475-7516/2011/03/019>. arXiv:1009.0224.
- [317] M. Cirelli, et al., PPPC 4 DM ID: A poor particle physicist cookbook for dark matter indirect detection, *J. Cosmol. Astropart. Phys.* 1103 (2011) 051. <http://dx.doi.org/10.1088/1475-7516/2012/10/E01>, <http://dx.doi.org/10.1088/1475-7516/2011/03/051>. arXiv:1012.4515.
- [318] P. Bruel, et al., Gamma rays, electrons and positrons up to 3 TeV with the Fermi gamma-ray space telescope, *J. Phys. Conf. Ser.* 404 (1) (2012) 012033. <http://dx.doi.org/10.1088/1742-6596/404/1/012033>. arXiv:1210.2558.
- [319] F. Acero, et al., Development of the model of Galactic interstellar emission for standard point-source analysis of Fermi large area telescope data, *Astrophys. J. Suppl.* 223 (2016) 26. <http://dx.doi.org/10.3847/0067-0049/223/2/26>. arXiv:1602.07246.
- [320] P.A.R. Ade, et al., Planck intermediate results. XXVIII. Interstellar gas and dust in the Chamaeleon clouds as seen by Fermi LAT and Planck, *Astron. Astrophys.* 582 (2015) A31. <http://dx.doi.org/10.1051/0004-6361/201424955>. arXiv:1409.3268.
- [321] I.A. Grenier, J.-M. Casandjian, R. Terrier, Unveiling extensive clouds of dark gas in the solar neighborhood, *Science* 307 (2005) 1292–1295. <http://dx.doi.org/10.1126/science.1106924>.
- [322] A.A. Abdo, et al., Fermi observations of cassiopeia and cepheus: Diffuse gamma-ray emission in the outer galaxy, *Astrophys. J.* 710 (2010) 133–149. <http://dx.doi.org/10.1088/0004-637X/710/1/133>. arXiv:0912.3618.
- [323] M. Su, T.R. Slatyer, D.P. Finkbeiner, Giant gamma-ray bubbles from Fermi-LAT: Active Galactic nucleus activity or bipolar Galactic wind? *Astrophys. J.* 724 (2010) 1044–1082. <http://dx.doi.org/10.1088/0004-637X/724/2/1044>. arXiv:1005.5480.
- [324] P.A.R. Ade, et al., Planck intermediate results. IX. Detection of the Galactic haze with Planck, *Astron. Astrophys.* 554 (2013) A139. <http://dx.doi.org/10.1051/0004-6361/201220271>. arXiv:1208.5483.
- [325] G. Dobler, D.P. Finkbeiner, Extended anomalous foreground emission in the WMAP three-year data, *Astrophys. J.* 680 (2008) 1222–1234. <http://dx.doi.org/10.1086/587862>. arXiv:0712.1038.
- [326] M. Ackermann, et al., A cocoon of freshly accelerated cosmic rays detected by Fermi in the cygnus superbubble, *Science* 334 (2011) 1103. <http://dx.doi.org/10.1126/science.1210311>.
- [327] G. Cowan, et al., Asymptotic formulae for likelihood-based tests of new physics, *Eur. Phys. J.* 71 (2011) 1554. <http://dx.doi.org/10.1140/epjc/s10052-011-1554-0>. arXiv:1007.1727.
- [328] A.A. Abdo, et al., The Fermi-LAT high-latitude survey: Source count distributions and the origin of the extragalactic diffuse background, *Astrophys. J.* 720 (2010) 435–453. <http://dx.doi.org/10.1088/0004-637X/720/1/435>. arXiv:1003.0895.
- [329] M. Ackermann, et al., The third catalog of active Galactic nuclei detected by the Fermi large area telescope, *Astrophys. J.* 810 (2015) 14. <http://dx.doi.org/10.1088/0004-637X/810/1/14>. arXiv:1501.06054.